Mirjam Ziselsberger, BSc

Landslides triggered in the Sindhupalchok District during the Mw 7.8 Nepal-Gorkha Earthquake of April 25, 2015

Photo-Interpretive Landslide Assessment

MASTER'S THESIS

to achieve the university degree of

Master of Science

Master's degree programme: Earth Sciences

submitted to

Graz University of Technology

Supervisor

Univ.-Prof. BA MSc PhD Daniel Scott Kieffer

Institute of Engineering Geology

Graz, April 2016

AFFIDAVIT

I declare that I have authored this thesis independently, that I have not used other than the declared sources/resources, and that I have explicitly indicated all material which has been quoted either literally or by content from the sources used. The text document uploaded to TUGRAZonline is identical to the present master's thesis dissertation.

Date

Signature

ACKNOWLEDGEMENTS

The work of the GEER Association, in general, is based upon work supported in part by the National Science Foundation through the Geotechnical Engineering Program under Grant No. CMMI-1266418.

The Center of Disaster Studies at the Institute of Engineering of Tribhuvan University was the primary collaborator in managing access to sites and providing local professionals and students to accompany the GEER team.

My sincerest thanks go to my supervisor D. Scott Kieffer, for the chance to be part of the GEER reconnaissance team, and for his motivation and support throughout the process of this master thesis. Furthermore, many thanks to my colleague Christoph Zambanini, for all the time we spent together in Nepal and in the office. I am also very grateful for all those who accompanied me in the last few years, especially Daniel de Pretis, Marcus Spitz, Felix Österreicher, Katharina Brandner and Esther Andel. Most importantly, I would like to express my gratitude to my parents Margaretha Bannert and Wilhelm Andel, for supporting me and all of my decisions. Finally, special thanks to my mother, for repeatedly proofreading this master thesis.

Mirjam Ziselsberger

ABSTRACT

The April 25, 2015 M_W 7.8 Nepal-Gorkha earthquake was caused by a fault rupture along the Main Himalayan Frontal Thrust. Due to a strong directivity effect, thousands of landslides were triggered in the districts southeast of Gorkha. This work focuses on mass movements in the district of Sindhupalchok, which is located northeast of the capital city Kathmandu.

By comparing pre- and post-earthquake satellite imagery, new and reactivated landslides were identified and mapped with a high resolution photo surveying tool (Google Earth Pro; images were provided by DigitalGlobe and CNES/Astrium). Besides some manually recorded parameters (e.g. surface area, slope aspect and affected infrastructure) further data was extracted from various sources, including the 1-arc-second SRTM DEM, ISRICS' soil cover, or ICIMOD's land cover. Calculations, statistical analyses and plots were performed, and several inventory maps were created with the software QGIS. Furthermore, some of the landslide data was plotted on empirical curves, like earthquake magnitude vs. area affected and magnitude vs. number of landslides, or the maximum epicentral distance as a function of earthquake magnitude.

Two site visits were done, the first in May right after the earthquake, and the second in October 2015, to examine the effects of the monsoon. Most of the observed landslides are shallow, dry slides composed of weathered rock and soil, and many of them exhibit steep joint detachment surfaces. Ridgetops, narrow gullies and road cuts are very common locations for landslides.

The compiled landslide data show several trends. The most affected areas are located between 1500 and 2500 meters above sea level. Longer landslides tend to occur preferably in higher elevations, and landslide areas increase towards the north where the mountains rise up to almost 7000 meters. Due to the high topographic relief of Sindhupalchok and the elevation-dependent climatic differences, correlations between altitude, soil- and landcover arise.

A tendency toward steep southern and gentle northern slopes exists in the affected region, which explains the pronounced occurrence of landslides on south and southeast facing hillsides. Landslide density also increased for slope angles above 35 degrees, and in geological formations consisting of slate or limestone.

A hydrological classification based on the orographic catchment areas of the main rivers passing through or along Sindhupalchok was performed. With a maximum of 1.2% of the drainage basin

area affected by landslides, the drainage basin of Bhotekoshi River was hit hardest.

The landslides were also grouped according to their distance from the epicenter. Approximately 75% of the triggered landslides lie within a radius of 100 to 130 km from the epicenter, which covers about half of Sindhupalchok's total area.

Contents

List of figures and tables

1. Introduction

On April 25, 2015 a M_W 7.8 earthquake struck Nepal as a part of the Main Himalayan Frontal Thrust ruptured. The hypocenter was located at 28.1473 N latitude and 84.7079 E longitude in the Gorkha district, in a depth of about 15 km. The earthquake and its aftershocks resulted in almost 9 000 deaths and hundreds of thousands of destructed or damaged houses.

Following this event, the Geotechnical Extreme Events Reconnaissance (GEER) Association assembled a team under the leadership of D. Scott Kieffer and Binod Tiwari. Two groups of international experts in the areas of (Engineering) Geology, Seismology, Geotechnical (Earthquake) Engineering and Civil Engineering visited Nepal in the weeks following the earthquake to evaluate the geotechnical impacts, and gather time-sensitive data. (Hashash et al. 2015) One of GEER's goals is to bring graduate students together with experts in post-event investigations, to advance the capabilities of individuals performing reconnaissance missions. (http://www.geerassociation.org/about-geer/goals, March 8, 2016). Thanks to Prof. Kieffer, I had the opportunity to become a member of the first team that visited Nepal from May 6th to May 12th. Goal of this trip was to "start a broad initial assessment of the earthquake's effects". (Hashash et al. 2015) The idea for this thesis emerged during our stay in Nepal, and it shall be a contribution to future landslide risk assessment. The aim is to statistically analyze and plot the landslides triggered in Sindhupalchok, which was one of the most badly affected districts of Nepal.

As this is an event-inventory, it is only a snapshot displaying the impact of the earthquake, not any previous or following events.

The thesis is subdivided into the following chapters:

1. The ***Introduction*** informs on background and aim of this thesis
2. ***Background and Research*** gives a short geographical, geological and seismological overview of Nepal.
3. ***Study area*** gives an overview of the district Sindhupalchok
4. ***Methods*** starts with a brief description of the used software, followed by an explanation of all landslide parameters.

5. In ***Results and Interpretation***, the trends and connections of all parameters are shown and described. Some of the inventory maps are integrated for better understanding of the discussed results. The effects of the monsoon are described briefly at the end of this chapter.
6. ***Conclusion*** summarizes the main goals and findings of this research, and gives some recommendations for future research.
7. ***References***
8. Further inventory maps and graphs are shown in the ***Appendix***.

2. Background and Research

2.1 Geographical and Geological Overview of Nepal

The Federal Democratic Republic of Nepal is located in South Asia, within the Himalayan arc, between China (in the north) and India (in the south) (Figure 1). About 80% of its area is characterized by mountainous terrain of the Himalaya. This orogeny developed due to the collision of the Indian and the Eurasian plate, which started about 50 Ma ago (Figure 2). It is the country with the highest relative relief (Figure 4), ranging from 64 m to 8848 m above sea level, both within an aerial distance of about 150 km (Dhital 2014).

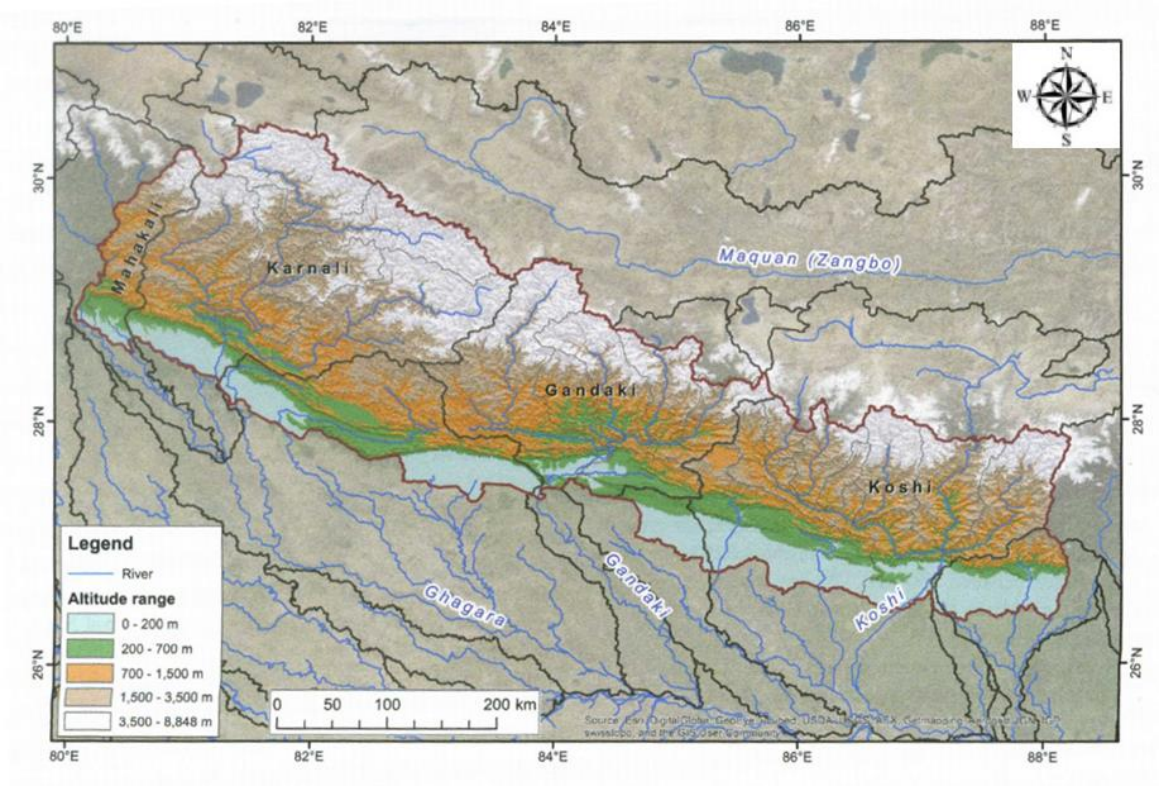

Figure 1 Map of Nepal (Source: Dhital 2014)

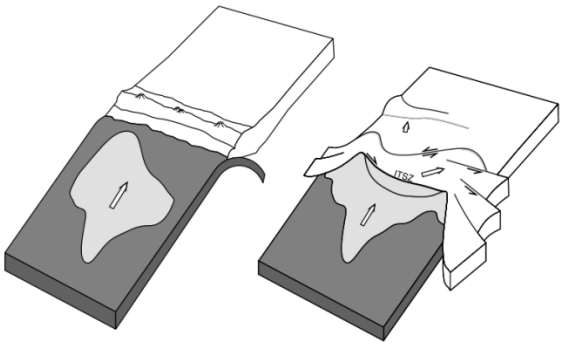

Figure 2 Indentation of India into Eurasia (Source: Avouac 2003)

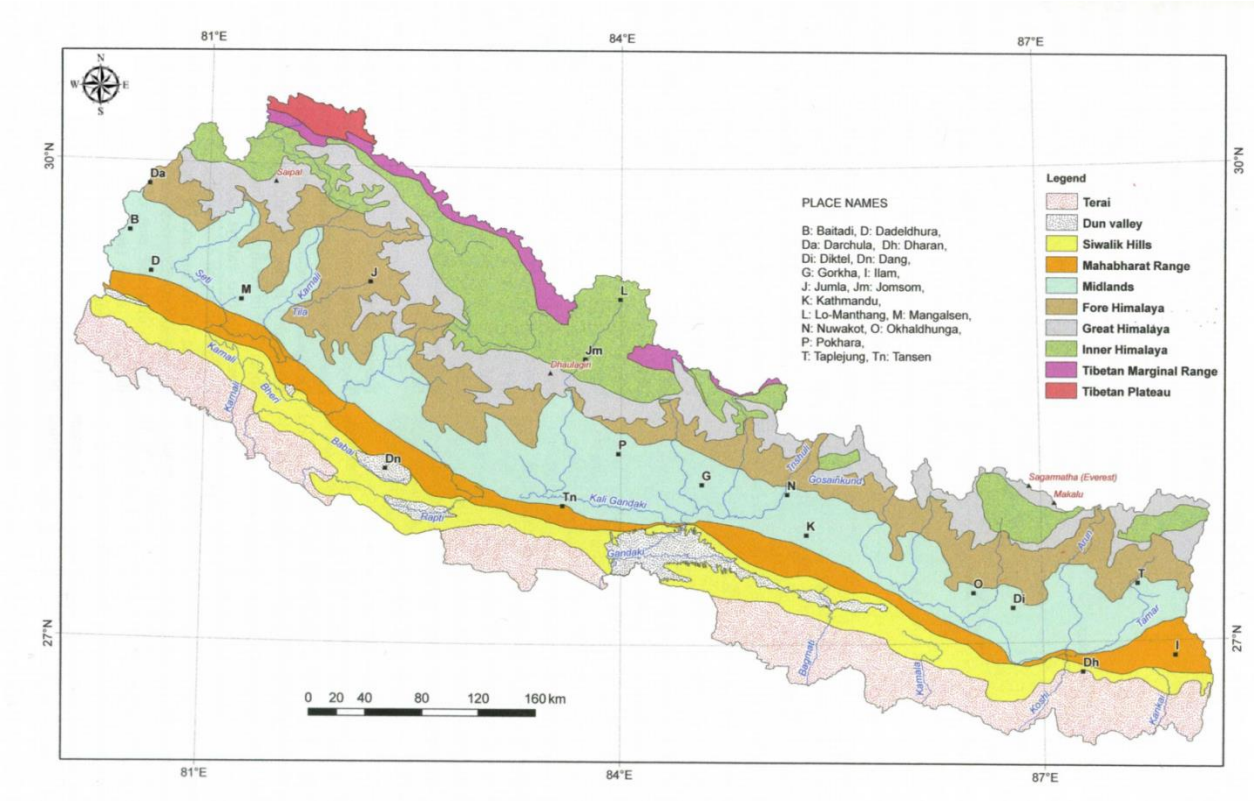

Figure 3 Physiograpic divisions of Nepal. (Source: Dhital 2014)

Hagen (1969) divided Nepal into the following physiographic subdivisions (Figure 3, Figure 4):

- Terai

This plain landscape is situated in the southern part of Nepal, between the Siwalik Range and the Indo-Gangetic Plain, and is covered with Pleistocene to Holocene sediments. It slopes towards the south and its height ranges from 100 to 200 m above sea level. The Terai is subdivided into three zones from south to north: Gangetic Alluvium, Marshy Land and Bhabar Zone. While the upper Terai zones are covered with coalescing alluvial fans made up of coarse sediments, the lower zones are composed of the finer grained sediments of the Gangetic Alluvium (Dhital 2014).

- Siwalik Range

The Siwalik Range, also known as the Sub-Himalaya, is the first topographic rise north of the Terai and consists of two or more ridges which are converging and diverging at different places. In between lie the wide “dun” valleys with altitudes of 100 to 700 m. The width of the Siwaliks decreases from 20 km at Nepal’s western border to less than 1 km in the eastern part, with some broader zones in between where the dun valleys are situated. The

topography is dominantly controlled by tectonic processes. This is shown by many parallel and rectangular drainage patterns, which reflect the bedding and joint planes, whereas centripetal and radial patterns are characteristic for synclinal and anticlinal cores. Another landscape affecting factor is the precipitation, as erosion and deposition of the soft and loose Siwalik strata result in the formation of gorges, rugged hills and alluvial fans (Dhital 2014). The Siwaliks are geologically delineated by the Himalayan Frontal Thrust in the south and the Main Boundary Thrust in the north. Their clastic sediments originate from the uplift and subsequent erosion of the Himalayas, and have been transported and deposited by streams and rivers. (Wilson, Wilson)

- Mahabharat Range

Further to the north lies the Mahabharat Range, which is separated from the Siwaliks by the Main Boundary Thrust and rises up to 3000 m. Apart from two major rivers (Karnali and Gandaki) which cut deep gorges through the Mahabharat Range, all other streams coming from the north are deflected to the east or west. Geologically, the Mahabharat Range is part of the Lesser Himalaya (Wilson, Wilson), although it comprises both Lesser and Higher Himalayan rocks. The central part, which extends between the Karnali and the Gandaki, exhibits sedimentary or slightly metamorphosed sequences, whereas the eastern and western part consist of metamorphic and crystalline rocks (Dhital 2014). These high-grade metamorphic rocks once slid on the Main Central Thrust and overlay the Lesser Himalaya, but with time most of these rocks were eroded and only some remnants have been left. (Molnar 1986)

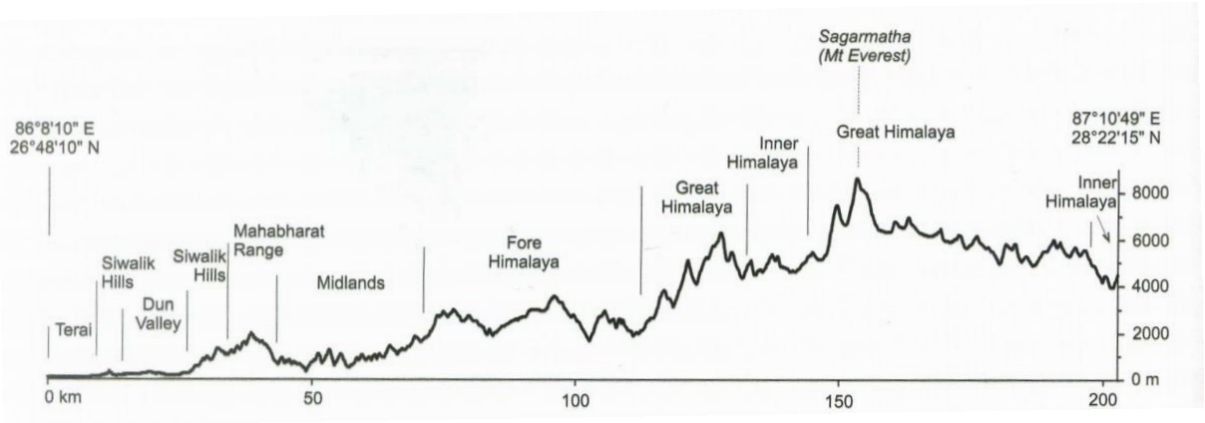

Figure 4 Profile of the Himalaya through east Nepal and position of physiographic regions. (Source: Dhital 2014)

- Midlands

Located between the Mahabharat Range and the Himalayan Mountain Ranges the midlands accommodate most of the densely populated areas in Nepal. Geologically, they are constituted of sedimentary, low-grade metamorphic and crystalline rocks, which are generally covered with alluvial, colluvial and residual soils. Due to constant channel shifting and vertical incision of the rivers, alluvial terraces are formed, which are used for agriculture. The very characteristic red soil of the midlands (Figure 5) emerges due to the humid subtropical climate, which benefits the oxidation of iron-containing minerals. (Dhital 2014)

- Fore Himalaya

The transition zone between the Midlands and the Great Himalaya is defined by an average altitude of 3000 m and lies within the crystalline thrust sheets and its surrounding valleys (Dhital 2014).

Figure 5 Red soil and morphology of the Midlands (© Ziselsberger); 27°51'51.02"N, 85°9'9.77"E

- Great Himalaya

The Great or Higher Himalaya is a discontinuous mountain range with altitudes exceeding 8000 m. It is composed of several subranges, and some massive transverse gorges cut through it from north to south. The Higher Himalaya consists of metamorphic and crystalline rocks (Himal Group) which are overlain by sedimentary rocks. It is separated from the Lesser Himalaya by the Main Central Thrust.

Its south facing slopes are generally shorter and steeper than those on the northern side. The morphology is controlled by glacial and fluvial processes, by precipitation and wind, and also by mass wasting processes like rock avalanches and rockslides. (Dhital 2014)

- Inner Himalayan Valleys

These areas are situated between the Great Himalaya and the Tibetan Marginal Ranges and are characterized by flat plains and deep gorges (Dhital 2014). Some of the Inner Himalayan Valleys are part of the Tethyan Himalayan sequence, which is located south of the Indus-Tsangpo suture zone. It consists of marine sediments that were deposited onto the Indian shelf before the subduction started. (Molnar 1986)

- Tibetan Marginal Ranges

The Tibetan Marginal Ranges are confined by the Inner Himalayan Valleys to the south and the Tibetan Plateau to the north. The major rivers flowing through the Himalaya towards India have their origin in these regions. (Dhital 2014)

2.2 Seismic Overview

The Indian plate moves northwards at a speed of 40-50 mm/year and is subducted under the Eurasian plate, which leads to recurring earthquakes (Figure 2). Nepal lies within this seismically active zone and has been hit by several devastating earthquakes in the last centuries (Bilham 1995; Avouac 2003; Hashash et al. 2015):

- 1255: Oldest known event with an estimated magnitude of M_L 7.8
- 1505: M_W 8.2 Central Himalayan Earthquake
- 1833: Two main shocks within one day with magnitudes between M_W 7.2 and 7.7
- 1934: M_S 8.1 Nepal-Bihar Earthquake.[1]

Nepal-Gorkha Earthquake 2015

"The M_w 7.8 Gorkha earthquake occurred on April 25, 2015 at 06:11:26 UTC at 28.1473 N latitude and 84.7079 E longitude with a hypocentral depth of 15 km." (Hashash et al. 2015)

The hypocenter lay on or close to the main frontal thrust, which is a highly active fault system. The fault rupture extended from the southern end of the earthquake in 1505 to the northern edge of the earthquake in 1934 (Hashash et al. 2015). Five aftershocks with M_w larger than 6.0 followed the main shock, "one of which was a M_w 7.3 event that occurred on May 12, 2015 approximately 140 km east of the main shock epicenter." (Hashash et al. 2015)

[1] There are different magnitude scales used to describe the intensity of an earthquake (http://www.usgs.gov/faq/categories/9828/3357, March 7, 2016):

1. Richter scale (M_L): A logarithmic scale to compare the size of earthquakes, developed by Charles Richter in 1935. As this method is only valid for certain frequency and distance ranges, it is also known as local magnitude scale (M_L).
2. Body wave magnitude (M_b), Surface wave magnitude (M_s): Extensions to the Richter scale, but also only valid for particular frequency ranges.
3. Moment magnitude (M_w): This scale gives the most reliable results for very large earthquakes.

2.3 (Remote Sensing) Landslide Mapping

Landslides are downslope movements of rock, debris or soil which can be triggered by extensive rainfalls, snow melting, earthquakes, volcanic activities or human actions. “Slope failures are the result of the interplay of physical processes, and mechanical laws controlling the stability or failure of a slope.” (Guzzetti et al. 2012) Mass movements leave morphological signs, which are characteristic for the type and the rate of motion. Furthermore, they change the land cover, which modifies the optical properties of the surface. These signs are useful for recognizing landslides in the field or on aerial/satellite images (Guzzetti et al. 2012).

There are several types of landslide maps for different purposes, like hazard, risk or zone maps. Inventory maps are the basis for following map products, as they show the occurrence, extent and activity (active/historic/dormant) of prior landslides. Recognizing past slope failures is important, as landslides tend to occur where something happened before (Kieffer 2015).

Remote sensing techniques can reduce the required time and resources for the compilation of a landslide inventory, especially when covering bigger areas. “Selection of a specific technique depends on the purpose of the inventory, the extent of the study area, the scale of the base maps, the scale and resolution and characteristics of the available imagery.” (Guzzetti et al. 2012)

2.4 Existing data on landslide occurrence after the M_W 7.8 earthquake

"The highest areal densities of landslides are developed on the downdropped northern tectonic block [Figure 6], which is likely explained by momentary reduction of the normal stress along planes of weakness during downward acceleration. Within this block, landslide densities increase southward and then abruptly decrease near the tectonic hinge line, which separates the downdropped and upthrown blocks." (Kargel et al. 2016)

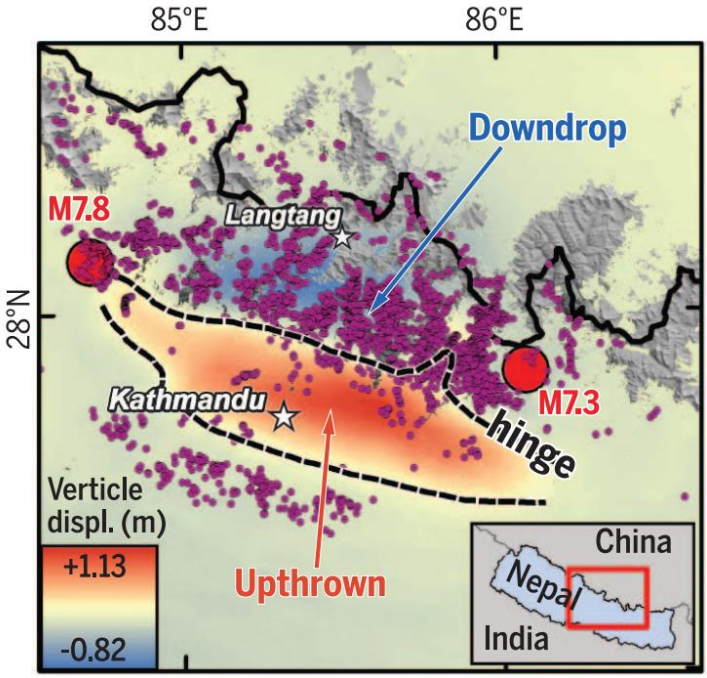

Figure 6 Landslides (purple dots) are concentrated mostly north of the tectonic hinge line (Source: Kargel et al. 2016)

According to Keefer (2002), the areal extent of landslides caused by an earthquake can be estimated with Equation 1 for magnitudes > 5.5 and ≤ 9.2.

Equation 1 Areal extent of landslide occurrence (according to Keefer (2002)):

$$log_{10} A = M - 3.46\ (\pm 0.47)$$

A = affected area [km²]

M = magnitude

Therefore, the areal extent of landslide occurrence due to the M_W 7.8 Nepal-Gorkha earthquake should be between 7000 km² and 65 000 km². Kargel et al. (2016) state that an area of 550 by 200 km (about 110 000 km²) was severely damaged by the earthquake, but no exact size of

affected area is given. Figure 7 shows the relation between area affected by landslides and earthquake magnitude (according to Keefer (2002)).

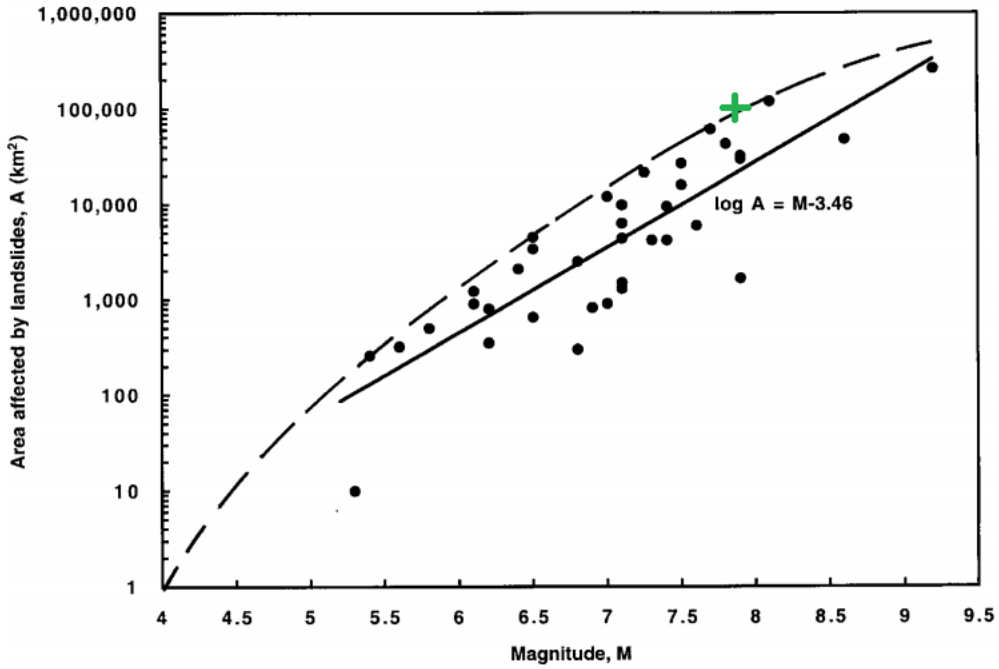

Figure 7 Relation between area affected by landslides and earthquake magnitude. Solid line is upper bound of Keefer (1984), dashed line is upper bound of Rodriquez et al. (1999) (Source: Keefer (2002)). Green cross indicates Nepal-Gorkha earthquake.

3. Study area

3.1 Sindhupalchok

Sindhupalchok is one of the seventy-five districts of Nepal and lies within the Central Development Region (Figure 8). It is located northeast of Kathmandu, and the only road that links Nepal to Tibet (China) is passing through it. Sindhupalchok extends over more than 2500 km² and can be divided into two morphologically different parts: the northern mountainous region with altitudes exceeding 3500 m, and the more densely populated, hilly terrain in the south. (OSOCC 2015; http://www.statoids.com/ynp.html, March 7, 2016)

Figure 8 Sindhupalchok, Central Development Region, Nepal (Source: https://de.wikipedia.org/wiki/Sindhupalchok#/media/File:Sindhulpalchok_district_location.png)

4. Methods

In this work, the terms “landslide”, “mass movement”, and “slope failure” are used as synonyms, as well as “inventory” and “landslide map”.

4.1 Google Earth Pro (GEP)

Google Earth Pro is an open source geographical information program where satellite and aerial images are projected onto a virtual globe. For the coordinate system the geographical coordinates of the World Geodetic System of 1984 (WGS84) are used. The underlying digital elevation model (DEM) originates from NASA’s Shuttle Radar Topography Mission (SRTM), and has a spatial resolution of 30 meters. There are several tools to display and map features, like a ruler to measure distances or areas.

By comparing pre- and post-earthquake images fresh and reactivated mass movements were located (Figure 9, Figure 10). Up-to-date images of the affected areas in Nepal were available within a few days after the earthquake to help relief organizations. The imagery covering the study area was provided by DigitalGlobe and CNES/Astrium[2]. After determining all identifiable landslides, several other parameters were recorded: size, length, width, slope relief, landslide relief, slope aspect and affected infrastructure (roads, houses, villages).

Figure 9 Before (left) and after (right) April 25 M7.8 earthquake, 27°52'3.57"N, 85°39'5.41"E (Source: Google Earth)

[2] DigitalGlobe operates four commercial earth imaging satellites (WorldView (1, 2 and 3) and GeoEye-1) and is a global provider of high-resolution satellite images (DigitalGlobe). CNES (Centre national d’études spatiales) is the French government space agency.

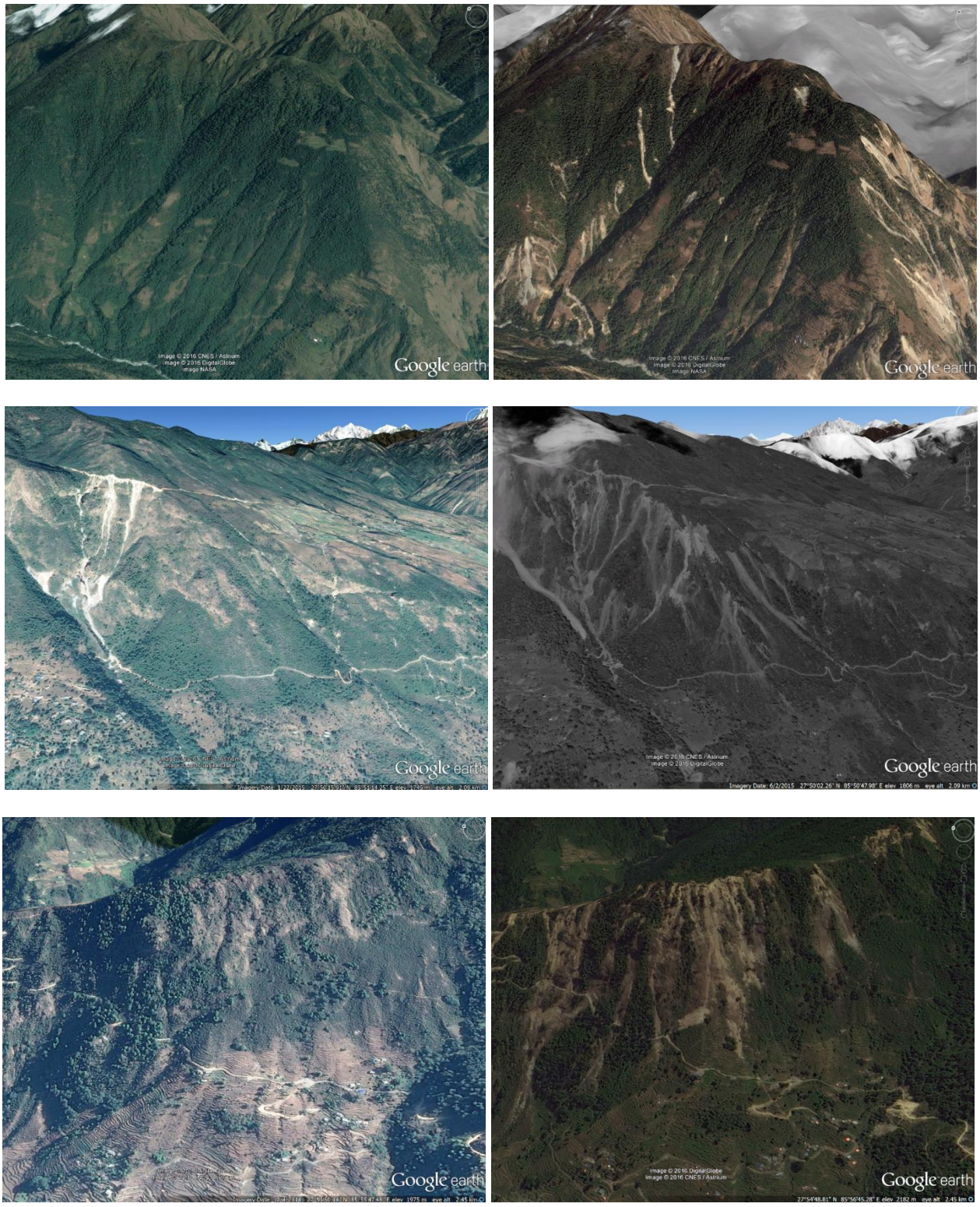

Figure 10 Before (left) and after (right) April 25 M7.8 earthquake (Source: Google Earth):
top (28° 1'7.70"N, 85°39'42.38"E), middle (27°50'23.76"N, 85°50'59.28"E), bottom (27°53'50.14"N, 85°55'47.48"E)

4.1.1 Limitations

Due to differing quality of the satellite images, not all landslides could be clearly identified and/or measured. These quality differences are caused by several factors like radiometric resolution, distortion and weather effects (clouds).

4.1.2 Completeness of the inventory

"A formal definition of completeness requires that a landslide inventory includes all landslides associated with a landslide event (a single trigger). This definition assumes that all landslides are visible and recognizable, and that the entire study area affected, even marginally, by the trigger(s) is fully and thoroughly investigated. A functional definition of completeness requires that the landslide inventory includes a substantial fraction of all landslides at all scales. A substantially complete inventory must include a substantial fraction of the smallest landslides." (Malamud et al. 2004) Although definitely not all triggered landslides could be identified, the documentation was done in all conscience.

4.2 Microsoft Excel 2010

The spreadsheet MS Excel was used as database for the recorded data (Appendix: Figure 1) and to calculate parameters like slope relief, slope angle and aspect ratio. Further on, statistical analysis and plots were made by using Excel's functions.

4.3 Quantum GIS Lyon (QGIS)

QGIS is an open source geographic information system to display, edit and analyze geographical data. It was used to calculate new information (e.g. altitude), combine different parameters (slope angle and aspect) and finally to create the inventory maps.

4.4 RoboGEO

The software RoboGEO was used to geocode the photographs by synchronizing these with the GPS track logs. Thereby latitude, longitude and altitude were added to the image's EXIF data.

4.5 Field Reconnaissance

After the initial reconnaissance in May 2015, a second phase of reconnaissance field work took place in October 2015. Kathmandu and the districts Sindhupalchok, Nuwakot, Rasuwa and Dhading were visited (Figure 11). The aim of this work was to observe the landslide affected areas (Figure 12, Figure 13) and examine the effects of the monsoon (Figure 14 and Chapter 5.15 Field observations).

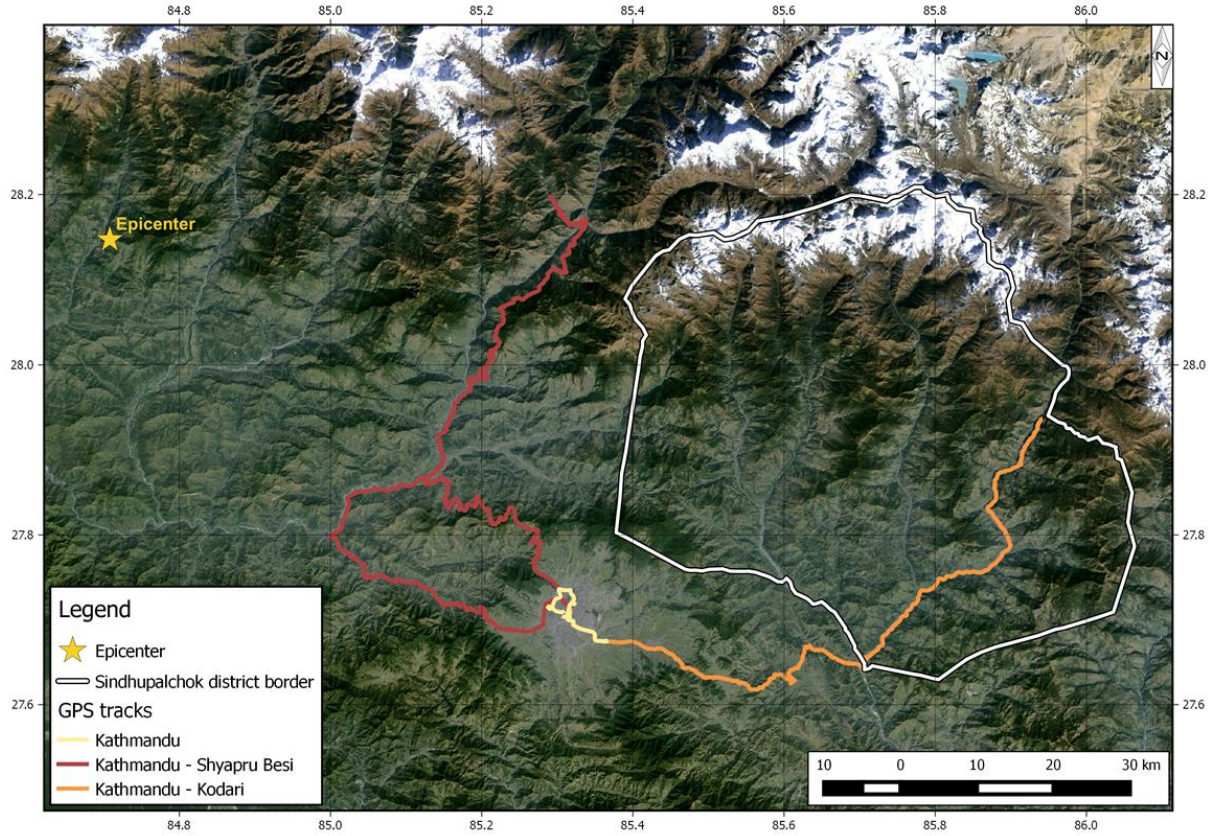

Figure 11 GPS tracks: yellow: Kathmandu, orange: Sindhupalchok, red: Nuwakot, Rasuwa, Dhadin (© Ziselsberger; Basemap: Google Earth Image)

Figure 12 Google Earth screenshot (top; Source: Google Earth) vs. on the ground taken photograph (bottom; © Ziselsberger). 28°2'28.75"N, 85°13'11.80"E

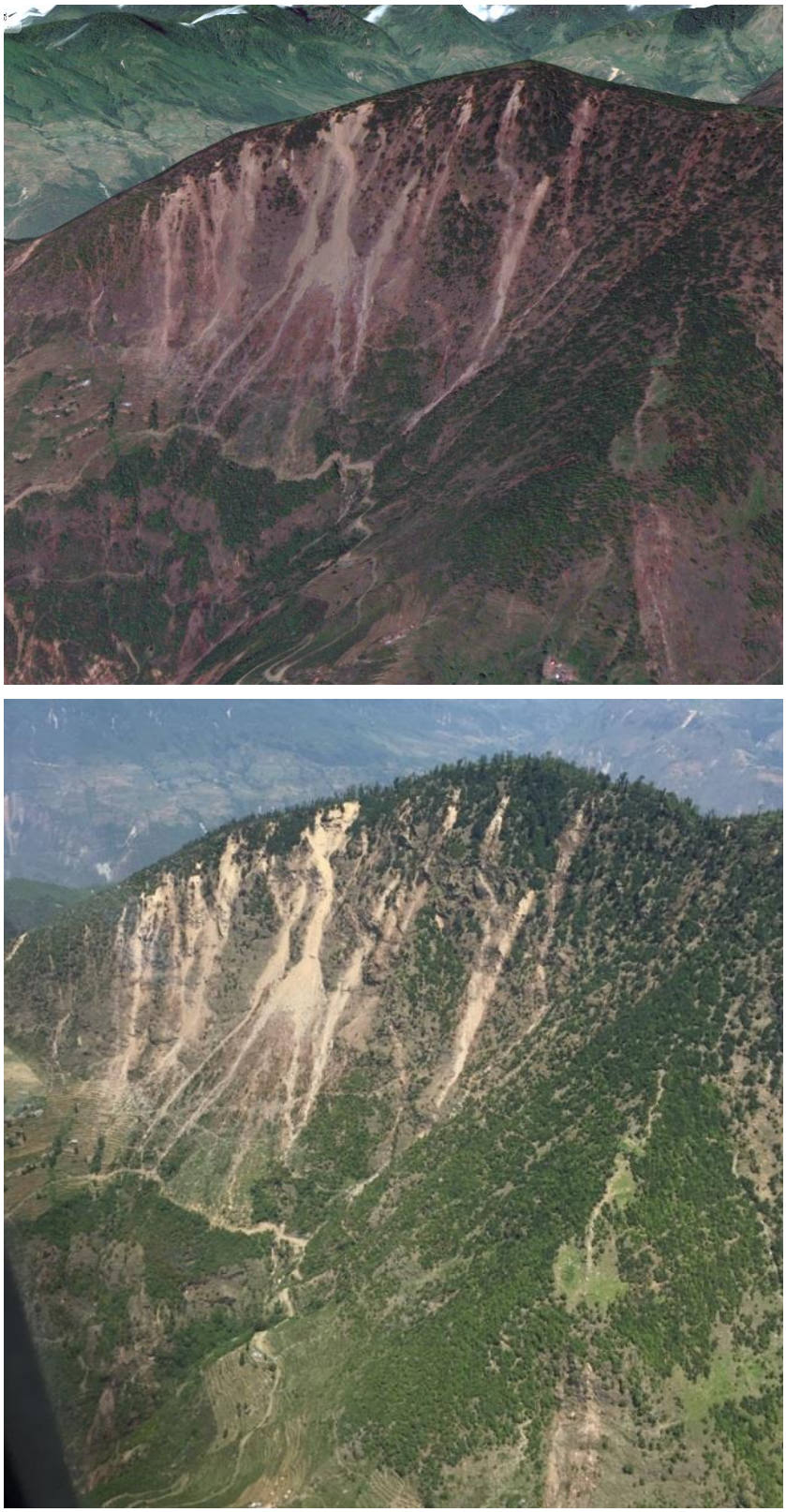

Figure 13 Google Earth screenshot (top; Source: Google Earth) vs. photograph taken in the helicopter (bottom; © Pehlivan). 27°49'25.00"N, 85°55'47.00"E

Figure 14 Before (top) and after (middle) April 25 M7.8 earthquake, and after the monsoon (bottom). 27°57'49.22"N, 85°32'25.20"E (Google Earth)

4.6 Landslide Attributes from Satellite Imagery

4.6.1 Landslide area

As can be seen in Figure 15, a polygon is drawn with Google Earth's ruler tool along the landslide's outline. The resulting surface area is given in square meters.

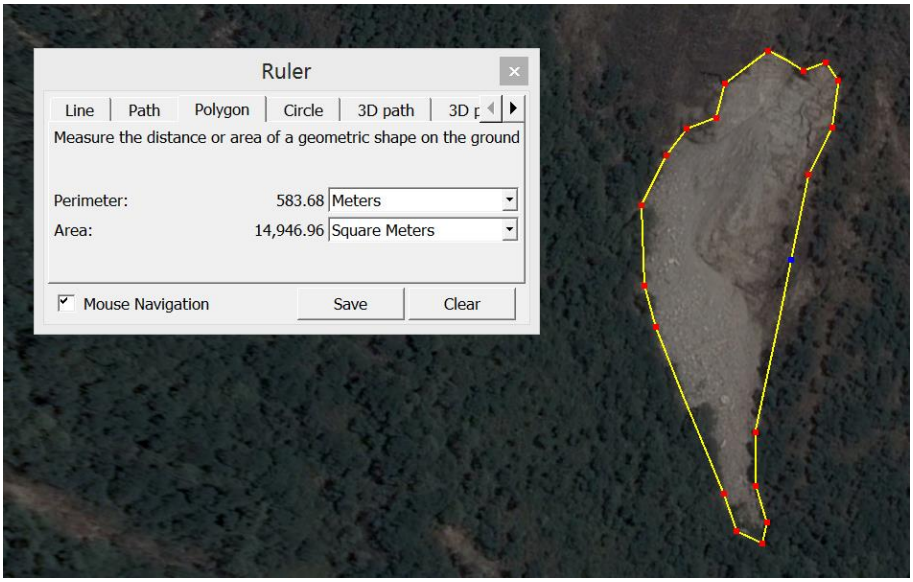

Figure 15 Polygon measurement of landslide with Google Earth Pro (28° 1'19.99"N, 85°40'25.94"E; Source: Google Earth)

4.6.2 Length and width

For further calculations (see 4.6.3 Aspect ratio), the length and width of each landslide were measured. Another option of the ruler tool was used which gives two different length measurements: "Map Length" is the horizontal distance between two points, whereas "Ground Length" is the slope distance between two points (Figure 16, Figure 17).

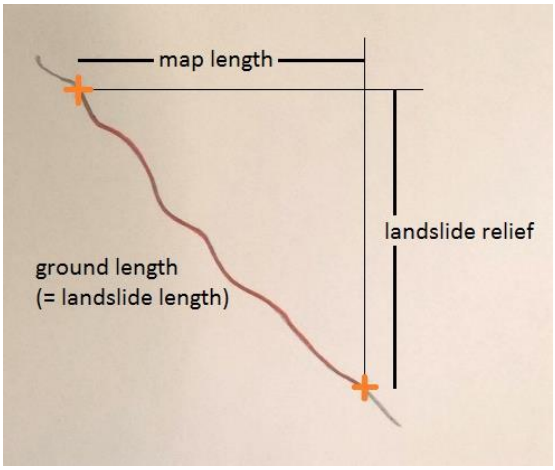

Figure 16 Sketch of map length, ground length and landslide relief (© Ziselsberger)

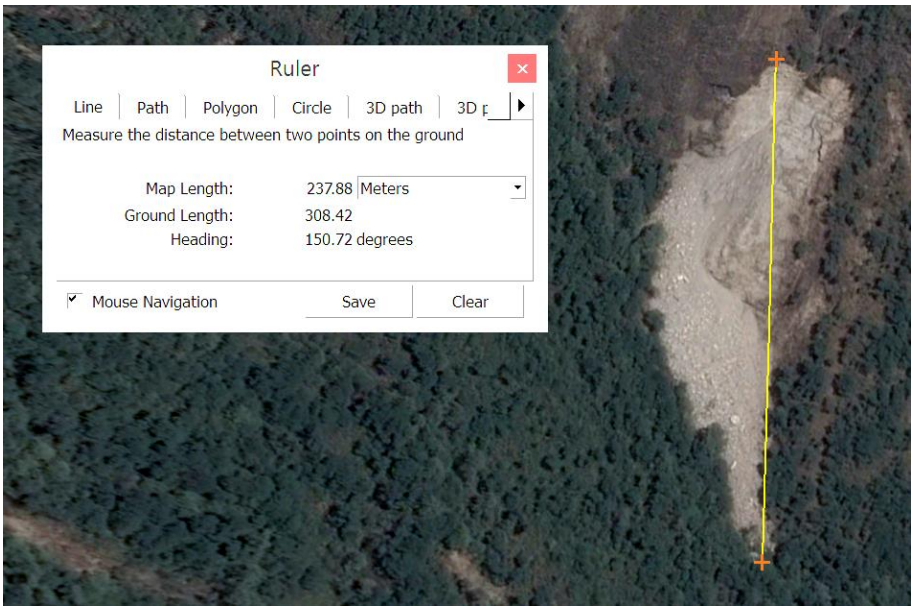

Figure 17 Vertical distance measurement (yellow line) = map length of landslide (Source: Google Earth)

Due to aberrations of the given ground lengths, the map length was used to approximately calculate the landslide length (Equation 2). The results were rounded to the nearest multiple of ten.

Equation 2 Ground length

$$\boldsymbol{ground\ length_{ls}}\ [\boldsymbol{m}] = \sqrt{(\boldsymbol{landslide\ relief})^2 + (\boldsymbol{map\ length})^2}$$

The $width_{ls}$ of each landslide was measured (Figure 18) and rounded to the nearest multiple of ten.

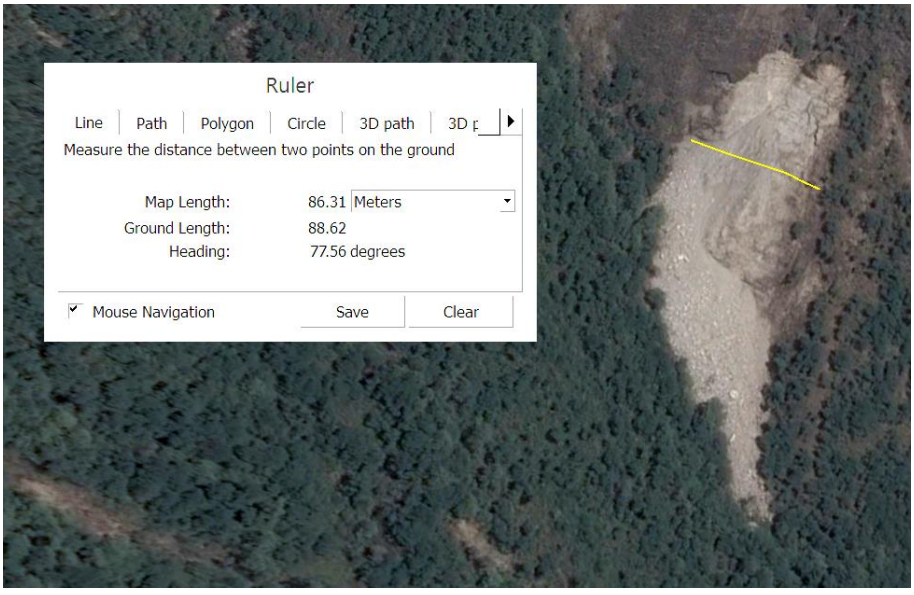

Figure 18 horizontal distance measurement (yellow line) = width of landslide (Source: Google Earth)

4.6.3 Aspect ratio

The aspect ratio describes the width-to-length relationship (Equation 3) of a landslide, indicating its shape (Figure 19).

Equation 3 Aspect ratio

$$aspect\ ratio\ = \frac{width_{ls}\ [m]}{length_{ls}\ [m]}$$

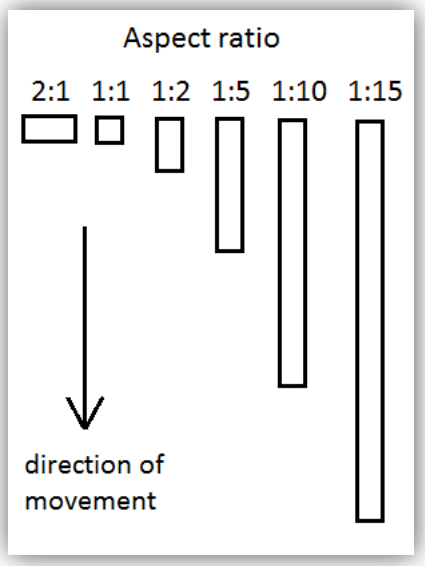

Figure 19 Aspect ratio sketch (© Ziselsberger)

4.6.4 Slope angle

The slope angle expresses the steepness of a mountain slope. First, it was calculated with Excel (Equation 4), and then for comparison computed from an 1-arc-second DEM (http://srtm.usgs.gov/index.php, March 7, 2016) with QGIS.

Equation 4 Slope angle

$$slope\ angle\ [°] = degrees\left(tan^{-1}\frac{map\ length}{landslide\ relief}\right)$$

The steepness is one key parameter in slope stability, especially when loose, cohesion less materials accumulate on a hillside.

4.6.5 Slope aspect

There are several factors which can influence the stability of a slope, and they often vary for different slope aspects. Rain and temperature play an important role, especially in mountainous regions, as they are key parameters of weathering processes and soil development.

The slope aspect (Table 1) of each landslide was estimated during the acquisition with Google Earth, and later on computed with QGIS for comparison. Furthermore, the distribution of slope aspects within the whole study area was calculated.

Table 1 Slope aspect classification

Degrees	Aspect
337.5° - 22.5°	North (N)
22.5° - 67.5°	Northeast (NE)
67.5° - 112.5°	East (E)
112.5° - 157.5°	Southeast (SE)
157.5° - 202.5°	South (S)
202.5° - 247.5°	Southwest (SW)
247.5° - 292.5°	West (W)
292.5° - 337.5°	Northwest (NW)

4.6.6 Slope and landslide relief

"Slope relief" is the height difference between the top and the toe of a slope (Figure 20, Figure 21), whereas "landslide relief" is the height difference between the uppermost and the lowermost point of a landslide (Figure 16, Figure 20, Figure 21).

Figure 20 Height measurement points: slope relief (yellow stars) and landslide relief (orange crosses) (Source: Google Earth)

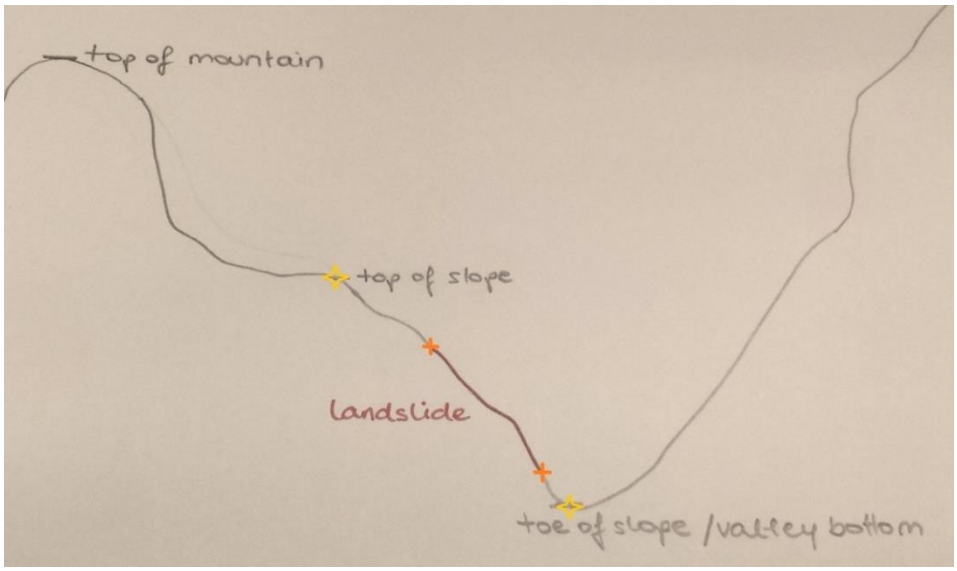

Figure 21 Sketch of valley cross section with height measurement points for slope and landslide relief (© Ziselsberger)

4.6.7 Affected infrastructure

Affected infrastructure – including houses, roads or pipelines – was documented whenever a landslide was responsible for the damage (Figure 22).

Figure 22 Village destroyed by a landslide, 27°55’08.95’’N, 85°54’52.64’’E (Source: Google Earth)

4.6.8 Landslide density

Landslide density describes the number of landslides within one square kilometer (circle with a radius of 564m). The data was computed with QGIS by creating a "heatmap", with the landslides' locations as input layer.

4.6.9 Altitude

The altitude of each landslide was extracted from the DEM (http://srtm.usgs.gov/index.php, March 7, 2016) by using the "point sampling tool" in QGIS.

4.6.10 Soil

Data concerning the soil cover of Nepal is publicly available from SOTER – Soil and Terrain Database of Nepal (http://www.isric.org/projects/soter-nepal, March 7, 2016).

4.6.11 Geology

The geological units were gathered from the Geological Map of Nepal (Amatya, Jnawali 1993) and the Geological Map of Central Nepal (Neupane). According to their description, the formations were merged into five groups (Table 2):

Table 2 Geological Formations

		Formation	Description
1	**Gneiss**	(Himal Group)	Gneisses, Shists, Quartzites
		(Ulleri)	Gneiss
		Gneiss	Gneisses
		Himal Group	Gneisses, Shists, Quartzites
		Ulleri	Gneiss
2	**Limestone**	Chandragiri	Limestones (fine grained crystalline)
		Lakharpata	Limestone/Dolomite, Shale
		Sangram	Shales, Limestone, Quartzite
3	**Quartzites, Phyllites**	Kushma	Quartzites, Phyllites
		Maksang	Quartzites
		Nautanda	Quartzites, Phyllites
		Ranimatta	Phyllites, Conglomerates, Quartzites
		Syanja	Quartzites (calcareous), Limestones (quartzitic), Shales
4	**Shists**	Sarung Khola	Schists
		Shiprin Khola	Schists (coarse crystalline)
		Tawa Khola	Schists (coarse grained)
5	**Slates**	Galyang	Slates
		Ghanapokhara	Slates (calcareous), Shales

4.6.12 Landcover

A publicly available dataset of Nepal's land cover is provided by the International Centre for Integrated Mountain Development (http://rds.icimod.org/Home/DataDetail?metadataId=9224, March 7, 2016). The data regarding Sindhupalchok was extracted from this dataset by using QGIS.

The original dataset was divided into ten different classes, which were merged into five groups in this study (Table 3).

Table 3 Land cover

1	Forest	Broadleaved closed forest
		Broadleaved open forest
		Needleleaved closed forest
		Needleleaved open forest
2	Sparse vegetation	Shrubland
		Barren area
3	Grassland	Grassland
4	Cultivated land	Agriculture area
5	Rest	Rivers
		Built-up area

4.6.13 Distance from the epicenter

The distance of each landslide from the epicenter was calculated with the spherical law of cosines (Equation 5) (Veness 2002-2016).

Equation 5 Law of cosines

$$d = \cos^{-1}(sin\varphi_1 * sin\varphi_2 + cos\varphi_1 * cos\varphi_2 * \cos\Delta\lambda) * R$$

d… distance [km]

φ_1… latitude 1 [rad]

φ_2… latitude 2 [rad]

Δλ… longitude 2 – longitude 1 [rad]

R… radius [km]

4.6.14 Drainage Basins

Five major rivers drain the district of Sindhupalchok: Indrawati, Sunkoshi, Bhotekoshi, Trishuli and Tama Koshi. There is a sixth drainage basin (Langtang Khola) shown in Figure 23, but no landslides were identified in this region due to a lack of new satellite images.

About 1090 km² are covered by Indrawati's drainage basin, followed by the catchment area of Sunkoshi, which extends over 740 km². On third place lies Bhotekoshi's drainage area with 690 km². The residual area of Sindhupalchok is drained by Trishuli in the northwest, Tama Koshi in the east and Langtang Khola in the north.

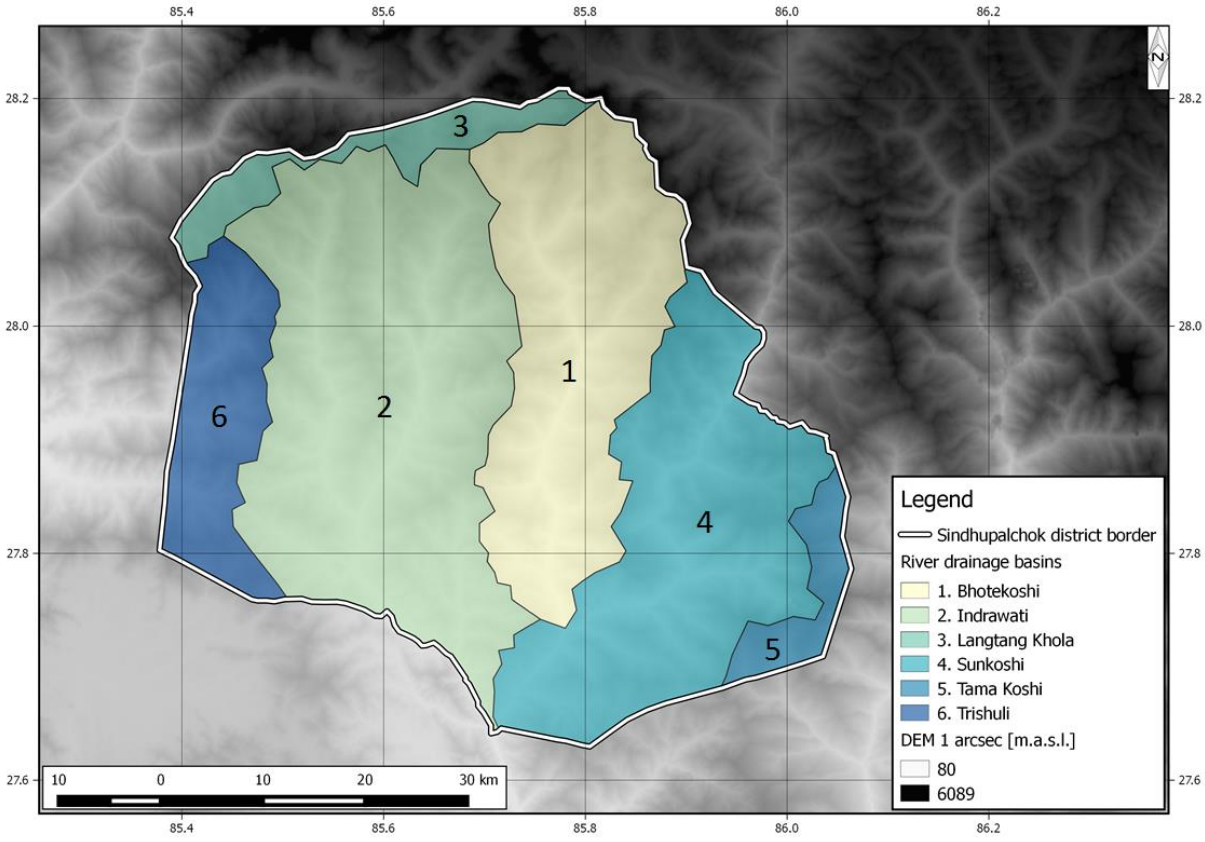

Figure 23 Map of main drainage basins in Sindhupalchok (© Ziselsberger; Basemap: SRTM DEM)

5. Results and interpretation

All numerical parameters were statistically analyzed in Excel, and the results can be seen in Table 4 .

The arithmetic mean is the sum of values divided by the number of landslides. The standard deviation quantifies the amount of variation of a set of data values. The bigger the standard deviation, the wider is the range of values. “Min”, “q1”, “Median”, “q3” and “max” are the quartile values, representing 0, 25, 50, 75 and 100% (Figure 24).

Table 4 Statistical analysis

	Landslide area [m²]	Landslide density [ls/km²]	Slope angle [°]	Slope aspect [°]	Slope relief [m]
Arithmetic mean	4579	5.7	34	166	394
Standard deviation	12075	6.2	10	83	289
min (0%)	10	1.0	5	0	3
q1 (25%)	553	2.0	28	108	183
Median (50%)	1532	4.0	35	159	326
q3 (75%)	4464	7.0	40	223	538
max (100%)	558055	52.0	89	360	2027
	Aspect ratio	**Landslide width [m]**	**Landslide length [m]**	**Altitude [m.a.s.l.]**	**DEPI [km]**
Arithmetic mean	0.31	32	174	1953	108
Standard deviation	0.34	31	193	652	12
min (0%)	0.01	5	10	645	71
q1 (25%)	0.12	10	50	1485	101
Median (50%)	0.22	20	110	1832	108
q3 (75%)	0.38	40	230	2315	117
max (100%)	6.00	400	3670	4295	139

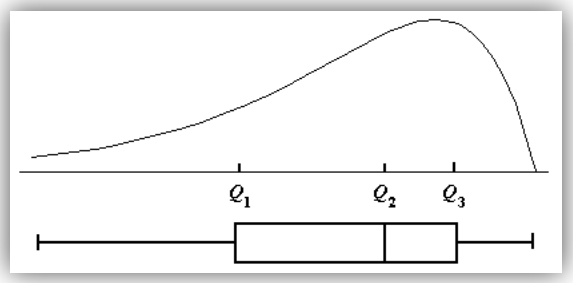

Figure 24 Quartile distribution (Source: https://onlinecourses.science.psu.edu/stat500/sites/onlinecourses.science.psu.edu.stat500/files/lesson02/left_skew.gif, March 7, 2016)

Plots (histograms, column charts, line charts, ...) and descriptions are shown in the following subchapters:

- Old, new and reactivated landslides
- Landslide area
- Aspect ratio
- Slope angle
- Slope aspect
- Slope relief
- Affected infrastructure
- Altitude
- Soil
- Geology
- Landcover
- Distance from Epicenter (DEPI)
- Drainage Basin (DB)
- Landslide density hotspots
- Field observations

5.1 Old, new and reactivated landslides

By comparing the satellite images taken before and after the earthquake, 6284 landslides were recorded in the Sindhupalchok district, 1143 of which are old (pre-earthquake), 1103 reactivated and 4038 new (Figure 25).

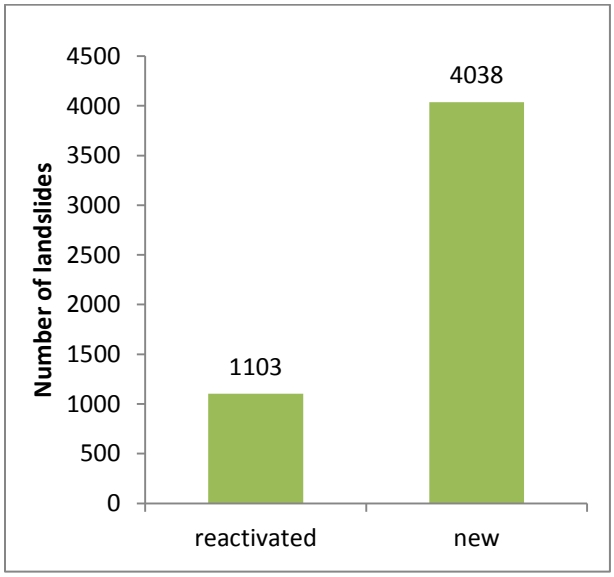

Figure 25 By comparing the satellite images taken before and after the earthquake 1103 reactivated and 4038 new landslides were recorded.

An empirical relation between the total number of former reported landslides and earthquake magnitude is shown in Figure 26 (from Keefer 2002). As the total number of landslides due to the Nepal-Gorkha earthquake is not known, only the number of landslides triggered in Sindhupalchok is indicated (green cross) in this Figure.

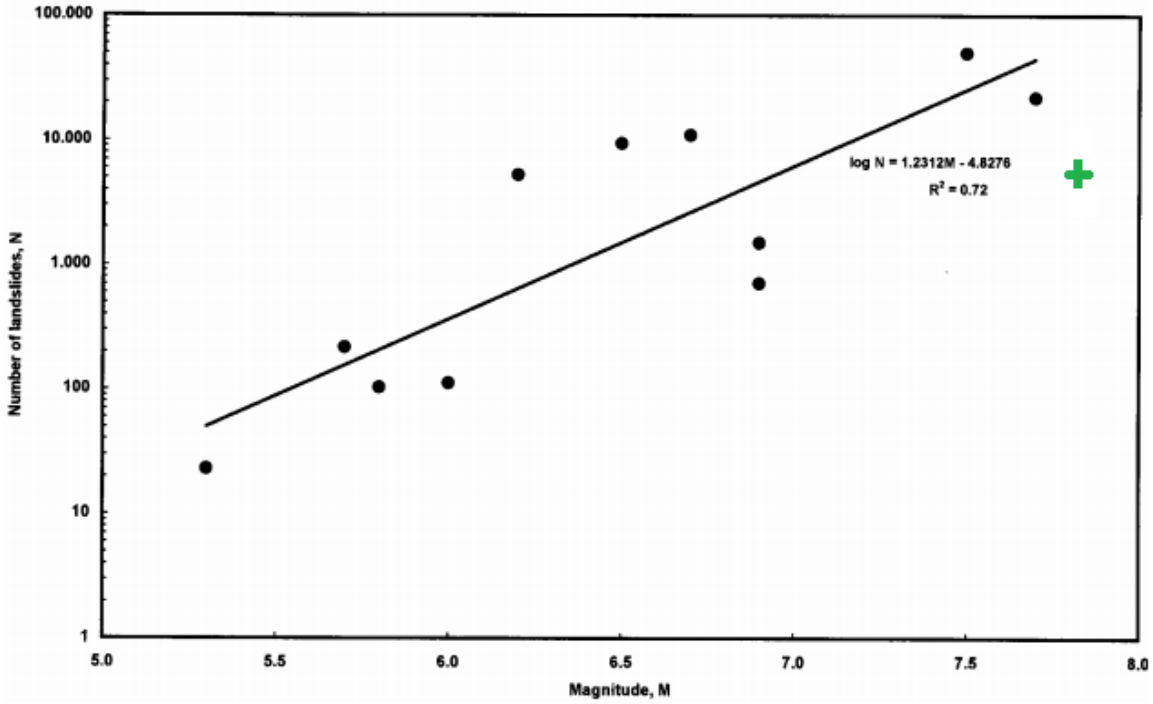

Figure 26 Empirical relation between total number of reported landslides and earthquake magnitude for earthquakes with comprehensive inventories of landslides (Source: Keefer 2002). Green cross depicts the number of landslides in Sindhupalchok due to the Nepal-Gorkha earthquake. Total number is not known.

Figure 27 shows an increase in reactivated landslides with rising landslide area. This trend might be caused by the fact that traces of former landslides are easier to identify, the bigger the landslides had been.

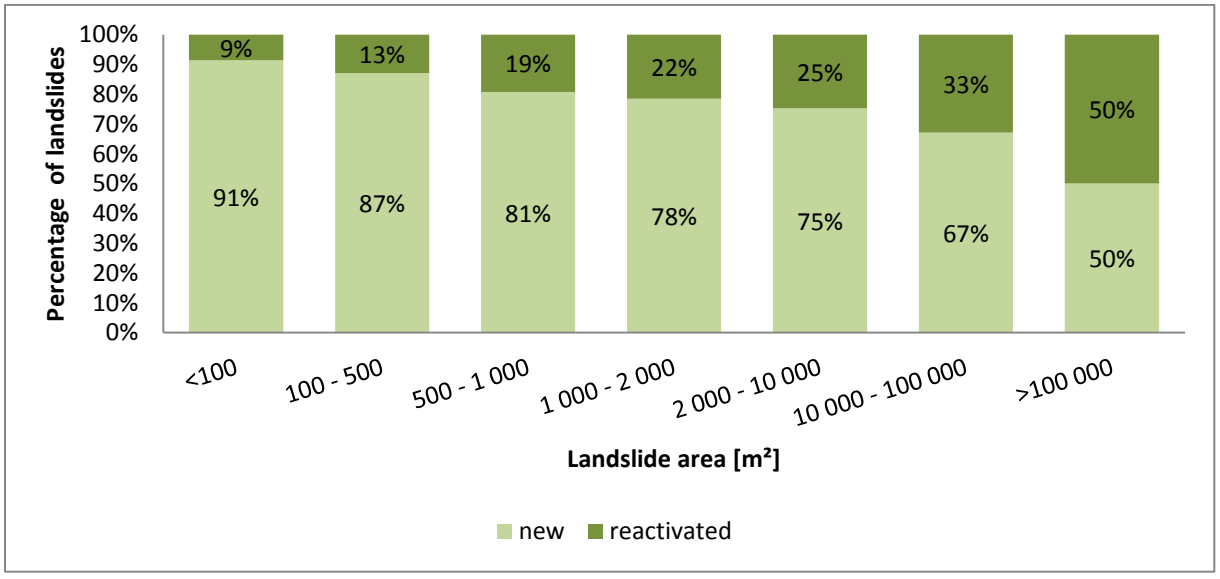

Figure 27 By comparing the size of new (light green) and reactivated (dark green) landslides, an increase in the number of reactivated landslides with rising area can be seen.

5.2 Landslide area

Landslide areas range from 10 m² to 558 055 m² with a median size of 1532 m² (Figure 28, red dashed line). As shown in Figure 28, the number of landslides increases up to a size of 200 m², which seems to be the resolution threshold (blue dash-dot line). This means that probably not all landslides smaller than 200 m² have been recorded due to bad image quality caused by distortion or weather effects (clouds).

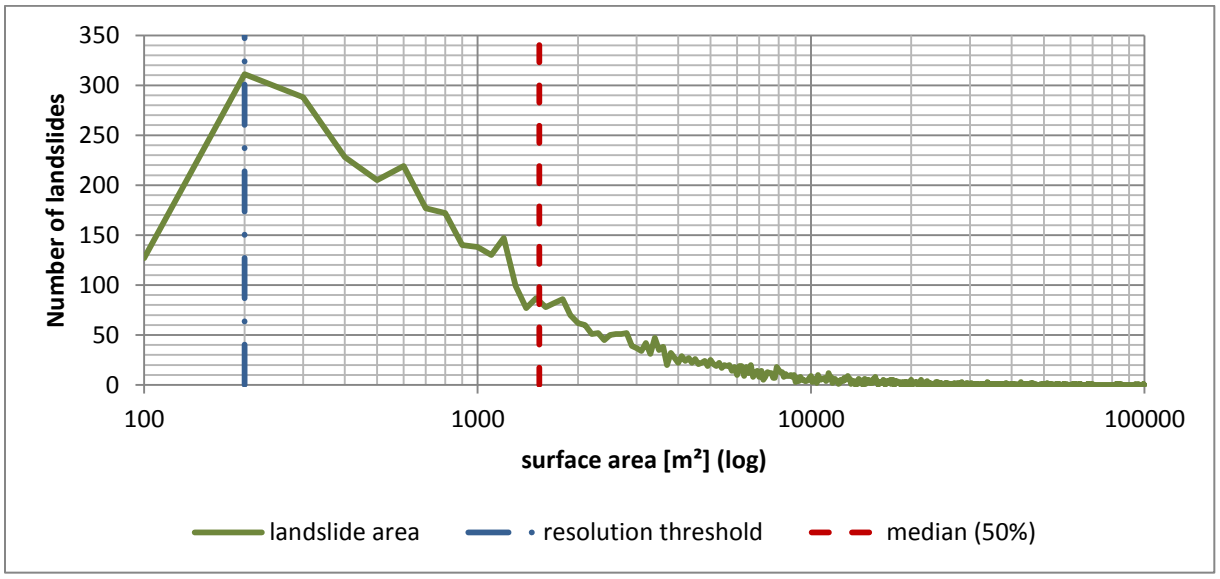

Figure 28 Distribution of landslides depending on the landslide area [m²], blue dashed line indicates resolution threshold

After the peak, the distribution shows a decrease in landslide occurrence which follows a power law regression of $\boldsymbol{y = 10^6 x^{-1.295}}$ (Figure 29, black line).

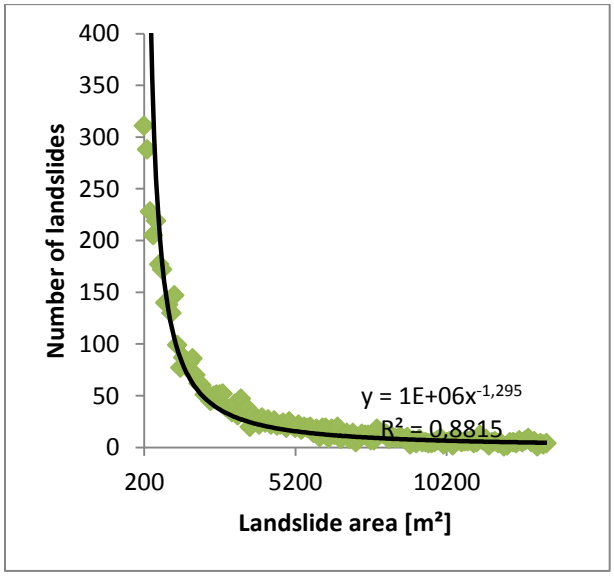

Figure 29 Power law regression for landslides with an area between 200m² and 13500m²

Figure 30 illustrates the percentage of landslide occurrence as a function of landslide area and altitude (given in meters above sea level). The higher the altitude, the longer the landslides get. Therefore, an increase of landslide areas can be seen from south to north (Appendix: Figure 3).

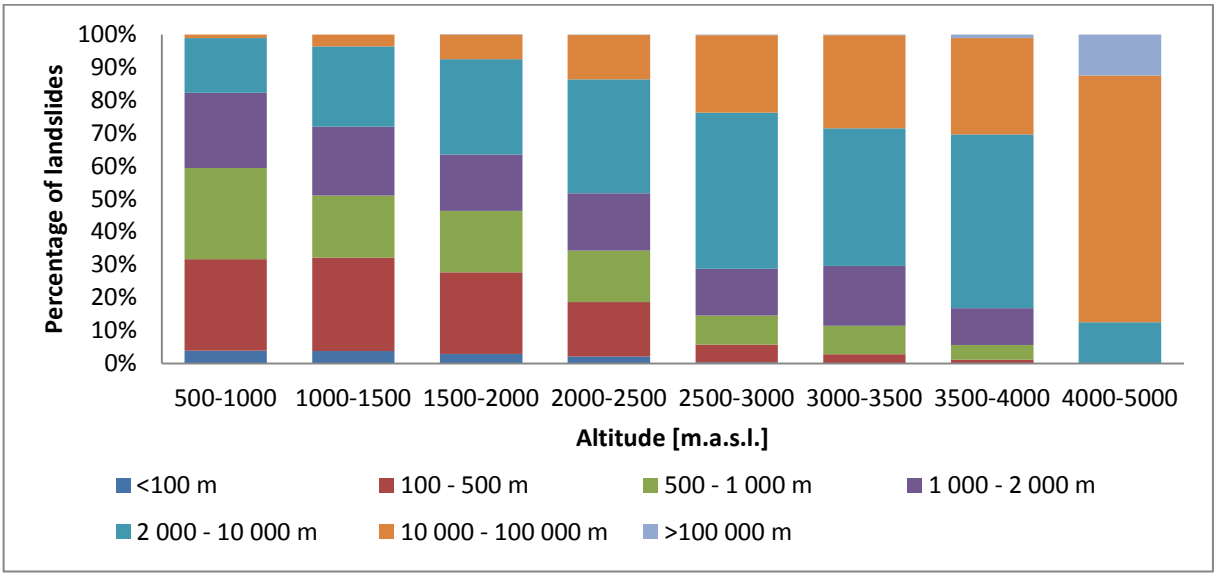

Figure 30 Percentage of landslide occurrence (y-axis) as a function of landslide area [m²] and altitude (x-axis).

5.3 Aspect ratio

Three quarters of all landslides have an aspect ratio between 1:9 and 1:1. Figure 31 depicts the steady rise from 1:100 to 1:3, with a short break between 1:9 and 1:7. After the distribution reaches the peak, it drops sharply. The same trend can be seen in Figure 32 where the aspect ratio is combined with the geological information of each landslide. The little anomaly in the limestone curve might explain the break in the aspect ratio histogram (Figure 31) between 1:9 and 1:7.

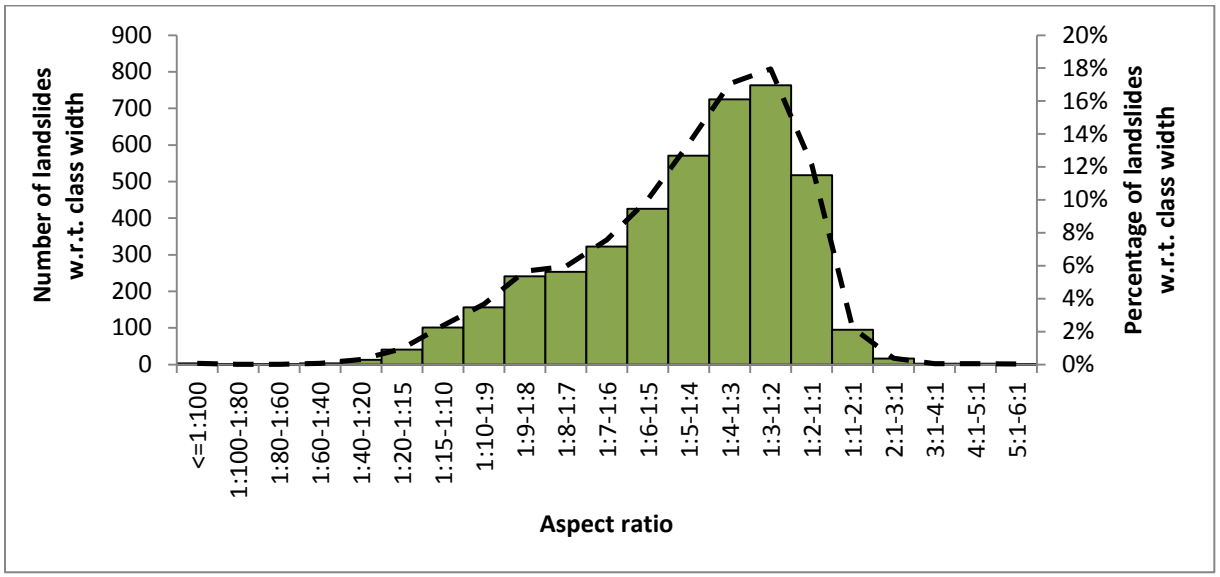

Figure 31 The aspect ratio histogram depicts the steady rise from 1:100 to 1:3, with a short break between 1:9 and 1:7. After the distribution reaches the peak, it drops sharply. The black dashed line represents the percentage of landslides with respect to the class width.

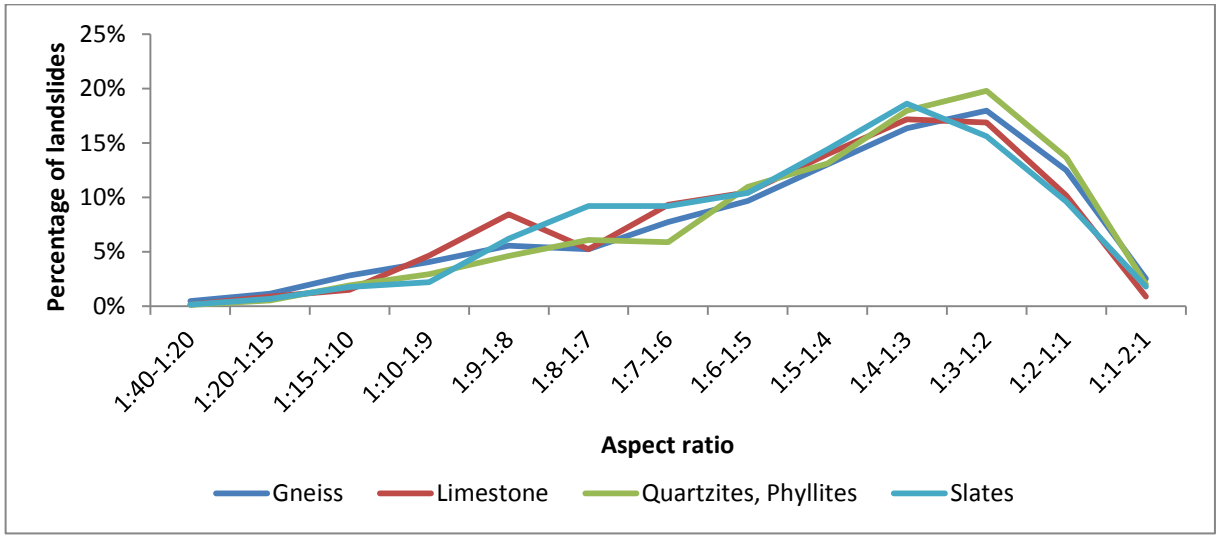

Figure 32 Geology vs. aspect ratio. The little anomaly in the limestone curve (red) might explain the break in the aspect ratio histogram (Figure 31) between 1:9 and 1:7.

5.4 Slope angle

Figure 33 shows the rate of landslides (green line) and the landslide density (black dashed line) in dependence of the slope angle. Compared to the normal distribution of landslide occurrence, the density is shifted to steeper angles and shows two breaks at about 50-55° and 60-65°. As listed in Table 4, 50% of the landslides happened on slopes with an inclination between 28° and 40°, the mean slope angle being 34°. Despite the fact that only 20% of Sindhupalchok's ground is steeper than 35° (Figure 34), almost 50% of all landslides occurred in these areas. Up to a slope angle of 25° the percentage of affected ground remains nearly the same, whereas the total area increases almost linearly. While the total area distribution decreases above slope angles of 25°, the percentage of affected terrain starts to rise from 25° to 45°. This trend is not surprising, as hillsides tend to get unstable with increasing steepness because friction is not strong enough to hold cohesionless materials back from sliding.

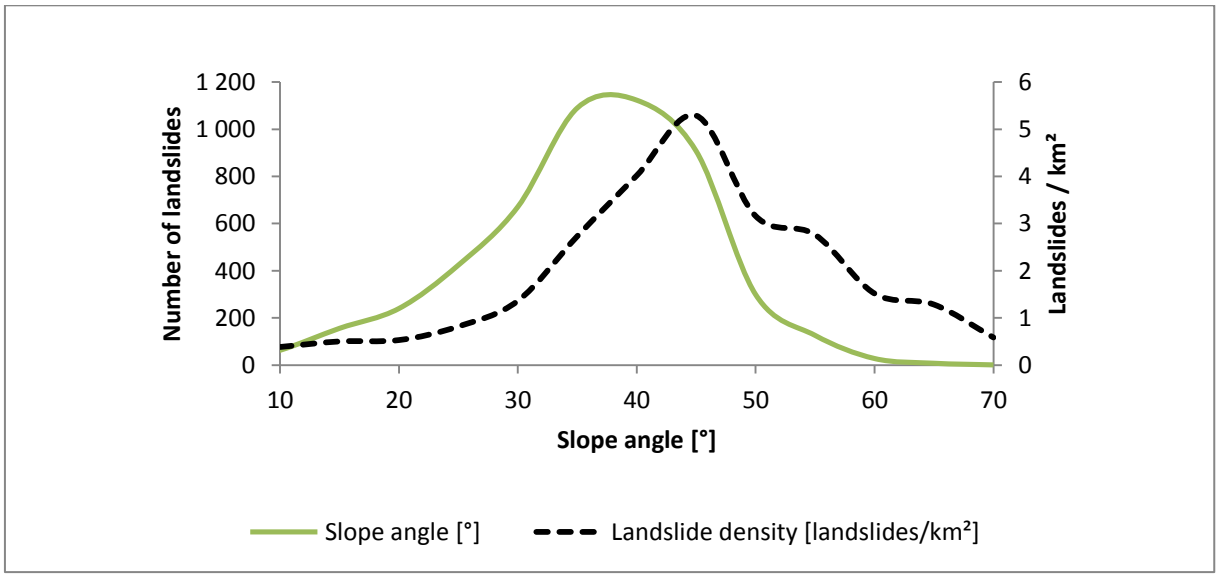

Figure 33 Slope angle distribution

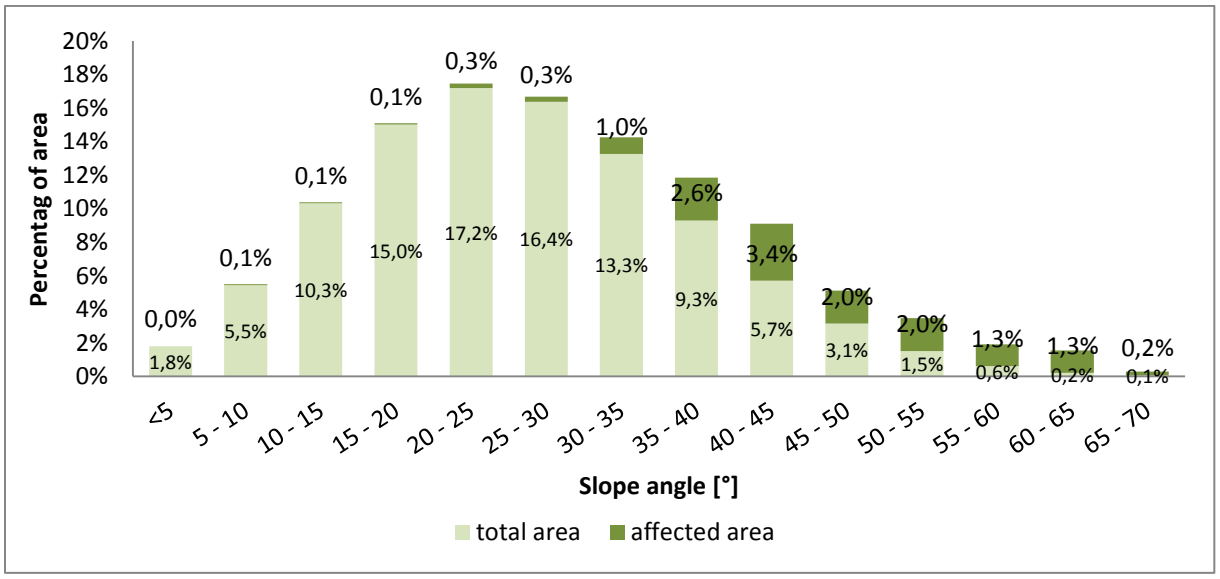

Figure 34 Slope angle distribution of the total area (light green), and percentage of affected terrain (dark green) within each class.

Figure 35b shows that up to a height of 2000 meters, the percentage of slopes with an angle of 20° (black line) dominates over those with an angle of 45° (green line). Despite this distribution, the percentage of landslides triggered on slopes with an angle of 45° already surpasses those triggered on shallower slopes at an altitude of 1500 m (Figure 35a).

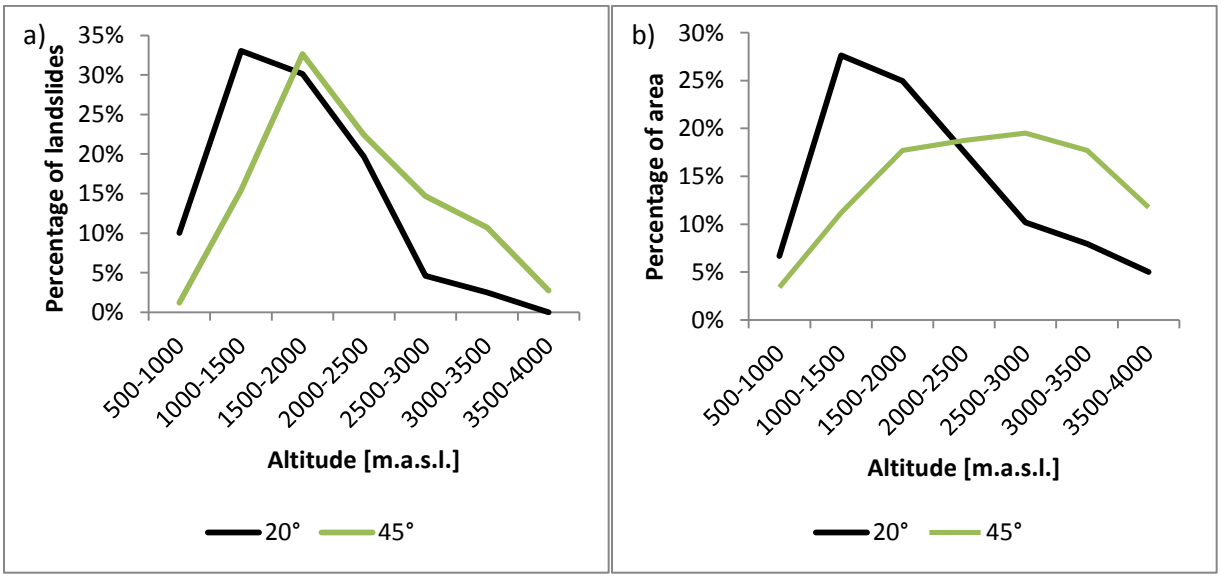

Figure 35 (a) Slope angle vs. altitude: the percentage of landslides triggered on slopes with an angle of 45° surpasses those triggered on shallower slopes at an altitude of 1500 m; (b) slope angle area distribution: up to a height of 2000 meters, the percentage of slopes with an angle of 20° (black line) dominates over those with an angle of 45° (green line).

5.5 Slope aspect

The slope aspects of Sindhupalchok's hillsides are shown in the Appendix: Figure 5. In Figure 36 two lines are plotted, showing the landslide density based on the slope aspect. The blue line was computed with the slope aspects recorded in Google Earth, whereas the data for the red line was extracted from the DEM. While there are two different results regarding the most affected slope aspect, northwestern slopes were definitely the least affected. In Figure 37, a slight trend towards more slopes oriented in southwestern direction (light green) can be seen.

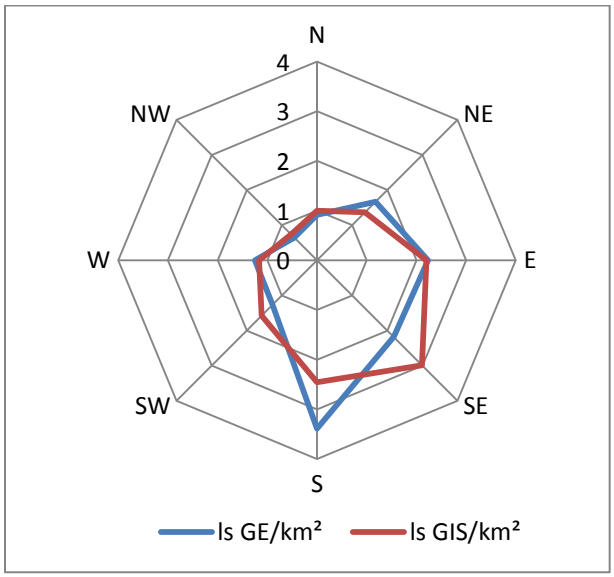

Figure 36 Landslide density (ls/km²) depending on slope aspect: The blue line represents the data recorded with Google Earth (GE), whereas the data for the red line was computed with a GIS-software.

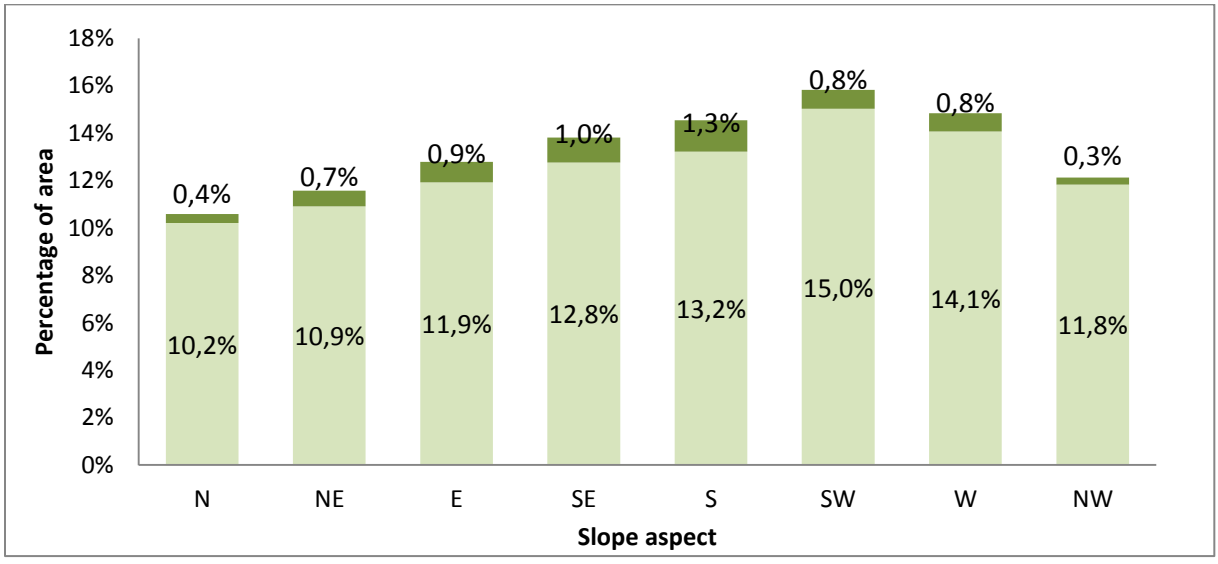

Figure 37 Total area distribution of slope aspects (light green), and percentage of affected areas (dark green)

The cause for the prevalence of triggered landslides on the southern and southeastern slopes (Figure 38a) is a tendency of steeper southern slopes and more shallow hillsides facing north, which was proved by plotting the percentage of area of two different slope angles against the slope aspects (Figure 38a). While slopes with an angle of about 25° (green line) are almost equally common in all directions, the distribution shifts towards the south with increasing inclinations (45°, purple line).

Figure 38b shows the quite equally distributed overall occurrence of the two most affected soil types (RGe and CMu).

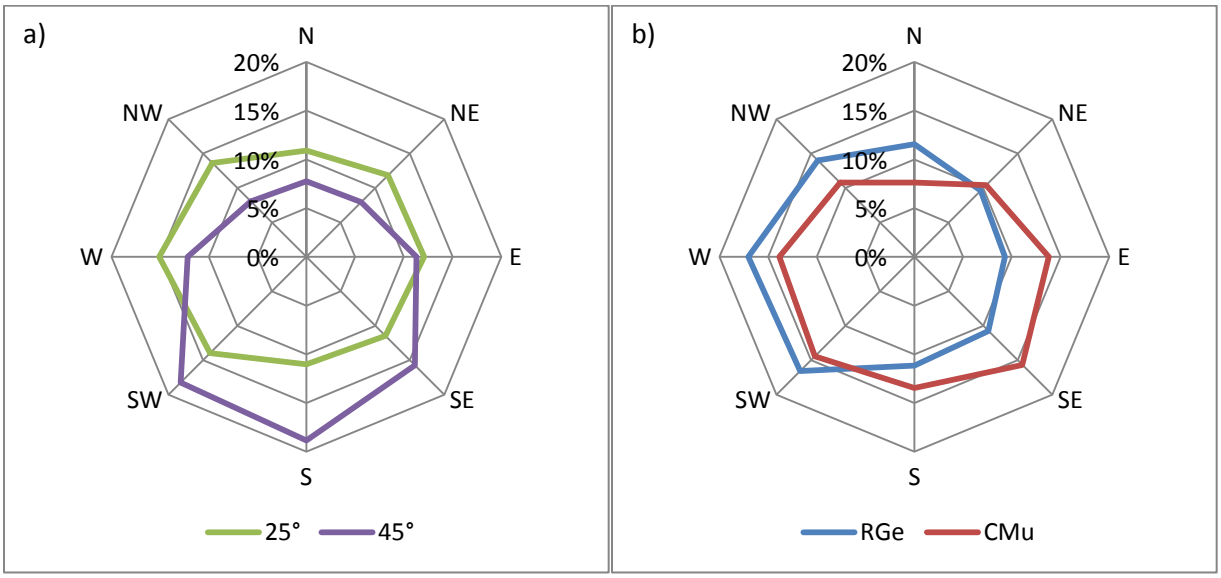

Figure 38 (a) Area distribution of slopes with 25° and 45° regarding their slope aspect (b) Area distribution of RGe and CMu soils depending on the slope aspect. RGe = eutric Regosol, CMu = humic Cambisol;

5.6 Slope relief

The number of landslides increases up to a slope relief of 260 m and decreases continuously to the maximal slope relief of 2027 m (Figure 39). The median slope relief is 326 m, whereas the average relief equals 394 m (Table 4).

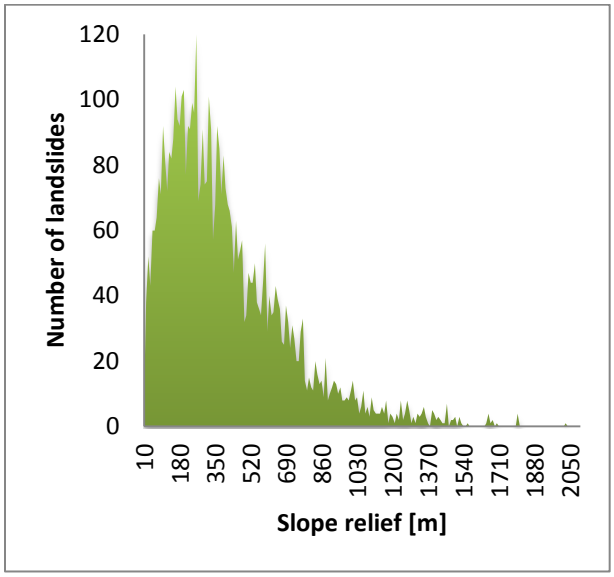

Figure 39 Number of landslides depending on the slope relief, which describes the vertical height difference between the top and the toe of a slope.

5.7 Affected infrastructure

A map of affected infrastructure is shown in the Appendix: Figure 2).

Although a lot of villages in Sindhupalchok were destroyed during the earthquake, the number of villages and houses hit by landslides can be counted on two hands. Compared to those few incidents, the number of affected roads is much higher (Figure 40).

In the rural areas of Sindhupalchok, roads are often built by local people who do not take into account the geological and geotechnical properties of the ground. This leads to poor stability conditions, and further to a high number of landslides. Figure 41 supports this theory, as most of the affected infrastructure is located in cultivated areas.

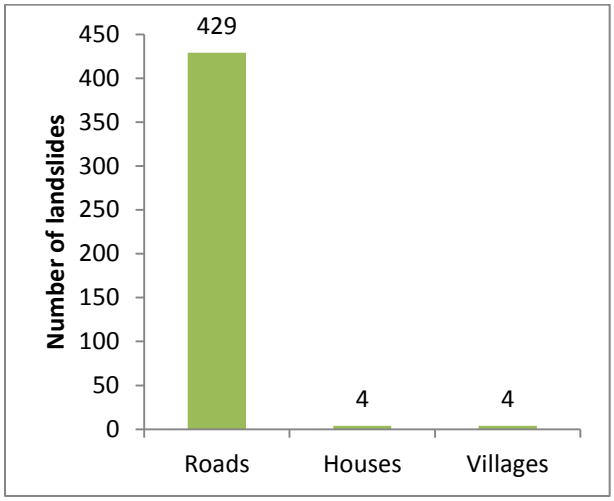

Figure 40 Affected infrastructure: Out of all recorded landslides in Sindhupalchok 429 affected roads, four destroyed houses and another four landslides hit villages.

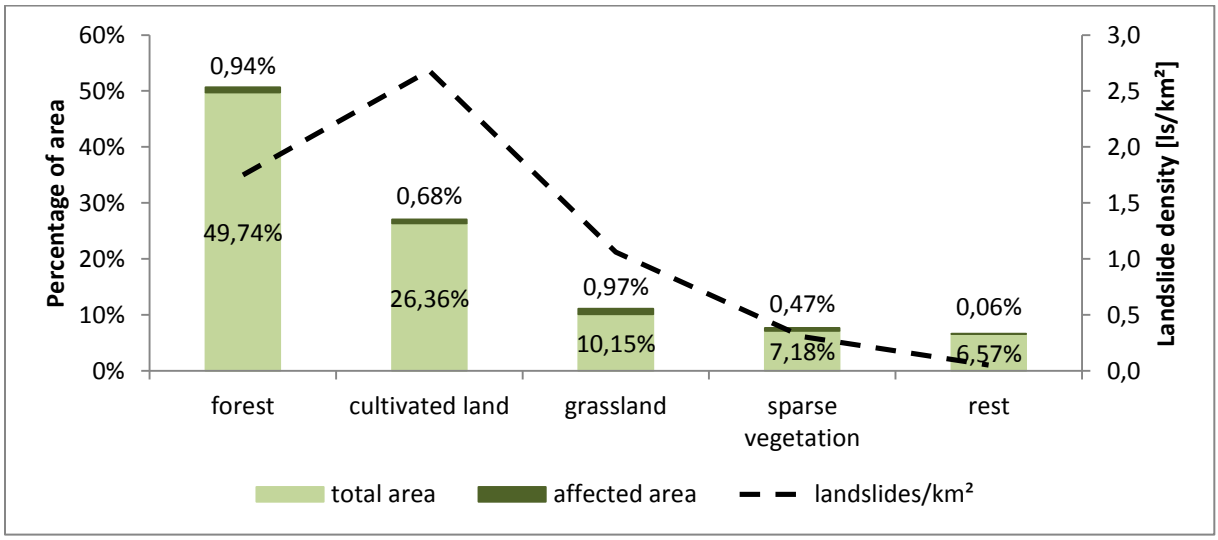

Figure 41 Affected infrastructure vs. landcover: Most of the affected infrastructure is located in cultivated areas.

5.8 Altitude

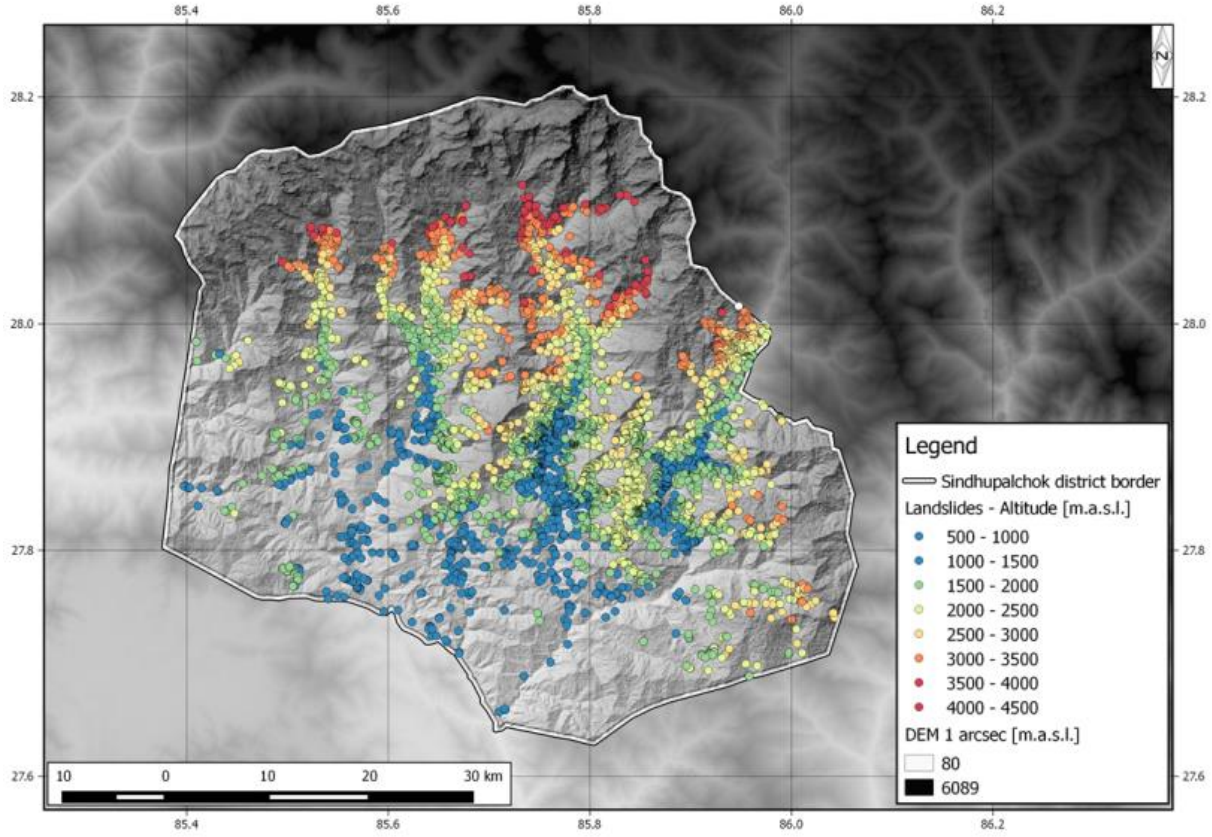

Figure 42 Map: Altitude of landslides within Sindhupalchok (© Ziselsberger; Basemap: SRTM DEM)

Landslides were triggered in altitudes ranging from 600 to 4300 m above sea level (Table 4, Figure 42). The number of landslides (Figure 43, black dashed line) rises steeply until it reaches a peak at an altitude of 1500 to 2000 m. After this peak the rate declines steadily.

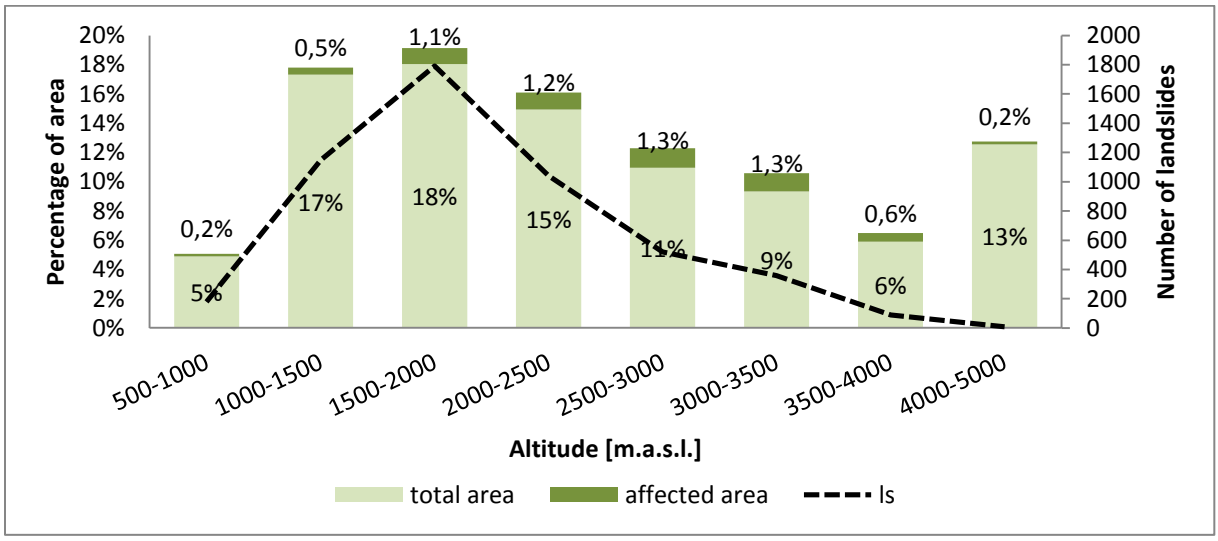

Figure 43 Altitude: Total area distribution (light green) and percentage of affected areas (dark green) depending on the altitude. Black dashed line represents the number of landslides (ls).

5.9 Soil

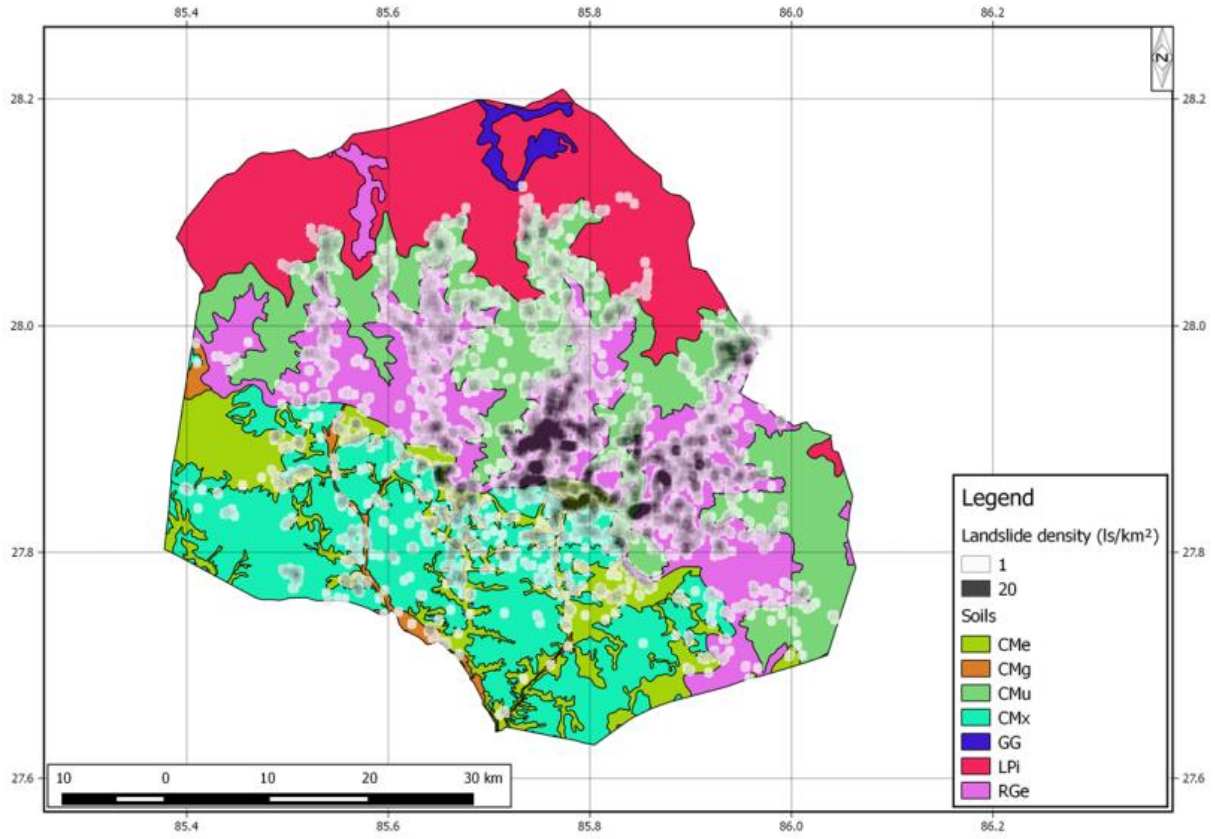

Figure 44 Map: Soil types (© Ziselsberger)

There are different types of soil covering the slopes of Sindhuplachok (Figure 44, Table 5). Figure 45 illustrates the total area (light green) as well as the percentage of affected ground (dark green) for each soil type.

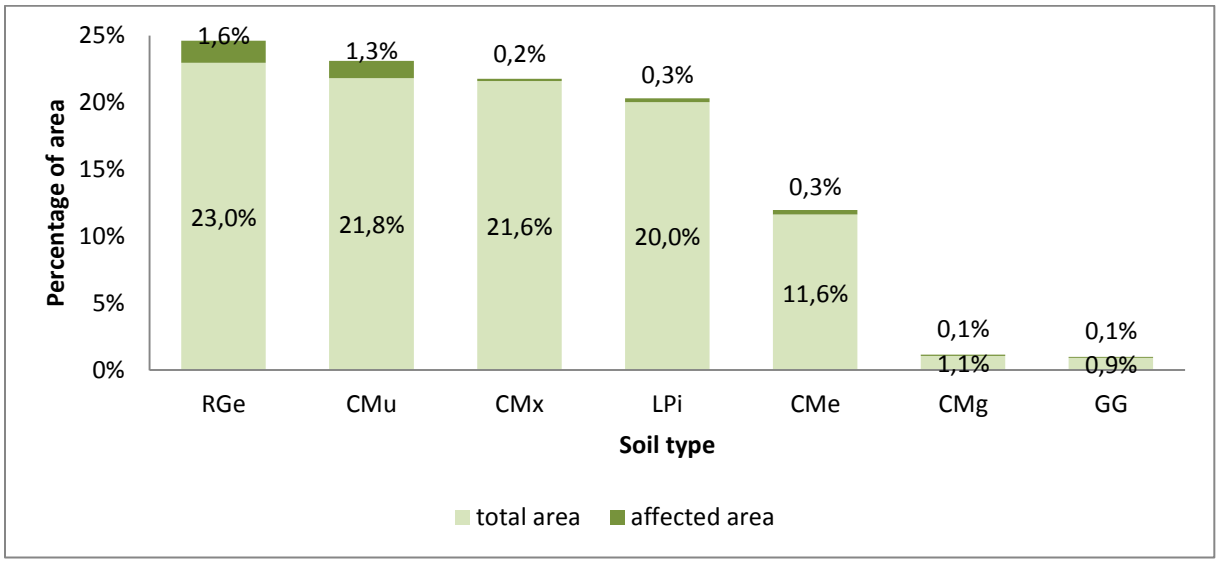

Figure 45 Total area distribution (light green), and percentage of affected ground (dark green) of different soil types.

Table 5 Soil Types

Abbreviation	Soil name
CMe	Eutric Cambisols
CMg	Gleyic Cambisols
CMu	Humic Cambisols
CMx	Chromic Cambisols
GG	Glaciers
LPi	Gelic Leptosols
RGe	Eutric Regosols

RGe and CMu are not only the most common, but also the most affected soil types. RGe (eutric Regosol) is a "very weakly developed mineral soil in unconsolidated materials". (FAO 2006) CMu (humic Cambisol) is characterized by "at least the beginnings of horizon differentiation in the subsoil". (FAO 2006) Both are typical for mountainous terrains in all climates. As they are poorly developed soils, they are probably easier to erode, especially on steep slopes.

In Figure 46a the landslides occurring within one of those two soil types are plotted depending on their altitude. The same trend as in Figure 43 can be seen here. Especially the occurrence pattern of CMu looks very similar to the rise and fall of affected area in Figure 43. The proportion of each soil type in different altitudes is shown in Figure 46b. Due to changing climatic conditions, the distribution of soils is highly dependent on the altitude.

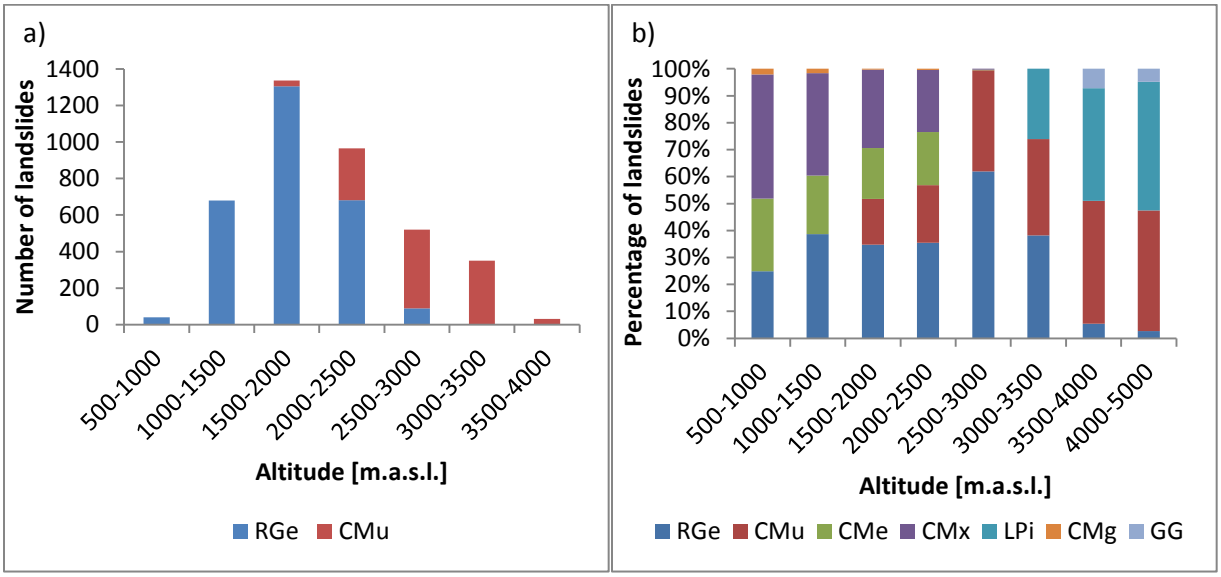

Figure 46 (a) Number of landslides occurring in areas covered with RGe or CMu, as a function of the altitude (b) Percentage of landslides with varying soil covers in different altitudes.

5.10 Geology

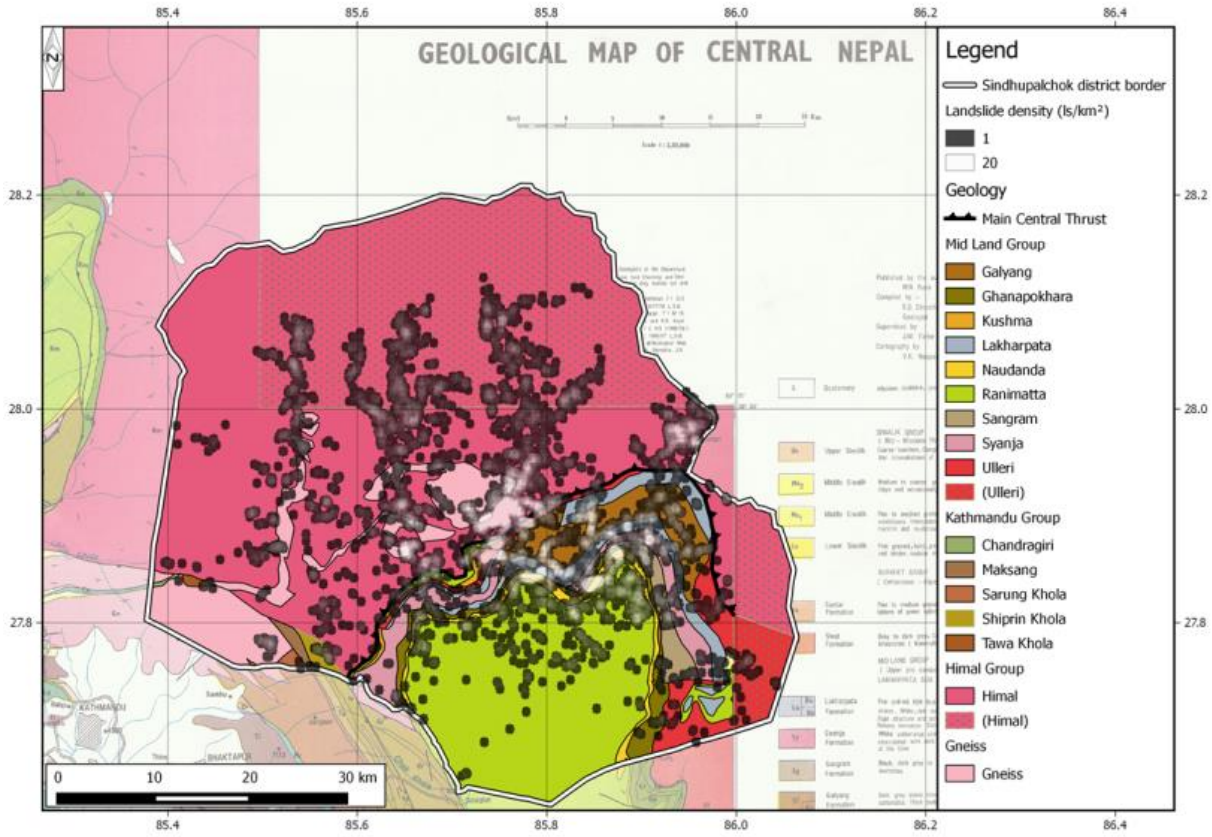

Figure 47 Map: Geology of Sindhupalchok (© Ziselsberger; Basemap: Geological Map of Central Nepal (Neupane))

About three quarters of Sindhupalchok are made out of Gneiss (Figure 47), and 20% consist of Quarzites and Phyllites (Figure 48a). The highest landslide density, on the other side, is in Limestone or Slate bearing formations (Figure 48b). According to Kargel et al. (2016), the majority of landslides were triggered in Proterozoic Phyllite, Amphibolite, Metasandstone, and Schist rock sequences of the Lesser and High Himalaya.

Table 6 Description of geological formations

Formation	Description	Formation	Description
(Himal Group)	Gneisses, Shists, Quartzites	Maksang	Quartzites
(Ulleri)	Gneiss	Nautanda	Quartzites, Phyllites
Gneiss	Gneisses	Ranimatta	Phyllites, Conglomerates, Quartzites
Himal Group	Gneisses, Shists, Quartzites	Syanja	Quartzites (calcareous), Limestones (quartzitic), Shales
Ulleri	Gneiss	Sarung Khola	Schists
Chandragiri	Limestones (fine grained crystalline)	Shiprin Khola	Schists (coarse crystalline)
Lakharpata	Limestone/Dolomite, Shale	Tawa Khola	Schists (coarse grained)
Sangram	Shales, Limestone, Quartzite	Galyang	Slates
Kushma	Quartzites, Phyllites	Ghanapokhara	Slates (calcareous), Shales

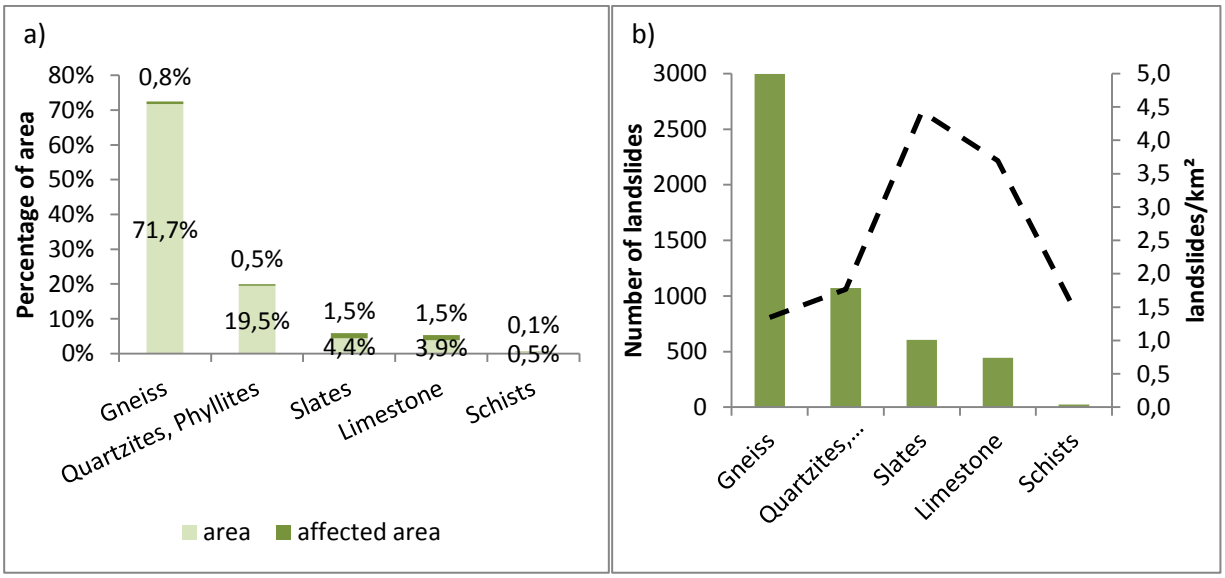

Figure 48 (a) Total area distribution (light green) and percentage of affected areas (dark green) as a function of the lithology, (b) Number of landslides and landslide density (black dashed line) depending on the lithology

When looking at the landslides' geology and their altitude (Figure 49), a similar trend like in Figure 43 is observable. As the altitude rises from 500 to 1500 meters, the number of landslides occurring in Limestone and Slates increases rapidly. After this peak, the distribution of landslides in one of those two lithologies starts to decrease again.

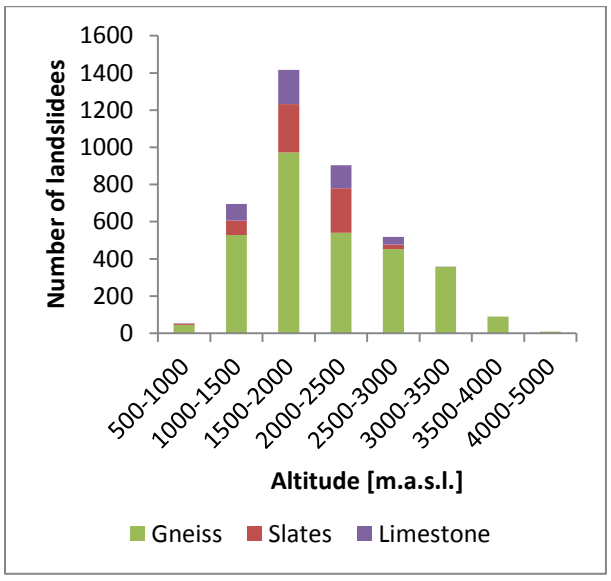

Figure 49 Geology vs. altitude: Number of landslides occurring within different lithologies, plotted as a function of their altitude

5.11 Landcover

One quarter of Sindhupalchok's ground is used for agriculture and about half of its area is covered with forest. Beside those two parts, another highly affected form of land cover seems to be grassland (Figure 50). The high landslide density in agricultural land is probably linked to the highly affected altitudes of 1500 to 2500 meters. Figure 51 shows that more than 40% of the slope failures in cultivated land are located in these altitudes.

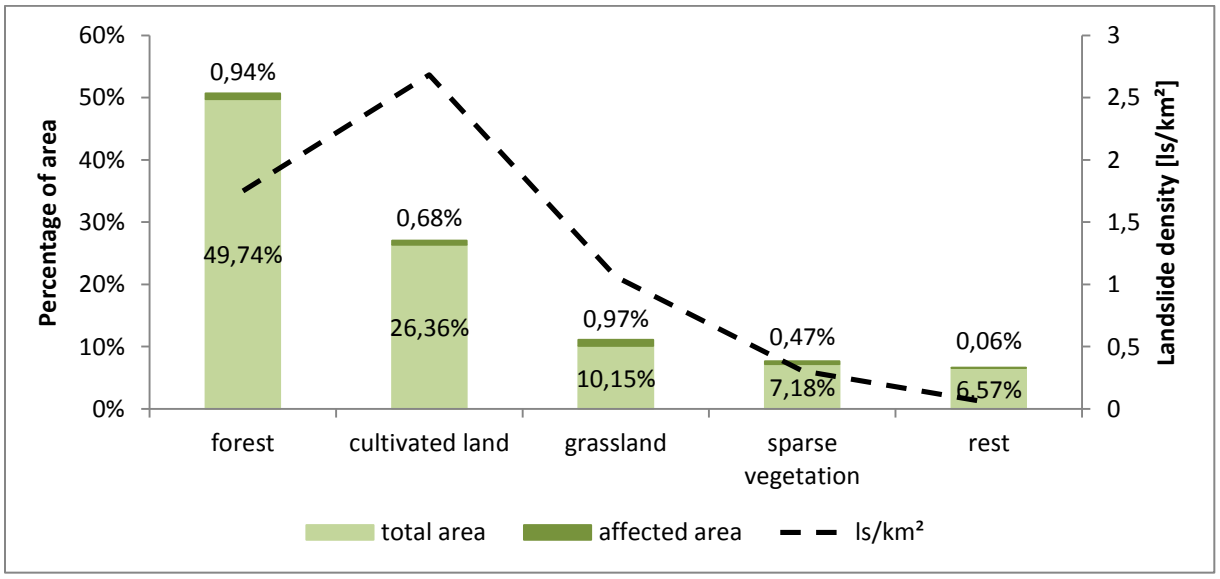

Figure 50 Landcover: Total area distribution (light green) and percentage of affected areas (dark green). Black dashed line describes landslide density (landslides/km²)

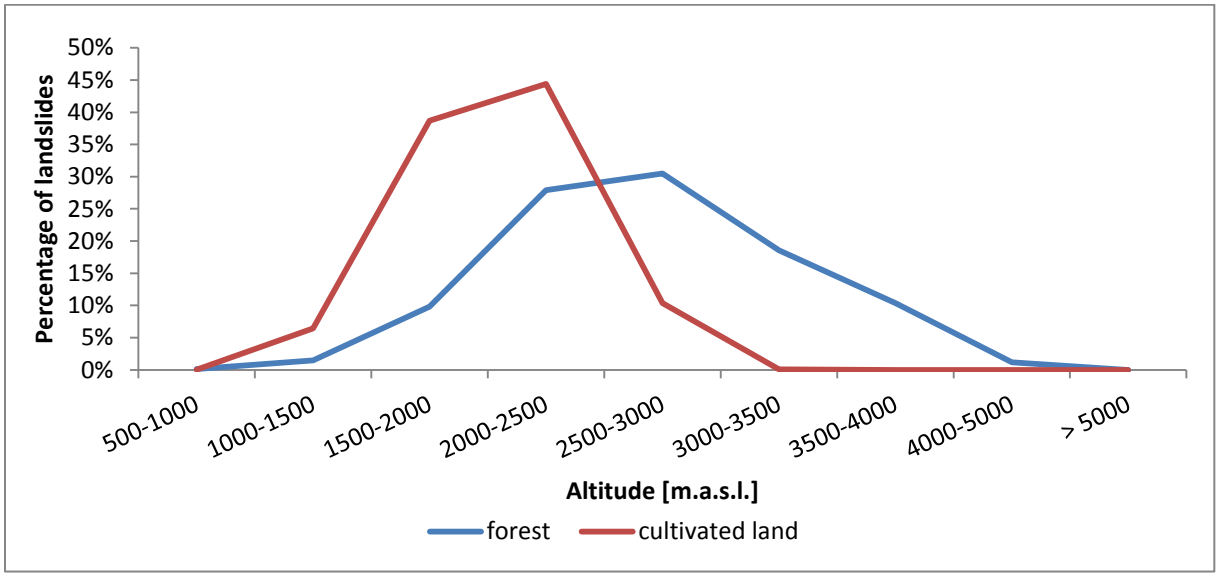

Figure 51 Land cover vs. altitude: Percentage of landslides occurring in forests (blue) and cultivated areas (red), as a function of the altitude

5.12 Distance from epicenter (DEPI)

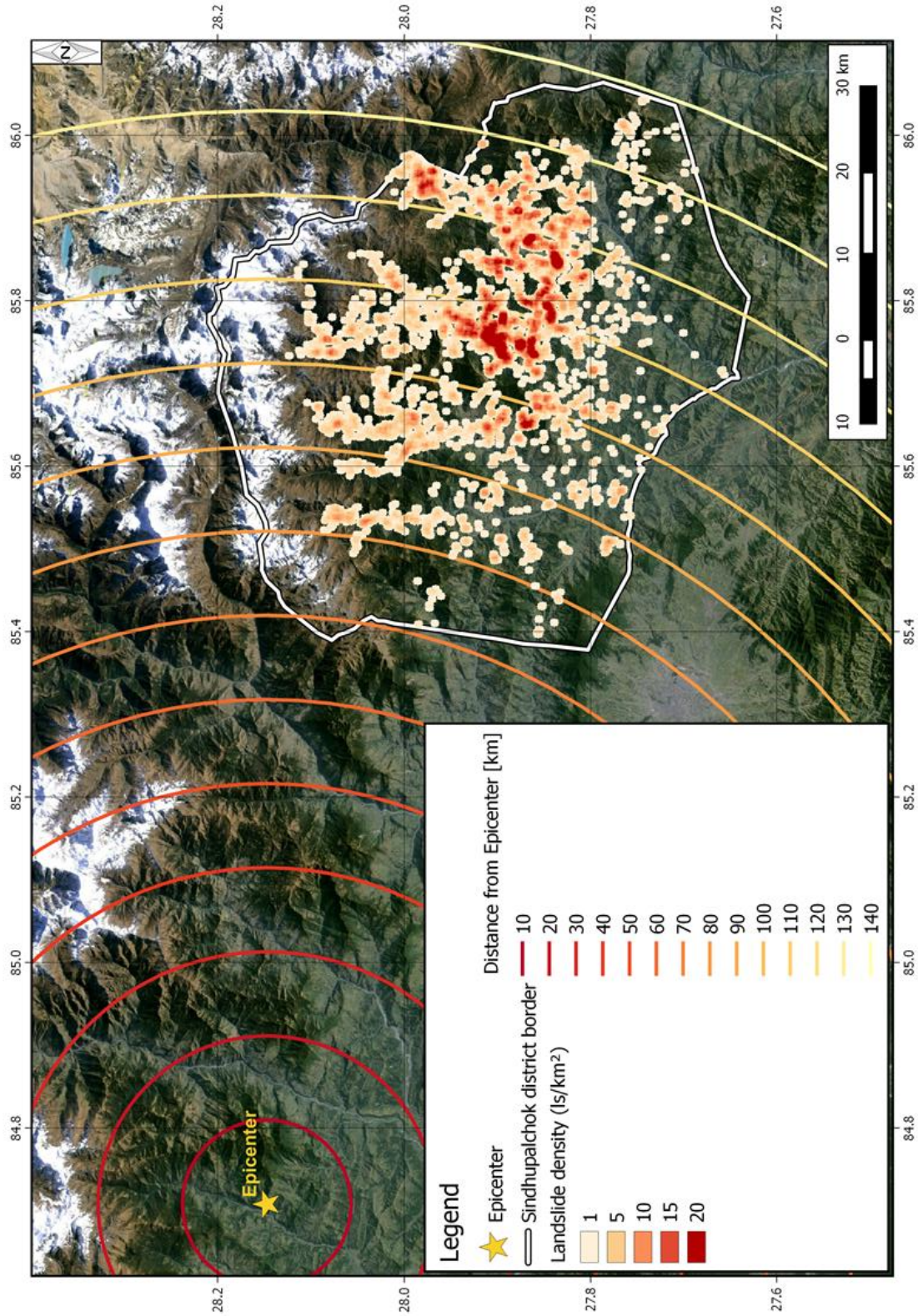

Figure 52 Map: Distance from epicenter – Landslide density shown in combination with distance from the epicenter (© Ziselsberger; Basemap: Google Earth Image)

About 75% of all landslides occur within a distance of 100 to 130 km from the epicenter (Figure 52). There is no identifiable trend of growth or fall in landslide occurrence with increasing distance from the epicenter. Instead, three regions seem to have been hit harder than all others, and this trend is not a function of area distribution (Figure 53).

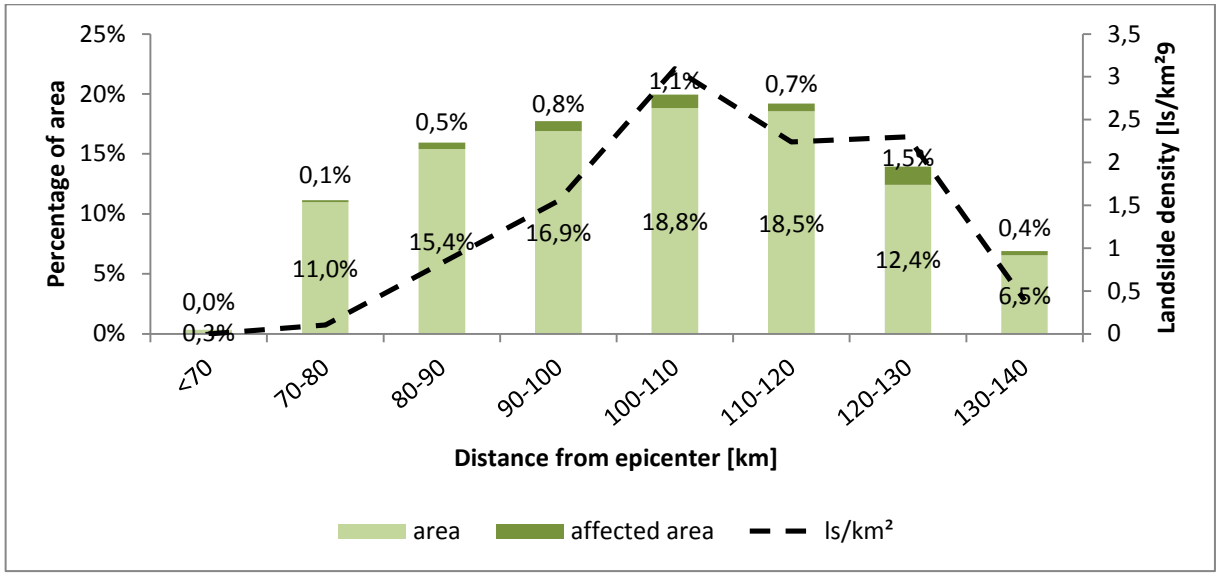

Figure 53 Total area distribution (light green) and percentage of affected areas (dark green) depending on the distance from epicenter. The landslide density (ls/km²) is shown by the black dashed line.

Figure 54 illustrates the number of landslides depending on their distance from the epicenter and their altitude. In this plot, the classes 100 - 110 km and 120 – 130 km stand out, which might explain the shape of the landslide density graph in Figure 53.

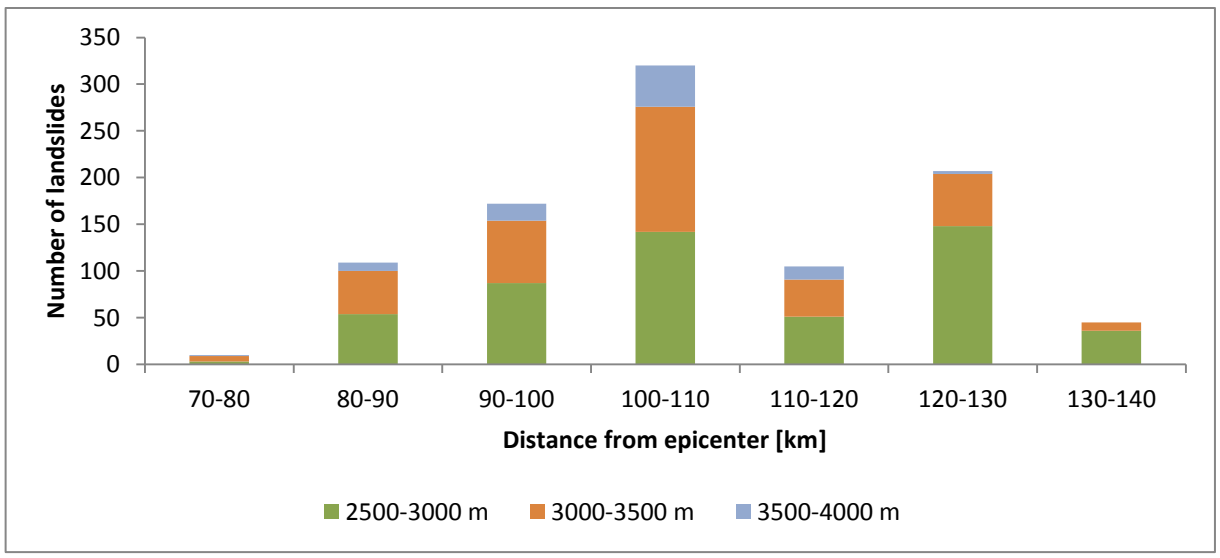

Figure 54 Altitude vs. DEPI: Number of landslides occurring within altitudes of 2500-3000 m (green), 3000-3500 m (orange) and 3500-4000 m (grey), plotted according to their distance to the epicenter

Figure 55 shows the relationship between epicentral distances of landslides and the magnitude of the earthquake (from Khazai, Sitar (2004)). Besides landslides triggered by other earthquakes, like the M 6.7 Northridge Earthquake (1994) or the M 7.6 Chi Chi Earthquake (1999), the landslides of Sindhupalchok are plotted in this diagram.

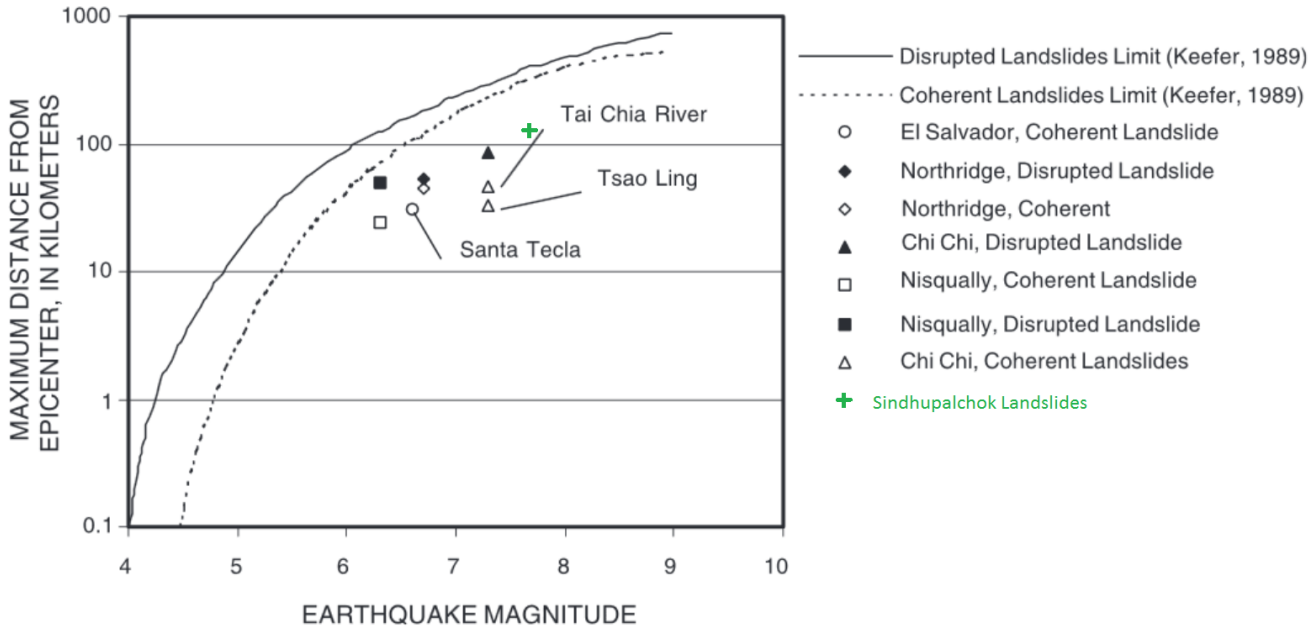

Figure 55 Maximum distance from epicenter for seismically induced landslides as a function of earthquake magnitude (limits from Keefer, 1989). (Source: Khazai, Sitar (2004)) Green cross indicates landslides in Sindhupalchok.

5.13 Drainage Basin (DB)

A map of the drainage basins is shown in Figure 23 and in the Appendix: Figure 6. Figure 56 illustrates the area distribution and the percentage of affected terrain for each drainage basin. The black dashed line indicates the landslide density.

As can be seen from this diagram, most landslides were triggered in the drainage basins of Sunkohsi and Bhotekoshi. This trend can be explained with the two following graphs (Figure 57):

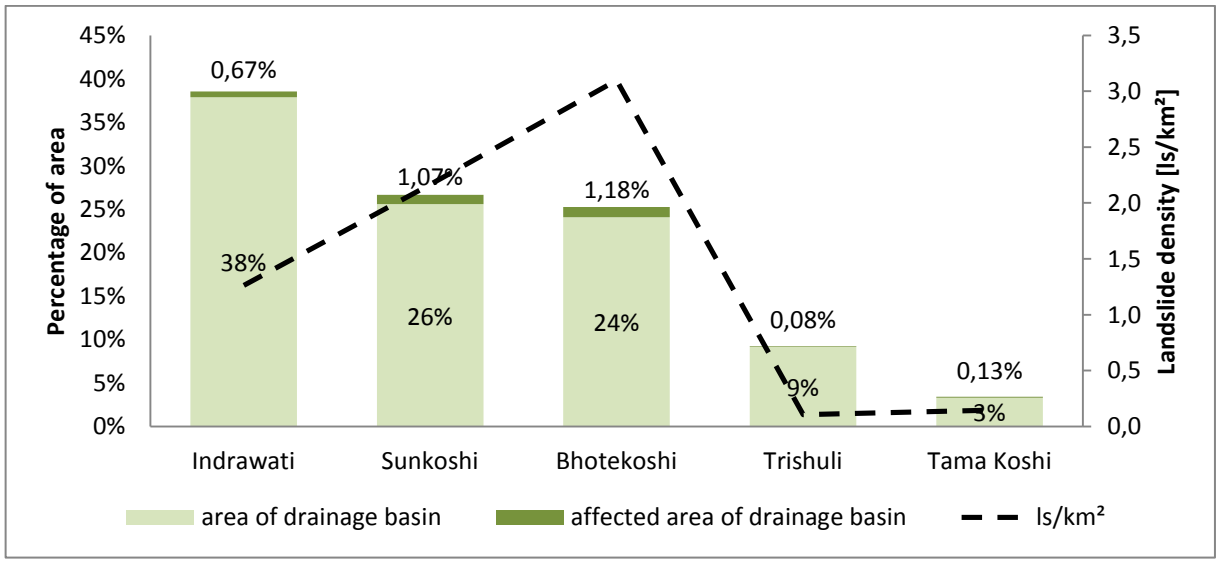

Figure 56 Drainage basins: Total area of drainage basins (light green) and percentage of affected area within each drainage basin (dark green). The landslide density (ls/km²) is shown by the black dashed line.

The percentage of landslides within one of the two most affected soil types (Figure 57a) or lithologies (Figure 57b) shows the same trend when they are divided into the given drainage basins.

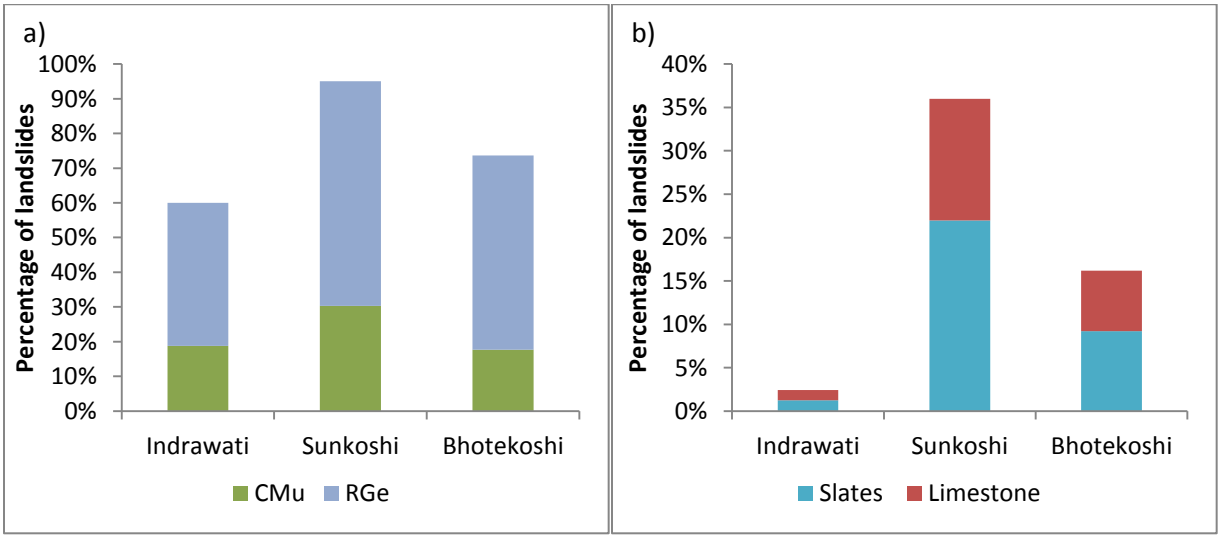

Figure 57 Percentage of landslides in different drainage basins, shown depending on their (a) soil cover or (b) geology

5.14 Landslide density hotspots

Six areas (Figure 58, Table 7) have been analyzed in more detail to find out why landslide density is so much higher there than in other places.

Table 7 Hotspot data

Hotspot (HS)	HS1	HS2	HS3	HS4	HS5	HS6
All landslides	76	707	124	105	99	67
Area [km²]	6.0	33.7	7.6	4.1	2.8	1.5
Landslide density [ls/km²]	12.6	21.0	16.4	25.9	34.9	45.3

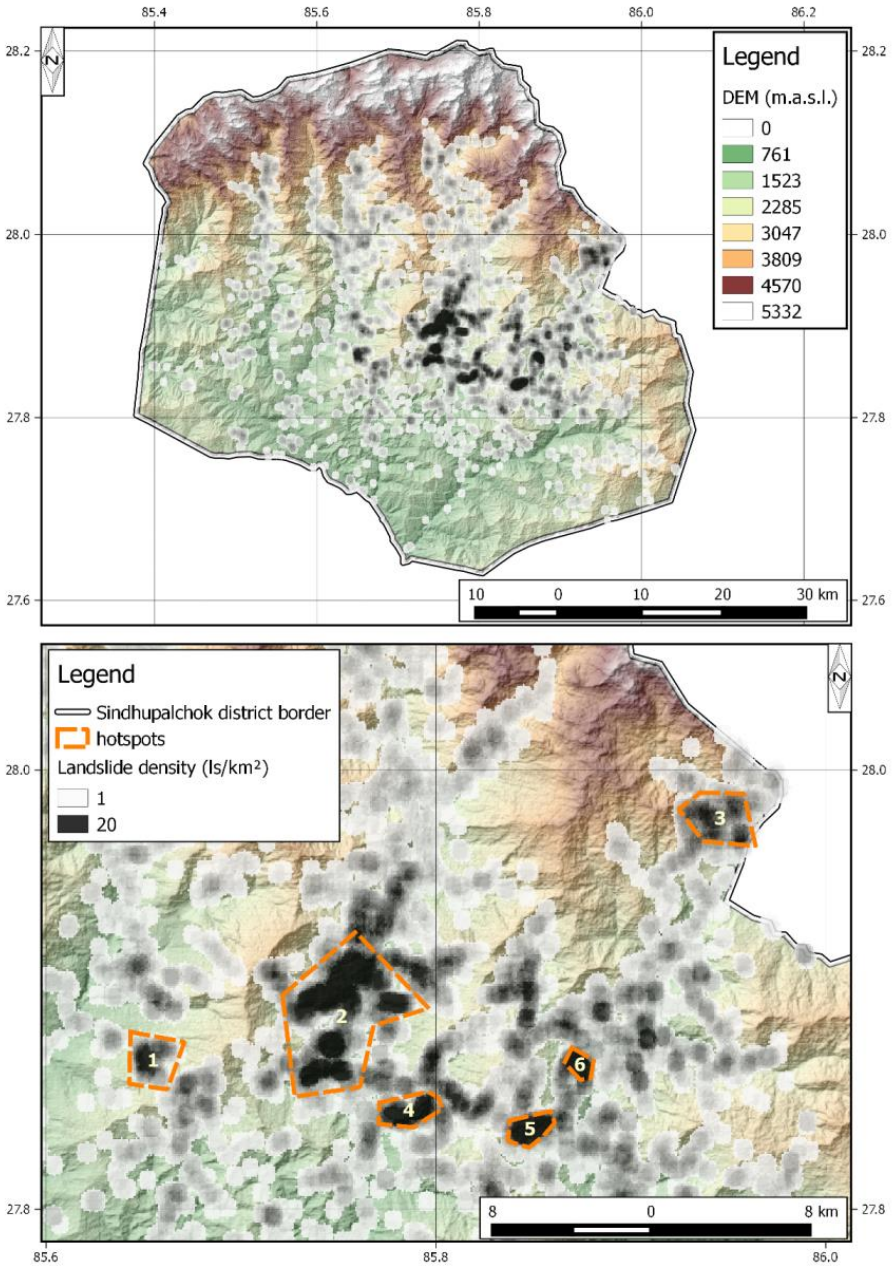

Figure 58 Map of landslide hotspots: Due to their high landslide density, these six areas have been analyzed more precisely. (© Ziselsberger; Basemap: colored SRTM DEM)

5.14.1 Soil

Two hotspots (HS2 and HS6) are almost completely covered with RGe, and HS3 with RGe and CMu. In none of the other three areas is one of those two soils dominant (Figure 59).

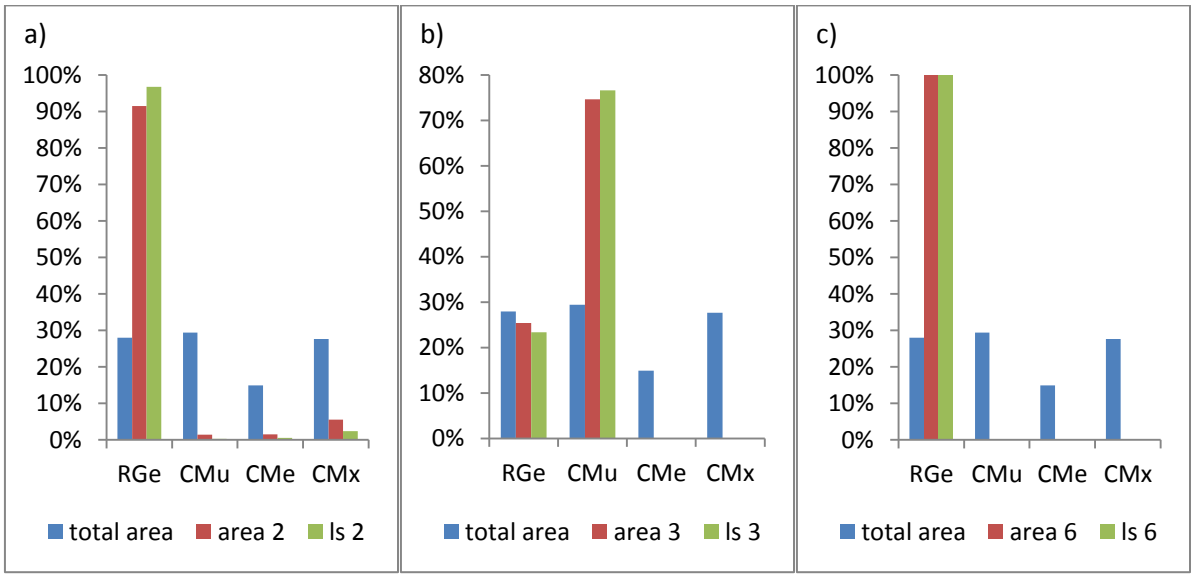

Figure 59 The overall area distribution (blue) of four soil types, compared to the occurrence of these soils within three different hotspots (red) and the percentage of triggered landslides (green): (a) HS2, (b) HS3 and (c) HS6

5.14.2 Geology

HS4, HS5 and HS6 lie within geological units composed of Quartzites, Phyllites, Slates and Limestone (Figure 60). As already described in previous chapters, Limestone and Slate bearing formations are prone to landslide occurrence.

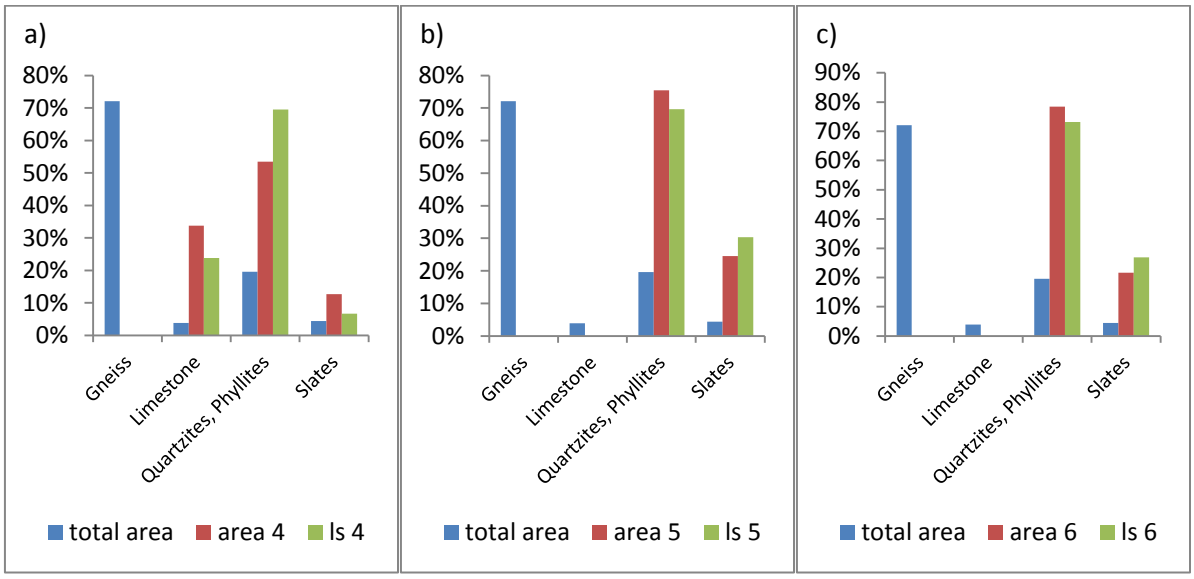

Figure 60 The overall area distribution (blue) of different lithologies, compared to the occurrence of these lithologies within three different hotspots (red) and the percentage of triggered landslides (green): (a) HS4; (b) HS5; (c) HS6

5.14.3 Altitude

As described earlier, the highly affected areas in Sindhupalchok are located between 1500 and 2500 meters above sea level. Four of the six hotspots lie almost entirely between 1000 and 2500 m (Table 8). HS3 is situated considerably higher (Figure 61), in elevations of 1500-3000 m, which is due to the far more northern position (Figure 58). Compared to the rest, HS4's altitude distribution is shifted to the left and has its peak between 1000 and 15000 m (Figure 61).

Table 8 Area distribution of hotspots as a function of the altitude

Altitude [m.a.s.l.]	Total area	HS1	HS2	HS3	HS4	HS5	HS6	HS1	HS2	HS3	HS4	HS5	HS6
500 - 1000	5%	0%	4%	0%	13%	0%	2%						
1000 - 1500	18%	5%	45%	0%	60%	5%	85%						
1500 - 2000	19%	59%	36%	13%	27%	65%	13%	100%	96%	86%	87%	100%	98%
2000 - 2500	16%	36%	15%	28%	0%	30%	0%						
2500 - 3000	12%	0%	0%	45%	0%	0%	0%						
3000 - 3500	10%	0%	0%	13%	0%	0%	0%						
3500 - 4000	6%	0%	0%	1%	0%	0%	0%						

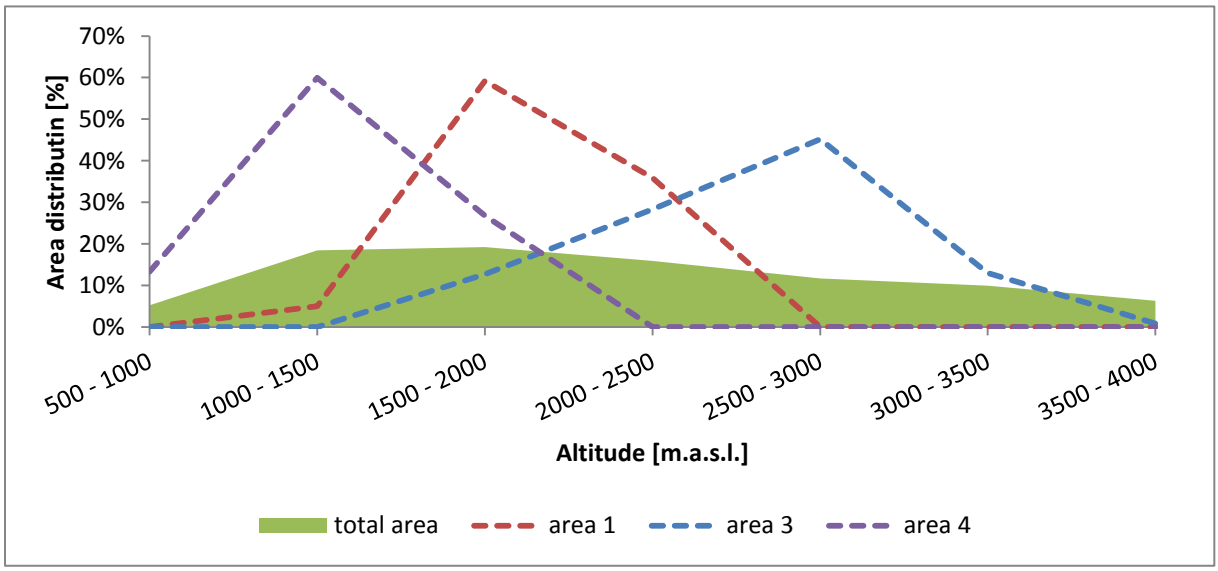

Figure 61 The total area distribution as a function of the altitude is shown in green, compared to the area distribution of three hotspots (dashed lines): HS1 (red), HS3 (blue) and HS4 (purple)

5.14.4 Slope Aspect

When comparing the slope aspect distribution of all hotspots, no common trend can be seen (Table 9, Figure 62). Four out of six are primarily exposed to the southeast. The reverse is true for HS1, which faces northwest, which was proved to be the least affected slope aspect.

Table 9 Area distribution of hotspots as a function of the slope aspect

		Area distribution					
Slope aspect	**Total area**	**HS1**	**HS2**	**HS3**	**HS4**	**HS5**	**HS6**
N	10.2%	22.2%	11.8%	3.1%	1.9%	0.4%	0.5%
NE	10.9%	8.8%	11.3%	17.1%	1.0%	1.8%	2.6%
E	11.9%	6.0%	17.4%	18.3%	7.0%	21.6%	38.3%
SE	12.8%	0.4%	18.4%	29.5%	11.0%	55.3%	39.9%
S	13.2%	4.1%	12.3%	18.4%	22.6%	19.7%	3.8%
SW	15.0%	14.9%	9.9%	11.7%	29.5%	1.0%	1.8%
W	14.1%	21.7%	9.0%	1.7%	21.7%	0.3%	8.9%
NW	11.8%	21.9%	9.9%	0.2%	5.2%	0.1%	4.1%

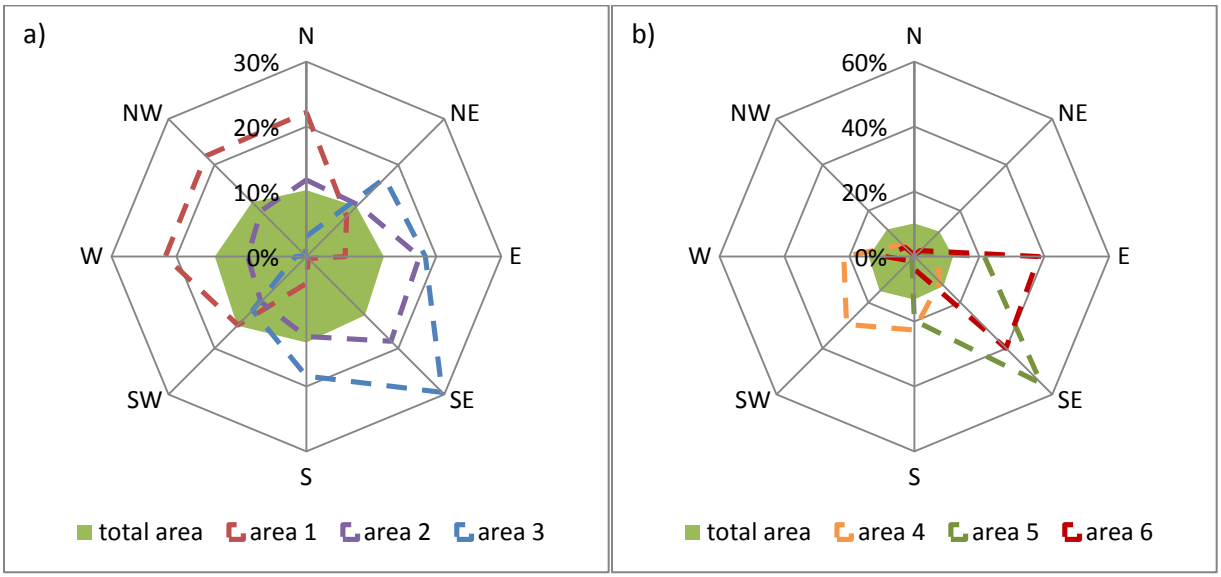

Figure 62 The total area distribution regarding the slope aspect is shown in green, compared to the area distribution of the hotspots (dashed lines): (a) HS 1, 2 and 3; (b) HS 4, 5 and 6)

5.14.5 Slope Angle

Apart from two hotspots (HS1 and HS3), none shows a deviation to the overall slope angle distribution (Table 10, Figure 63). The slopes in HS3 are generally steeper, which correlates to the higher altitude of this area. HS1 on the other side shows an increase in slope angles of 25 -30°. This might explain the high landslide density in this area.

Table 10 Area distribution of hotspots as a function of the slope angle

		Area distribution					
Slope angle [°]	**Total area [%]**	**HS1**	**HS2**	**HS3**	**HS4**	**HS5**	**HS6**
<10	6%	4%	3%	1%	5%	3%	5%
10 - 15	11%	8%	7%	3%	9%	7%	11%
15 - 20	15%	15%	13%	6%	15%	14%	17%
20 - 25	18%	19%	18%	10%	17%	18%	22%
25 - 30	17%	22%	20%	15%	16%	17%	20%
30 - 35	14%	17%	16%	19%	12%	15%	13%
35 - 40	9%	10%	10%	19%	9%	10%	6%
40 - 45	6%	4%	6%	13%	6%	6%	4%
45 - 50	3%	2%	3%	9%	5%	5%	1%
50 - 55	2%	1%	2%	4%	4%	2%	1%
55 - 60	1%	0%	1%	1%	2%	1%	1%
60 - 65	0%	0%	0%	0%	1%	0%	0%

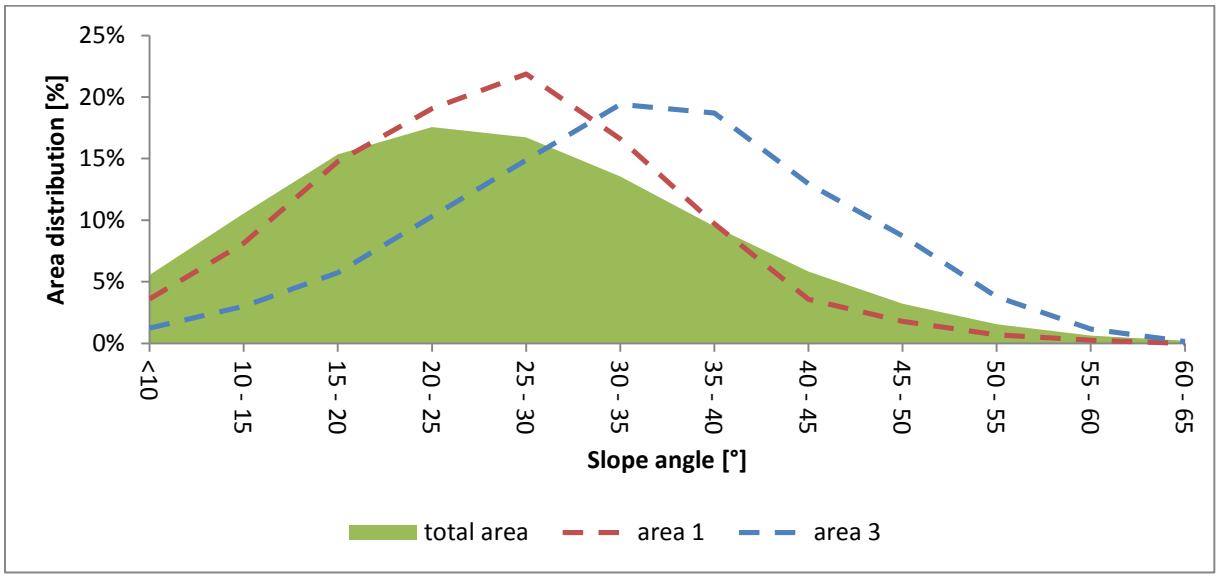

Figure 63 The total area distribution as a function of the slope angle is shown in green, compared to the area distribution of two hotspots (dashed lines): HS1 (red) and HS3 (blue)

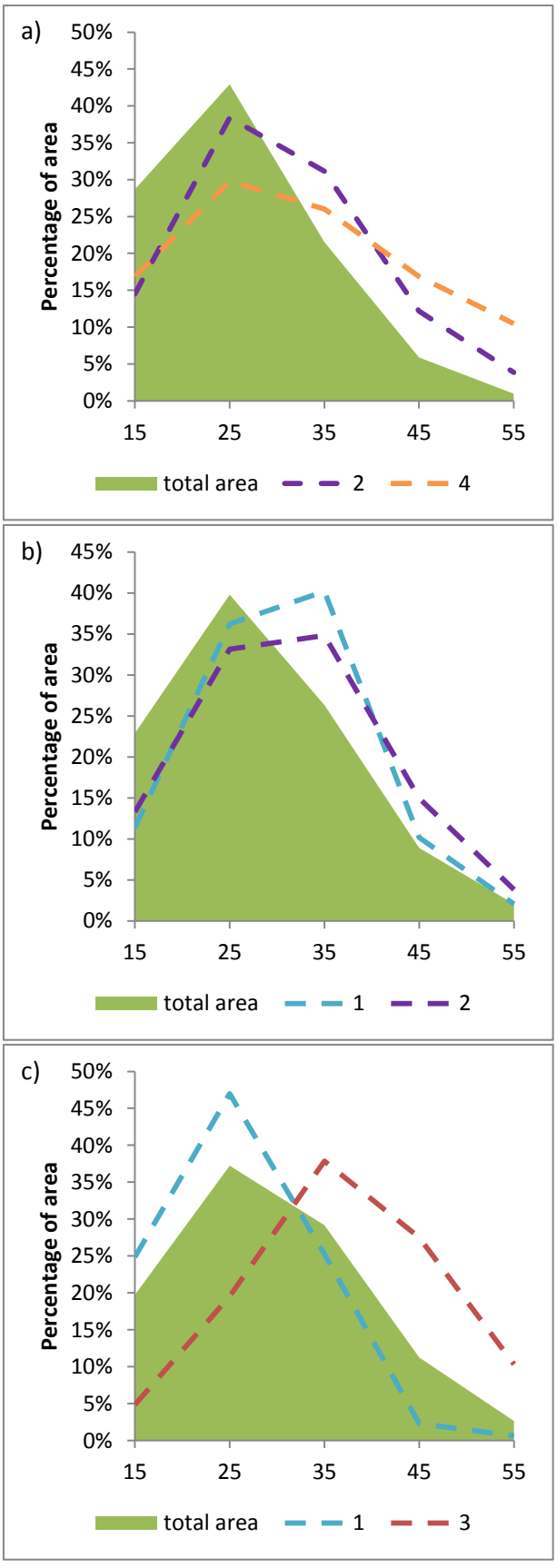

Figure 64 The area distribution as a function of the slope angle is shown for three different altitudes: (a) 1000-1500m, (b) 1500-2000m, (c) 2000-2500m. Total area (green), HS1 (blue), HS2 (purple), HS3 (red), HS4 (orange).

In Figure 64(a-c) the slope angle distribution of some hotspots compared the total area is shown for different altitudes.

Figure 64a displays the area distribution of HS2 and HS4, which largely lie between 1000 and 1500 m (Table 8). Both show a shift towards steeper slopes, especially HS4 has a lot more 45° and 55° inclined hillsides.

When taking a look on the Figure 64b, another shift towards steeper inclinations can be observed for HS1 and HS2.

In Figure 64c two different trends are shown. HS3 has a tendency towards steep hillsides, whereas HS1 shows an increase in moderately inclined slopes.

To sum up these results, the main influencing factor seems to be the altitude, followed by the slope angle. Despite its northwestern exposure, HS1 has a landslide density of 12.6 ls/km², which is caused by a bigger portion of moderate to steep slopes. HS2 is also the effect of steeper slopes, as well as of RGe being the main soil cover. Due to the more northern location, HS3 lies generally higher than all other hotspots, which correlates to steeper slope angles and a soil cover consisting of RGe and CMu.

Furthermore, its slope aspect distribution shows a distinct tendency towards southeast. Hotspots 4, 5 and 6 are very small and have a very high landslide density of up to 45 ls/km². This high occurrence appears to be related to the geological conditions, as all three hotspots are located in Slate, Limestone and Phyllite rich formations. Further on, HS6 is completely covered with the RGe soil type, HS5's slopes are almost exclusively facing southeast and HS4 has a higher concentration of steep slopes.

5.15 Field observations

Lying on the southern side of the Himalayan range, Nepal's climate is highly influenced by the monsoon during the summer months. As the earthquake occurred only weeks before the monsoon began, the soil and rocks covering the hillsides of Sindhupalchok were rather dry. The landslides examined during the first field trip in May were primarily shallow slips of regolith (Figure 65), which consists of loose material like soil or weathered rock that covers the underlying bedrock (Figure 66).

Figure 65 Shallow, dry slope failures (© Ziselsberger).
Left (27°52'33.74"N, 85°53'54.32"E), right (27°52'58.85"N, 85°54'48.81" E)

Figure 66 Some of the viewed outcrops along the road exhibited highly weathered rocks (mostly Gneiss), which are described as friable due to their preserved texture but high breakability (© Ziselsberger)

These slips were often seen along roads which are cut into the hillsides. Landslides started either on the outer edge of the cut or on the uphill slope, spilling onto and eventually blocking the road. Another common location for those dry earthflow-like slides was within steep gullies and along ridgetops. Besides all those landslides, lots of (tension) cracks were visible along the hillsides.

The monsoonal effects on those shaken slopes were studied during the second field trip in October 2015. Open cracks and loosened rocks and debris provided easy access for the water to penetrate into the ground. The rising water saturation lead to further destabilization of the hillsides and huge masses started to move down towards the valley. These mass movements were described as slow and continuous processes by the local inhabitants. Compared to the earthquake-induced landslides, these masses buried several villages and blocked many roads (Figure 67 - Figure 69). As can be seen in Figure 70 and Figure 71, the vegetation recovered rapidly between the two field trips. This fact once more underlines the time sensitivity of the gathered information. Under the right climatic conditions traces of landslide activity fade within a short period of time.

Figure 67 Massive debris masses blocked the roads during and after the monsoon (© Ziselsberger) 27°54'23.37"N, 85°55'15.37"E

Figure 68 Massive debris masses covered the roads after the monsoon (© Ziselsberger); 27°56'11.52"N, 85°56'28.56"E

Figure 69 Landslides reactivated by monsoonal rainfall (left; © Ziselsberger), Google Earth image (right) shows extent of landslides (white) and location of houses (yellow box) before monsoon; 27°56'16.33"N, 85°56'34.75"E

Figure 70 Destroyed house in Kodari (27°58'17.12"N, 85°57'41.78"E). Before (left) and after (right) the monsoon (© Ziselsberger).

Figure 71 Before (left) and after (right) the monsoon (© Ziselsberger)
27°54'23.36"N, 85°55'15.78"E

Figure 72 Google Earth image showing the landslides of Figure 71; 27°54'23.36"N, 85°55'15.78"E (Source: Google Earth)

One major difference between the landslides triggered during the earthquake and those caused by the monsoon is the angle of deposition of the moved material. With rising water content, the cohesion between the particles increases up to a certain point where the water starts to act as a lubricant (Figure 73). Therefore, the depositional angle of the landslides caused by the daily rainfall during the monsoon is flatter than of those triggered by the earthquake.

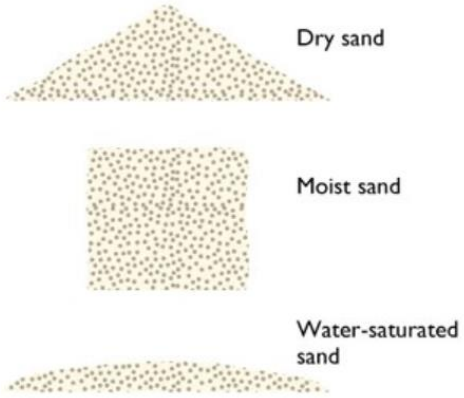

Figure 73 Behavior of dry, moist and water-saturated sand (Source: https://www.geocaching.com/geocache/GC3TY2P_geology-at-the-beach-presque-isle?guid=6d6905da-4228-4557-8d5b-888d65aaf4ca, 03.03.2016)

6. Discussion and Conclusions

Due to the Nepal-Gorkha earthquake on April 25, 2015 and its aftershocks, more than five thousand landslides were triggered in the district of Sindhupalchok. Of these, approximately 70% are new and 30% represent reactivated deposits.

There are more than one thousand landslides smaller than 500 m^2, and landslide frequency decreases with increasing surface area. The minimum area for a landslide to be definitely recognized on satellite imagery is approximately 200 m^2, which therefore represents the resolution threshold of this inventory. By comparing landslide areas as a function of altitude, a trend towards longer events at higher elevations is evident. Furthermore, most of the landslides were triggered in altitudes between 1500 and 2500 meters above sea level, which seems to be correlating with the soil cover, as the two most affected soil types dominate in these heights.

Altitude and soil cover were also the main influencing parameters in the following analyses:

- Landslide densities hit a peak within a distance of 110-120 km and 120-130 km to the epicenter.
- After dividing Sindhuplachok into six major orographic drainage basins, the percentage of affected area for each catchment area was computed. The highest proportions emerge in the drainage basins of Sunkoshi and Bhotekoshi.
- Six landslide density hotspots were analyzed to explain their high susceptibility. Most parts of these areas are located between 1000 and 2500 m. Furthermore, the slope angle distributions showed a tendency towards steeper inclinations.
- Regarding the landcover of Sindhupalchok, the highest landslide density can be seen in cultivated land, which dominates in elevations between 1500 and 2500 m.

The enhanced landslide density on southern and southeastern slopes is due to the general increase in landslide occurrence with rising slope inclinations and a tendency to steeper southern slopes.

As the geological information was extracted from geological maps, the classification is based on the formations' descriptions. For reasons of clarity and comprehensibility, the formations were merged into five groups based on their lithologies. Although Gneiss is the most common lithology, Limestone and Slate were far more affected. Possible reasons for this

trend are the structural and textural properties of the different rocks, as well as the occurrence of these formations in the highly affected altitudes between 1500 and 2500 m.

Despite the catastrophic destruction of villages and roads due to the shaking, in Sindhupalchok only little infrastructure was damaged by landslides triggered during the earthquake. Landslides during the monsoon, on the other side, buried several houses and blocked many roads.

7. References

Google Earth Satellite Images: DigitalGlobe and CNES/Astrium

DEM: Shuttle Radar Topography Mission (USGS)

Soils: SOTER – Soil and Terrain Database of Nepal (ISRIC)

Figure 13 was taken by GEER team member Dr. Menzer Pehlivan

8. Publication bibliography

Amatya, K. M.; Jnawali, B. M. (1993): Geological Map of Nepal (Scale 1:1 000 000): Department of Mines & Geology.

Avouac, Jean-Philippe (2003): MOUNTAIN BUILDING, EROSION, AND THE SEISMIC CYCLE IN THE NEPAL HIMALAYA. In, vol. 46: Elsevier (Advances in Geophysics), pp. 1–80.

Bilham, Roger (1995): Location and magnitude of the 1933 Nepal earthquake and its relation to the rupture zones of contiguous great Himalayan earthquakes. Current Science. Available online at http://cires1.colorado.edu/~bilham/1833Update09/1833CurrentScience.pdf, checked on 3/7/2016.

Dhital, Megh Raj (2014): Geology of the Nepal Himalaya. Regional Perspective of the Classic Collided Orogen. New York: Springer.

DigitalGlobe. Available online at https://www.digitalglobe.com/about/overview, checked on 1/19/2016.

FAO (2006): World reference base for soil resources, 2006. A framework for international classification, correlation, and communication. 2006 ed. Rome: Food and Agriculture Organization of the United Nations (World soil resources reports, 103).

Guzzetti, Fausto; Mondini, Alessandro Cesare; Cardinali, Mauro; Fiorucci, Federica; Santangelo, Michele; Chang, Kang-Tsung (2012): Landslide inventory maps. New tools for an old problem. In *Earth-Science Reviews* 112 (1-2), pp. 42–66. DOI: 10.1016/j.earscirev.2012.02.001.

Hagen, Toni (1969): Report on the geological survey of Nepal. Vol. 1.

Hashash, Y.; Tiwari, B.; Moss, R.; Asimaki, D.; Clahan, K.; Kieffer, D. et al. (2015): Geotechnical Field Reconnaissance: Gorkha (Nepal) Earthquake of April 25 2015 and Related Shaking Sequence.

ISRIC: Soil and Terrain database of Nepal. Available online at http://www.isric.org/projects/soter-nepal, checked on 1/18/2016.

Kargel, J. S.; Leonard, G. J.; Shugar, D. H.; Haritashya, U. K.; Bevington, A.; Fielding, E. J. et al. (2016): Geomorphic and geologic controls of geohazards induced by Nepal's 2015 Gorkha earthquake. In *Science (New York, N.Y.)* 351 (6269), pp. aac8353. DOI: 10.1126/science.aac8353.

Keefer, David K. (2002): Investigating landslides caused by earthquakes - A historical review. In *Surveys in Geophysics* 23 (6), pp. 473–510. DOI: 10.1023/A:1021274710840.

Khazai, Bijan; Sitar, Nicholas (2004): Evaluation of factors controlling earthquake-induced landslides caused by Chi-Chi earthquake and comparison with the Northridge and Loma Prieta events. In *Engineering Geology* 71 (1-2), pp. 79–95. DOI: 10.1016/S0013-7952(03)00127-3.

Kieffer, D. Scott (2015): GEO.708 Engineering Geologic Investigations. Mapping for Geologic Hazards - Landlides. TU Graz, 2015.

Malamud, Bruce D.; Turcotte, Donald L.; Guzzetti, Fausto; Reichenbach, Paola (2004): Landslide inventories and their statistical properties. In *Earth Surf. Process. Landforms* 29 (6), pp. 687–711. DOI: 10.1002/esp.1064.

Molnar, Peter (1986): The Geologic History and Structure of the Himalya. In *American Scientist* Vol. 74 (Issue 2).

Neupane, V. K.: Geological Map of Central Nepal (Scale 1: 250 000): Rana, M.N. (Department of Mines and Geology).

OSOCC (2015): Nepal Earthquake. District Profile - Sindhupalchok. On-Site Operations Coordination Centre. Available online at https://www.humanitarianresponse.info/sites/www.humanitarianresponse.info/files/assessments/150508_sindhupalchok_osocc_district_profile_-_for_publishing.pdfhttps://www.humanitarianresponse.info/sites/www.humanitarianrespo

nse.info/files/assessments/150508_sindhupalchok_osocc_district_profile_-_for_publishing.pdf, updated on 5/8/2015, checked on 3/7/2016.

USGS: Shuttle Radar Topography Mission (SRTM) 1 Arc-Second Global courtesy of the U.S. Geological Survey. Available online at https://lta.cr.usgs.gov/SRTM1Arc, checked on 1/18/2016.

Veness, Chris (2002-2016): Calculate distance, bearing and more between Latitude/Longitude points. Available online at http://www.movable-type.co.uk/scripts/latlong.html, checked on 3/1/2016.

Wilson, Liz; Wilson, Brant. Available online at http://www.geo.arizona.edu/geo5xx/geo527/Himalayas/geology.html, checked on 04,12,2015.

Appendix

ObjectID	Latitude	Longitude	new/reactivated	LA [m²]	width [m]	Map length [m]	max	min	LR [m]	max	min	SR [m]	SAs GE	SAn GE [°]	AR	ls length	ls length rd.	aff. Infra	SAn GIS [°]	SAs GIS [°]	Soil	DB	DEPI [km]	ls/km²	height	landcover
1	28.068186	85.539157	new	22 988	100	290	3195	2880	315	3519	2880	639	E	47.37	0.233	428.16	430		40.25	155.08	CMu	Indrawati	82.0	1.0	2922	1
2	28.079312	85.542412	new	35 943	210	160	3292	3117	175	4110	3117	993	SE	47.56	0.875	237.12	240		49.74	115.47	CMu	Indrawati	82.2	2.0	3159	1
3	28.068061	85.546349	new	19 882	50	460	3319	2945	374	3544	2885	659	W	39.11	0.085	592.85	590		23.44	312.83	CMu	Indrawati	82.7	3.0	3287	5
4	28.077882	85.546554	new	62 987	200	330	3711	3211	500	3790	3108	687	W	56.58	0.333	599.08	600		43.89	271.39	CMu	Indrawati	82.6	2.0	3218	2
5	28.072897	85.532724	reactivated	42 042	90	270	3437	3184	253	4008	3184	824	NE	43.14	0.243	370.01	370		24.61	76.79	CMu	Indrawati	81.3	1.0	3228	6
6	28.079138	85.539993	reactivated	8 610	50	200	3504	3311	193	4123	3116	1007	E	43.98	0.179	277.94	280		33.38	112.49	CMu	Indrawati	82.0	2.0	3354	2
7	28.077589	85.539628	new	1 528	10	100	3355	3264	91	4123	3264	859	E	42.30	0.071	135.21	140		55.54	139.32	CMu	Indrawati	81.9	1.0	3215	2
8	28.077594	85.538511	new	3 324	10	140	3407	3301	106	4123	3301	822	SE	37.13	0.056	175.60	180		51.77	143.45	CMu	Indrawati	81.8	1.0	3313	2
9	28.073990	85.541421	reactivated	6 427	50	180	3254	3007	247	3306	2987	319	SE	53.92	0.161	305.63	310		28.65	115.66	CMu	Indrawati	82.2	1.0	3000	1
10	28.073618	85.538826	new	8 201	20	390	3358	2974	384	3377	2968	409	SE	44.56	0.036	547.32	550		39.74	140.30	CMu	Indrawati	81.9	1.0	3218	1
11	28.072258	85.538309	new	5 931	50	120	3115	3026	89	3400	3026	374	S	36.56	0.333	149.40	150		30.69	173.25	CMu	Indrawati	81.9	1.0	3069	6
12	28.074644	85.537385	new	12 781	30	300	3397	3102	295	3400	3102	298	S	44.52	0.071	420.74	420		26.30	152.43	CMu	Indrawati	81.8	1.0	3347	2
13	28.084207	85.536246	new	1 666	10	90	3859	3759	100	4075	3152	923	SE	48.01	0.077	134.54	130		45.49	149.04	LPi	Indrawati	81.5	1.0	3766	6
14	28.082420	85.541839	new	686	10	100	3503	3408	95	4075	3198	877	SE	43.53	0.071	137.93	140		35.07	134.10	CMu	Indrawati	82.1	1.0	3398	1
15	28.081419	85.534901	new	874	10	310	3871	3613	258	4203	3254	949	SE	39.77	0.025	403.32	400		28.27	132.66	LPi	Indrawati	81.4	1.0	3735	6
16	28.083683	85.534269	reactivated	938	10	480	3970	3604	366	4245	3131	1114	SE	37.33	0.017	603.62	600		37.00	105.82	LPi	Indrawati	81.3	2.0	3855	2
17	28.084332	85.534415	reactivated	9 953	20	520	3980	3586	394	4245	3131	1114	SE	37.15	0.031	652.41	650		42.25	140.19	LPi	Indrawati	81.4	1.0	3871	6
18	28.075844	85.528866	reactivated	20 900	90	260	3647	3414	233	4329	3414	915	NE	41.87	0.257	349.13	350		53.36	86.03	LPi	Indrawati	80.9	1.0	3461	5
19	28.081551	85.523354	reactivated	11 070	50	230	3973	3666	307	4103	3666	437	E	53.16	0.132	383.60	380		30.63	45.00	LPi	Indrawati	80.3	2.0	3733	6
20	28.085528	85.523296	reactivated	4 399	10	270	3917	3753	164	4300	3753	547	SW	31.27	0.031	315.91	320		36.10	215.04	LPi	Indrawati	80.3	3.0	3813	6
21	28.078047	85.525885	new	7 235	50	160	3703	3589	114	4299	3589	710	NE	35.47	0.250	196.46	200		21.28	54.73	LPi	Indrawati	80.6	1.0	3572	2
22	28.072080	85.534868	new	35 243	120	260	3370	3155	215	3539	3155	384	N	39.59	0.353	337.38	340		23.22	77.47	CMu	Indrawati	81.5	2.0	3117	4
23	28.070826	85.536472	new	30 274	100	350	3378	3050	328	3439	3050	389	N	43.14	0.208	479.67	480		49.39	49.58	CMu	Indrawati	81.7	1.0	3174	4
24	28.069895	85.538935	new	4 366	30	190	3080	2915	165	3439	2915	524	E	40.97	0.120	251.64	250		36.09	90.61	CMu	Indrawati	82.0	1.0	2995	1
25	28.067990	85.535784	new	34 828	90	480	3369	2828	541	3439	2828	611	SE	48.42	0.125	723.24	720		38.49	98.13	CMu	Indrawati	81.7	2.0	3286	5
26	28.070148	85.537083	new	11 902	60	240	3342	3092	250	3439	3027	412	NE	46.17	0.171	346.55	350		51.56	68.33	CMu	Indrawati	81.8	1.0	3157	1
27	28.067531	85.543933	new	9 953	30	260	3128	2937	191	4160	2880	1280	W	36.30	0.094	322.62	320		50.35	272.03	CMu	Indrawati	82.5	2.0	3106	5
28	28.068950	85.547628	reactivated	16 796	30	610	3411	2976	435	4417	2918	1499	W	35.49	0.040	749.22	750		26.37	235.19	CMu	Indrawati	82.8	1.0	3349	5
29	28.070687	85.547953	new	15 702	20	610	3441	2999	442	3973	2928	1045	W	35.93	0.027	753.30	750		31.31	288.20	CMu	Indrawati	82.8	2.0	3416	5
30	28.071547	85.543874	new	10 582	30	320	3119	2949	170	3973	2949	1024	W	27.98	0.083	362.35	360		63.44	219.18	CMu	Indrawati	82.4	1.0	3071	2
31	28.072246	85.548491	new	11 872	20	610	3443	3014	429	3973	2989	984	W	35.12	0.027	745.75	750		28.94	307.59	CMu	Indrawati	82.9	1.0	3441	2
32	28.073016	85.549649	new	14 680	80	320	3480	3281	199	3973	3028	945	W	31.88	0.211	376.83	380		45.70	303.27	CMu	Indrawati	83.0	1.0	3467	5
33	28.074215	85.549631	reactivated	22 064	40	740	3605	3170	435	4256	3094	1162	W	30.45	0.047	858.39	860		52.99	263.62	CMu	Indrawati	83.0	2.0	3423	5
34	28.075689	85.548954	reactivated	12 906	50	260	3587	3268	319	3790	3094	696	S	50.82	0.122	411.53	410		50.00	214.93	CMu	Indrawati	82.9	1.0	3456	6
35	28.080258	85.548666	new	8 470	30	210	3500	3289	211	3790	3167	623	W	45.14	0.100	297.69	300		52.00	295.48	CMu	Indrawati	82.8	1.0	3507	5
36	28.087888	85.651022	new	55 196	180	610	3694	3330	364	4046	3330	716	NE	30.83	0.254	710.35	710		27.12	97.39	CMu	Indrawati	92.7	1.0	3472	5
37	28.093997	85.656597	new	6 541	20	240	3822	3687	135	4204	2988	1216	SE	29.36	0.071	275.36	280		22.89	135.74	LPi	Indrawati	93.2	2.0	3743	5
38	28.069099	85.662235	new	67 417	70	990	3398	2653	745	3434	2653	781	SW	36.96	0.056	1239.00	1240		27.58	204.09	CMu	Indrawati	94.0	2.0	3026	1
39	28.071303	85.648726	new	17 834	40	460	3268	2981	287	3775	2765	1010	SE	31.96	0.074	542.19	540		23.53	94.09	CMu	Indrawati	92.7	1.0	3154	1
40	28.079007	85.659986	new	20 546	150	200	3141	2921	220	3531	2921	610	W	47.73	0.500	297.32	300		38.22	268.03	CMu	Indrawati	93.7	1.0	3075	2
41	28.072297	85.651960	new	9 727	60	200	3031	2896	135	3775	2765	1010	E	34.02	0.250	241.30	240		35.42	125.68	CMu	Indrawati	93.0	2.0	2948	1
42	28.070892	85.652606	new	15 528	100	250	2978	2800	178	3775	2765	1010	E	35.45	0.323	306.89	310		39.07	86.44	CMu	Indrawati	93.0	3.0	2890	1
43	28.068890	85.648474	new	1 888	20	130	3107	3036	71	3780	2878	902	E	28.64	0.133	148.12	150		11.29	119.05	CMu	Indrawati	92.7	2.0	3110	1
44	28.070047	85.649448	new	7 333	50	180	3129	3009	120	3134	2878	256	S	33.69	0.227	216.33	220		20.27	50.96	CMu	Indrawati	92.7	1.0	3136	1
45	28.070160	85.650026	new	4 317	20	190	3104	2993	111	3134	2878	256	S	30.29	0.091	220.05	220		35.35	69.19	CMu	Indrawati	92.8	1.0	3102	1
46	28.069361	85.650766	new	16 165	60	370	3061	2886	175	3134	2878	256	SE	36.10	0.100	297.03	300		36.40	87.59	CMu	Indrawati	92.9	1.0	3052	1
47	28.068189	85.653164	new	4 994	30	240	2918	2650	268	3134	2650	484	S	35.92	0.130	456.86	460		35.69	135.44	CMu	Indrawati	93.1	1.0	2864	1
48	28.072170	85.649617	new	4 958	20	220	3135	2973	162	3775	2765	1010	E	36.37	0.074	273.21	270		41.73	89.00	CMu	Indrawati	92.7	2.0	3093	1
49	28.073500	85.650473	new	7 645	60	170	3098	3024	74	3775	2765	1010	E	23.52	0.316	185.41	190		25.36	74.83	CMu	Indrawati	92.8	3.0	3075	1
50	28.072990	85.654367	new	6 453	40	210	2920	2784	136	3043	2784	259	E	32.93	0.160	250.19	250		51.13	105.04	CMu	Indrawati	93.2	2.0	2912	1
51	28.073610	85.653780	new	5 431	30	200	2996	2851	145	3043	2816	227	NE	35.94	0.120	247.03	250		17.56	107.10	CMu	Indrawati	93.1	1.0	2971	1
52	28.072794	85.645222	new	5 016	40	180	3449	3325	124	3775	2765	1010	SE	34.56	0.182	218.58	220		35.32	124.30	CMu	Indrawati	92.3	1.0	3439	1
53	28.077381	85.649651	new	7 943	20	360	3324	3069	255	3373	2816	557	SE	35.31	0.045	441.16	440		34.09	148.59	CMu	Indrawati	92.7	1.0	3303	1
54	28.075832	85.645342	new	2 147	10	150	3376	3254	122	3736	3165	571	E	39.12	0.053	193.35	190		40.32	72.72	CMu	Indrawati	92.3	1.0	3408	1

Appendix: Figure 1 Excel spreadsheet: landslide data (example)

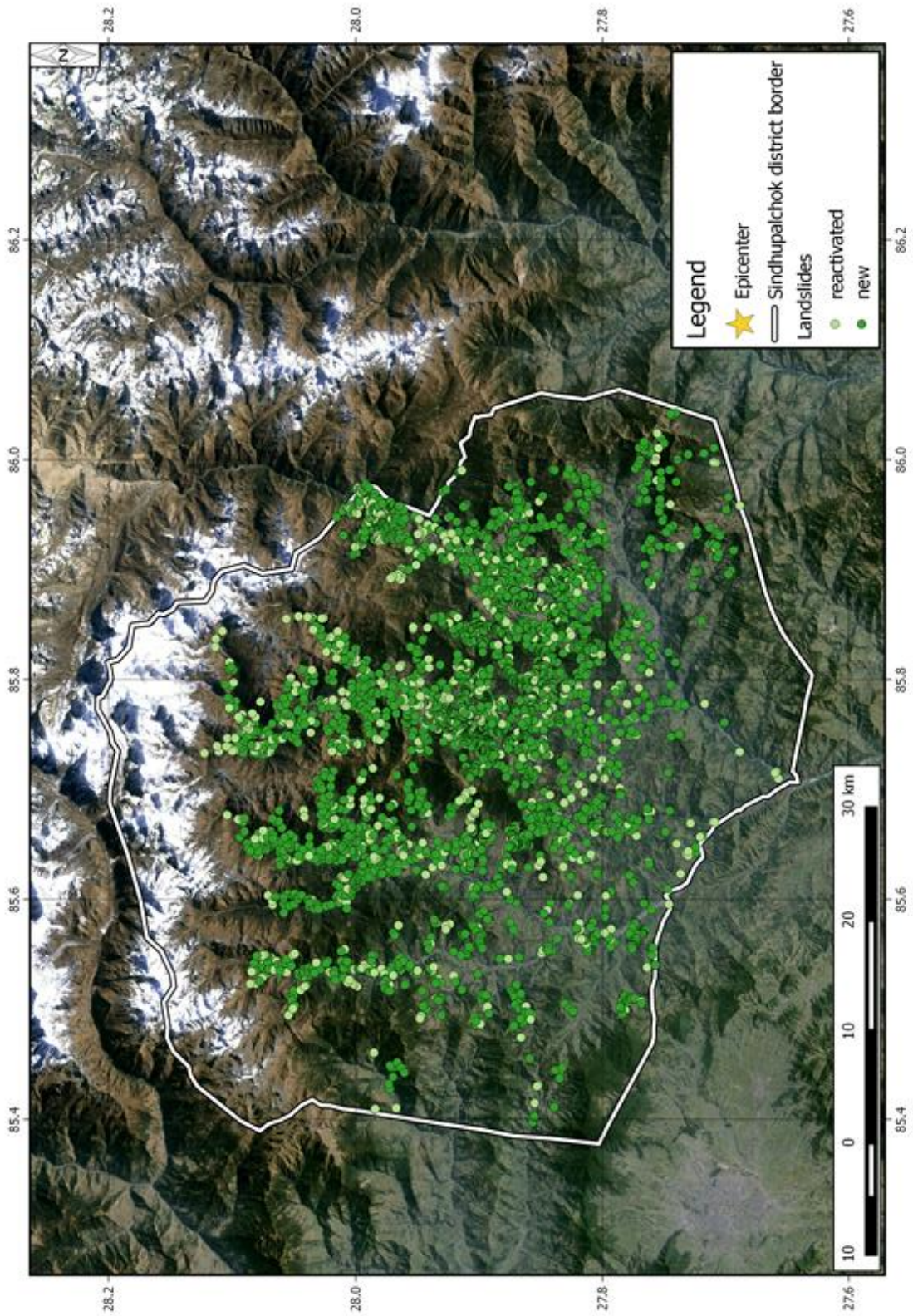

Appendix: Figure 2 Inventory map of new/reactivated landslides (© Ziselsberger; Basemap: Google Earth Image)

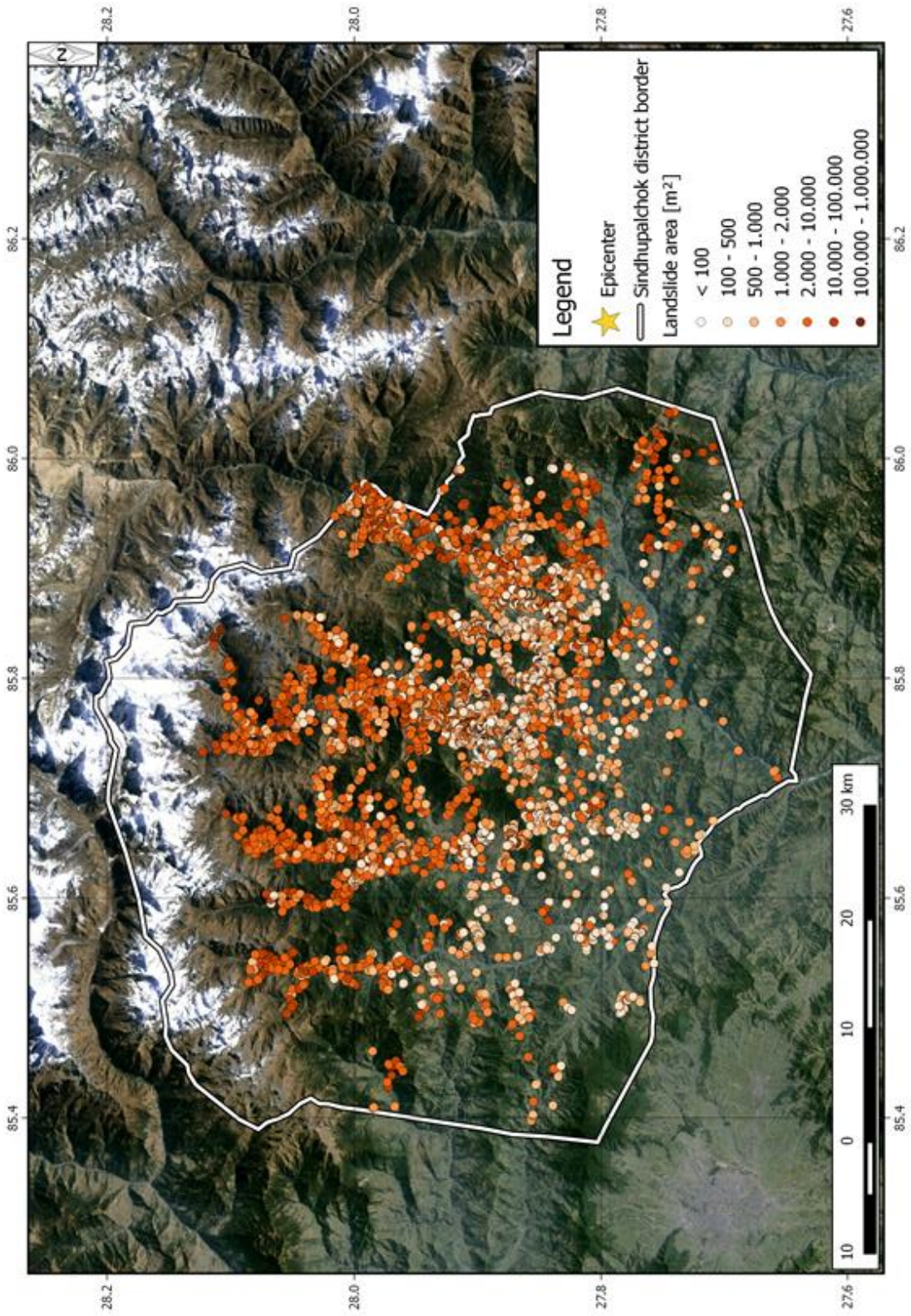

Appendix: Figure 3 Inventory map of landslide areas (© Ziselsberger; Basemap: Google Earth Image)

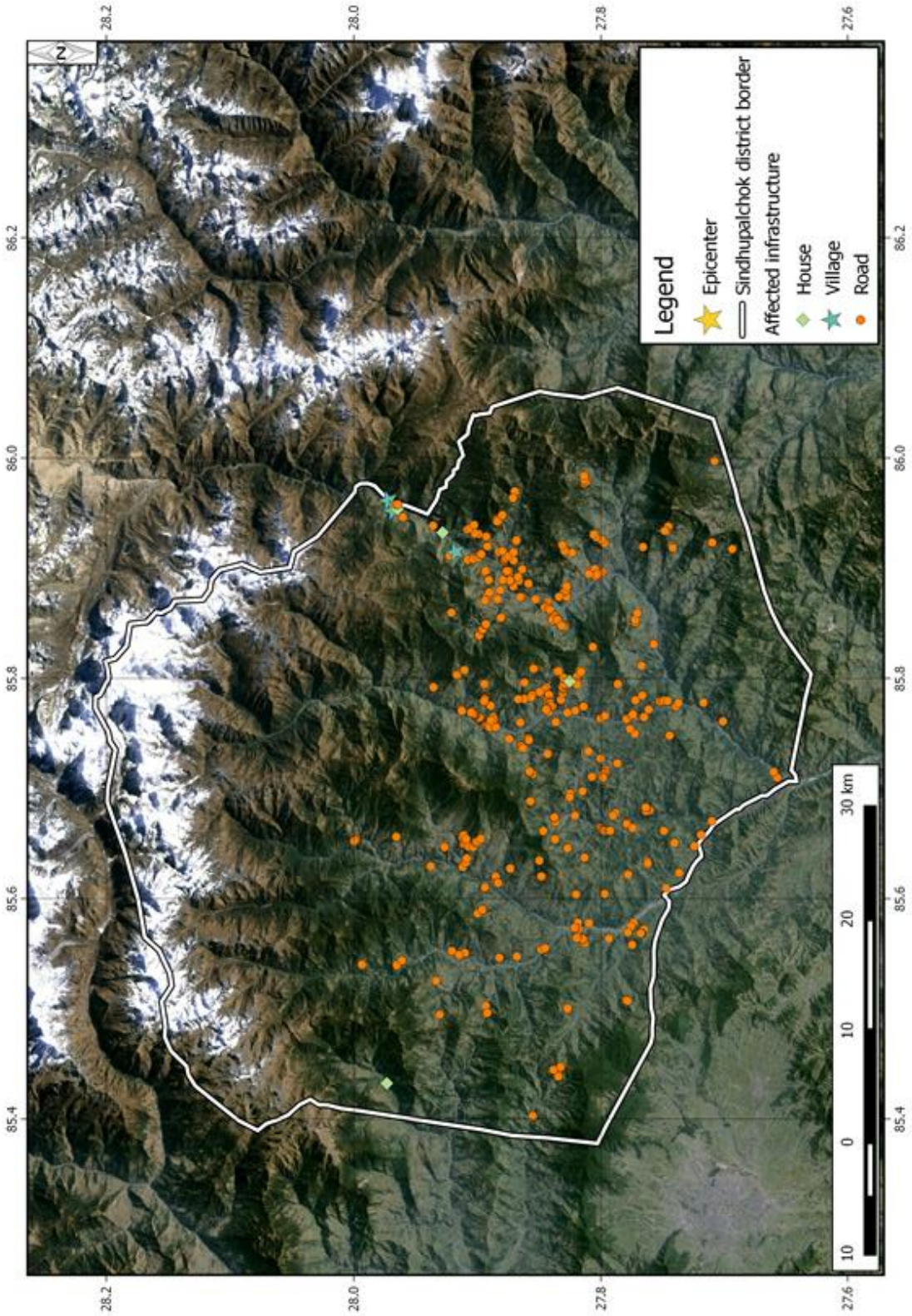

Appendix: Figure 4 Inventory map of affected infrastructure (© Ziselsberger; Basemap: Google Earth Image)

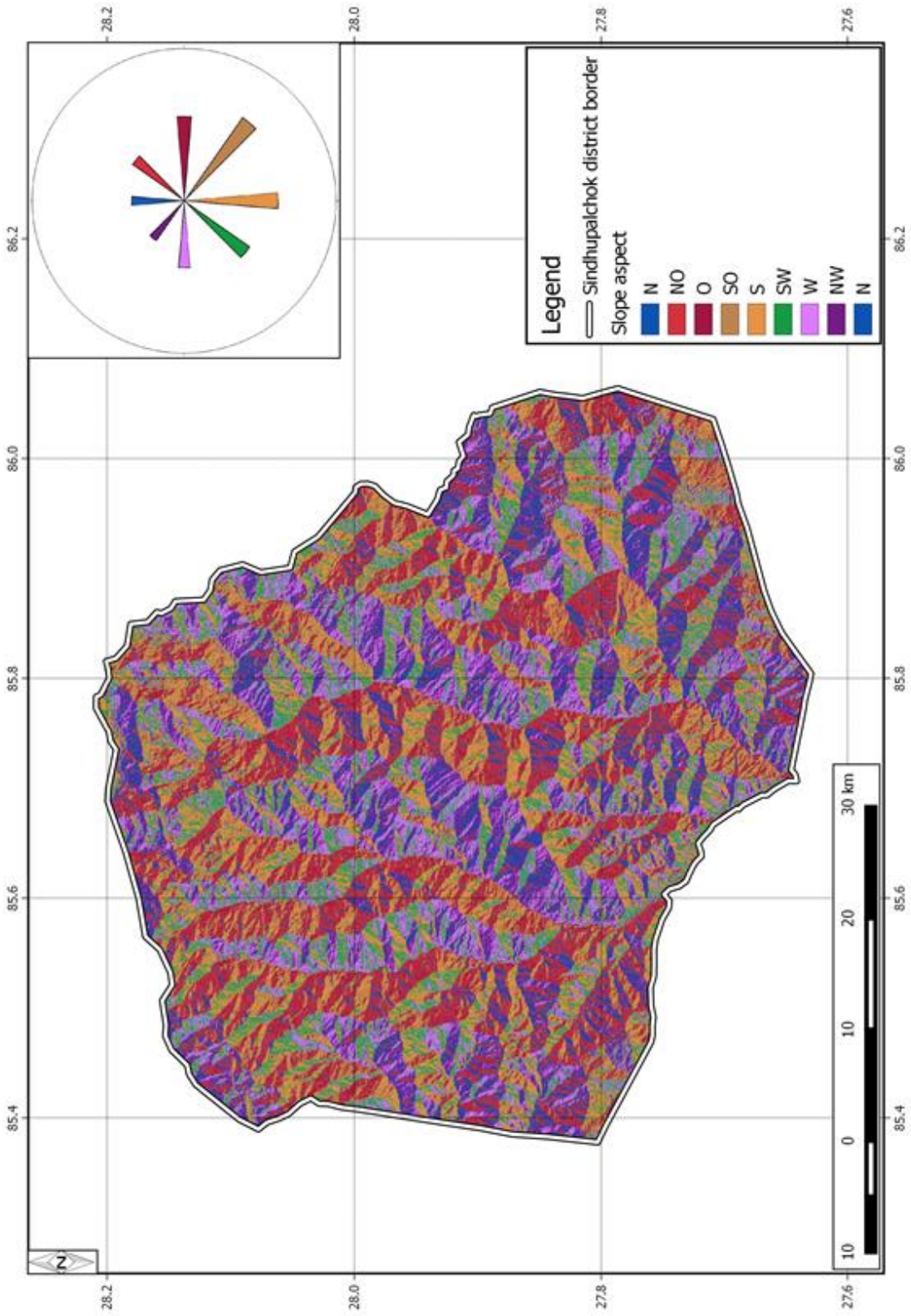

Appendix: Figure 5 Inventory map of slope aspects (© Ziselsberger)

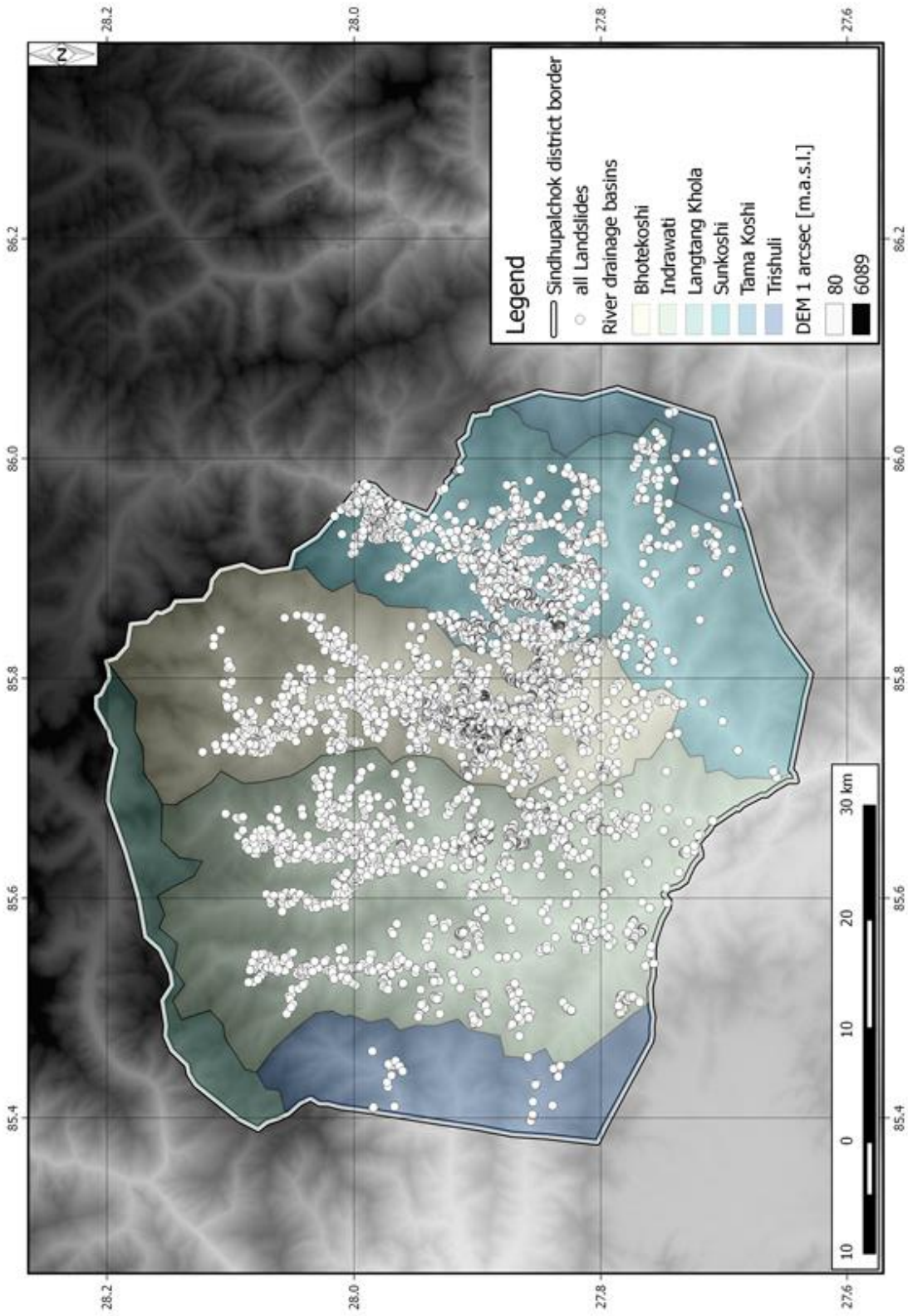

Appendix: Figure 6 Inventory map of drainage basins (© Ziselsberger; Basemap: SRTM DEM)